https://ntrs.nasa.gov/search.jsp?R=19680002453 2020-03-12T11:52:03+00:00Z

EE67-17
NASA Grant NsG-553
PRF 5120

PURDUE UNIVERSITY
SCHOOL OF ELECTRICAL ENGINEERING

DIGITAL COMMUNICATION SYSTEMS SUBJECT TO FREQUENCY SELECTIVE FADING

by
John C. Lindenlaub, Principal Investigator
Charles C. Bailey

N68-11921 (ACCESSION NUMBER) 124 (PAGES) CR-91078 (NASA CR OR TMX OR AD NUMBER) (THRU) 1 (CODE) 07 (CATEGORY)
FACILITY FORM 602

November 1967
Lafayette, Indiana

GPO PRICE $ _____
CFSTI PRICE(S) $ _____
Hard copy (HC) 3.00
Microfiche (MF) _____
ff 653 July 65

SUPPORTED BY THE NATIONAL AERONAUTICS AND SPACE ADMINISTRATION

PURDUE UNIVERSITY

SCHOOL OF ELECTRICAL ENGINEERING

ELECTRONIC SYSTEMS RESEARCH LABORATORY

DIGITAL COMMUNICATION SYSTEMS SUBJECT TO FREQUENCY SELECTIVE FADING

By

John C. Lindenlaub, Principal Investigator

Charles C. Bailey

November, 1967

Lafayette, Indiana

Supported by

NATIONAL AERONAUTICS AND SPACE ADMINISTRATION

Washington, D. C.

Under

Grant NsG-553

FOREWORD

This report is an interim report which summarizes one phase of research that is being carried out at Purdue University in the area of communication theory under NASA Grant NsG-553.

TABLE OF CONTENTS

TABLE OF CONTENTS (continued)

LIST OF TABLES

LIST OF FIGURES

LIST OF FIGURES (continued)

ABSTRACT

This research is concerned with the effects of frequency selective fading on binary digital communication systems and with a method of alleviating some of these effects. The frequency selective fading is assumed to be describable in terms of a filter whose transfer function is a sample function from a complex Gaussian random process. Matched filter detection at the receiver is assumed to be employed. Although the analytical methods used in this report are general, DPSK signaling is assumed for all the quantitative results.

In order to determine the probability of error for this system, a technique due to Bello and Nelin is used. This is applied to three cases:

1. Square pulse signaling and Gaussian-function-shaped channel frequency correlation function.
2. Square pulse signaling and sin(x)/x - shaped channel frequency correlation function.
3. Raised cosine signaling and sin(x)/x - shaped channel frequency correlation function.

The results of these three cases are compared and it is shown that significant differences in error probability

result from using the two different signals with the same channel while very little difference in performance results from using the two different channels with the same signal.

For the three cases mentioned above, an approximate error probability expression developed by Sunde is compared to the exact results. It is shown that this approximation does not provide a good estimate of the error probability when the frequency selective fading is of importance.

Next, some experimental results from computer simulations of communication systems subject to frequency selective fading are given. The first of these is an investigation of the relative effects of the amplitude and phase distortion introduced in such a system. It is shown that the phase distortion component has a deleterious effect on the system's performance while the amplitude distortion has a slight beneficial effect. These results provide the motivation for the development of an adaptive scheme for counteracting the effects of frequency selective fading. This is done by measuring the residual delay and delay distortion introduced by the channel fading with pilot tones and then using phase correction networks at the receiver to compensate for the measured phase characteristic. It is shown that this technique can result in error rate improvement factors of twenty or data rate increases by a factor of two to three. It is also shown that the system which corrects for both delay and linear delay distortion provides very little improvement over the system which corrects for delay only.

CHAPTER I: INTRODUCTION

1.1 General Description of the Problem

Communication channels which exhibit severe fading effects have been in use for several years. Important examples of these are the widely-used h-f channels and tropospheric scatter channels (1). Severe fading effects have also been experimentally observed on an orbital dipole channel (2) and a lunar reflection channel (3). There is also some evidence that fading due to multipath propagation through the atmosphere may exist in certain earth-space communication channels (4). With increasing use of telemetry, digital transmission of voice signals, and long-distance transmission of computer data, it is apparent that digital communication over such links will become more prevalent. Furthermore, with the increasing digital data rates being used in modern telemetry, computer, and telephone transmission equipment, it is expected that attempts at very high data rate transmission through such channels will be made. With the advent of such wideband transmission, the frequency selective behavior of the above-mentioned channels will play a great role in determining the design and performance of the systems to be used. It is therefore becoming increasingly important to understand the basic effects that

frequency selective fading has on digital transmission schemes and to determine methods of minimizing these effects.

Frequency selective fading can be defined as the phenomenon which occurs in fading channels when deep fades can be observed at some frequencies of transmission while relatively little fading is occurring at other frequencies in the band. If signals of wide bandwidths are transmitted over such a channel, then since the channel transmittance at one point in the transmission band may differ significantly from that at some other point, the received signal may be effectively transmitted through a frequency selective filter. This will result in distortion in the shape of the received pulse. When such distortion occurs in a digital communication system employing a matched filter-sampler receiver configuration, then the probability of correctly classifying the received signal is reduced due to two effects. These are:

1. Mismatch of the received signal's shape relative to the shape of the signal for which the matched filter is designed and
2. Intersymbol interference due to undesirable tails created in the pulse response characteristic of the system.

These distortion effects together with the effect of fluctuating strength of the received signal (even if not distorted) are the two effects which determine the basic limitations on error rate performance of digital communication systems

employing receivers of the above type. The purpose of the research discussed in this report is to compare exact and approximate methods of determining the error rate performance of such communication systems and to evaluate a novel method of reducing the effects of a frequency selective channel on these systems.

1.2 Outline of Previous Work

Much of the results to date have been based on considering the output of the fading channel to be a Gaussian random process. This random process can be related to the channel transmittance which will then be, in general, a complex-valued function of time and frequency. Using this representation, Bello and Nelin (5) were able to determine error probabilities for both incoherent FSK and differentially coherent PSK systems operating over such a channel. These results were based on the known Gaussian properties of the received signal and are valid for any order of postdetection diversity combining in the receiver system. Sunde (6) conjectured that the most serious distortion effects in such a system can be attributed to the phase distortion imposed on the transmitted signal by the channel. He further postulated that for narrow enough bandwidths, linear delay distortion alone could be considered to cause the pulse distortion. This is equivalent to approximating the phase response function by a truncated Taylor's series expansion about the center frequency of the transmission band. Thus using the

statistical properties of the linear delay distortion in a Gaussian fading channel, he developed an approximation to the error probability.

Hingorani (7) has extended the work of Bello and Nelin to the case of simultaneous time and frequency selective fading and an arbitrary number of independent diversity paths, where each diversity branch has identical statistics and may contain a specular component. His method was to reduce the receiver decision variable to a canonic form employed by Stein (8).

Several ideas have been advanced in an effort to try to reduce the effects of distortion in fading channels. Most of these are transmitted reference techniques where separate sounding signals are transmitted along with the data signal in order that the receiver may gain some knowledge of the state of the channel and use this to process the received signal in a better manner. Walker (9) considered the performance of a "frequency differential" system in which a sinusoid is transmitted near a PSK signaling channel and then translated at the receiver for correlation with the signal waveform. He derived the maximum likelihood receiver for this type of transmission and determined its performance in the presence of a fading channel plus noise. Hancock and Hingorani (10) considered a transmitted reference communication system employing a time-variant multipath channel and a general reference-message signal combination for which they derived the "one-shot" Bayes receiver. For Gaussian

multiplicative disturbance, white additive Gaussian noise, and binary PSK, the error probabilities for this receiver were also derived. They later extended this work by determining the Bayes receiver for sequential transmission of signals through a time-variant random channel whose delay spread is less than one baud (11). Spilker (12) investigated the effect of combined time and frequency offset between the information and reference signals for transmitted reference system communication through certain time-variant channels representable as tapped delay lines.

Descriptions of systems which have been experimentally shown to reduce error probability in communication systems employing selective fading channels have also been described in the literature. Price and Green (13) described the RAKE system, which used wideband signals to determine the path structure of an h-f radio channel and which uses this information in a tapped delay line recombining system at the receiver. This results in a receiver which can be interpreted either as a diversity combining operation or as an adaptive matched filter. Hollis (14) described a transmitter-receiver combination which combats the time spreading effects of fading channels by stepping the mark and space frequencies of an FSK link, thus reducing the intersymbol interference at the receiver's detector.

1.3 Review of Related Work

The problem of transmitting communication pulses through channels with frequency selective properties, but which are time invariant has received some attention in recent years. Often in these works the term "channel with memory" is used to describe what we have called "channel with frequency selective properties" above. Aein and Hancock (15) attacked this problem by deriving the optimum linear receiver filter for correlation detection of the overlapping signals which arrive at the receiver. They also considered a decision directed receiver structure which attempts to subtract out the pulse tails which interfere with the pulse being processed by the detector. Schwarzlander (16) then investigated the problem of designing signals to be transmitted through the channel which would reduce the degrading effects of intersymbol interference at the receiver. He succeeded in determining, from the class of signals which result in time-limited pulses at the channel output (i.e., they create no intersymbol interference), the signal which maximizes the pulse energy present at the receiver input. That is, he determined the pulse which minimizes probability of error out of the above-mentioned class of pulses. Quincy (17) then investigated a joint optimization problem wherein an attempt was made to simultaneously optimize the receiver structure and the transmitted signal shape. He formulated the optimum Bayes receiver for pulses with intersymbol interference, and using a variational technique found the signal

shape which, for a given allowed amount of intersymbol interference, maximized the energy transferred through the channel. It should be noted that all the above work is based on the assumption that the channel filtering operation is time invariant and completely known to the system designer.

The transversal equalizer has received much attention recently as a possible engineering solution to the problem of intersymbol interference in data transmission systems. Rappeport (18), Lucky (19, 20), Schreiver et al. (21), and Gorog (22) have suggested designs for transversal equalizer systems which could be automatically adjusted to correct for channel-induced distortion. These adaptive equalizers have been developed mainly for telephone transmission channels, but have not yet been applied to frequency selective fading radio channels.

1.4 Mathematical Assumptions

The general form of the communication system which will be considered in this report is shown in Figure 1.[1] In this figure, a very general receiver structure, known as the canonic receiver, is shown. Although we will later specialize our results to the differentially coherent phase shift keying (DPSK) case, the canonic receiver is shown here to indicate the very general class of modems that can be analyzed by techniques discussed in this report. For example, the DPSK

---

[1] In this figure and throughout this report, the symbol "*" denotes complex conjugate.

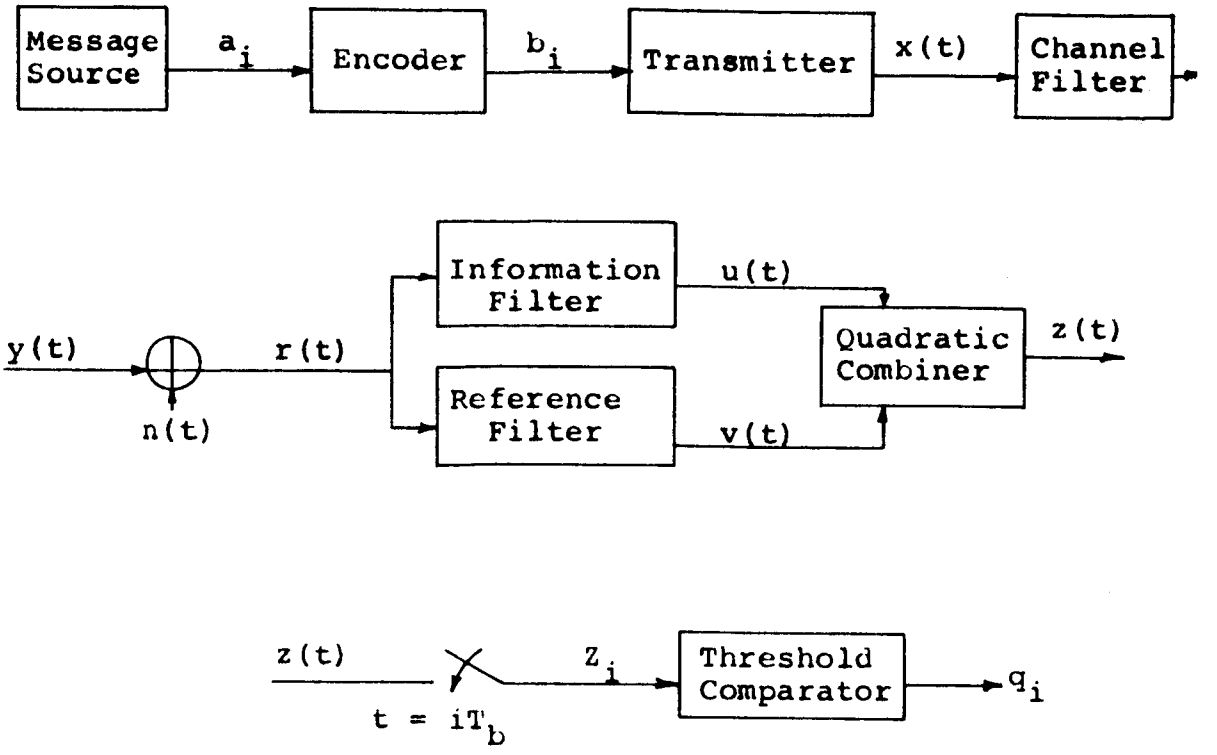

$$z = a|u|^2 + b|v|^2 + 2Re\{cu^*v\}$$

$$q_i = 0, \; Z_i \leq 0$$

$$q_i = 1, \; Z_i > 0$$

Figure 1. System to be Considered.

receiver is realized if the information filter is matched to the transmitted pulse, the reference filter is a similar matched filter plus a delay of one baud, and the combiner gains are a = 0, b = 0, c = 1. The canonic receiver becomes an incoherent FSK receiver if the information and reference filter are matched to the two FSK signals and a = -b, c = 0. Further applications of the canonic receiver model are discussed in (8).

In the system shown, all time functions are represented by their complex envelopes. Thus, for example, the actual output of the waveform generator we are attempting to model is $\mathrm{Re}\{x(t)e^{j\omega_0 t}\}$ where ω_0 is the frequency in radians per second. The value of ω_0 is unimportant, but it is necessary to assume that it is larger than the highest frequency component in x(t).

In this system the message source emits a sequence of binary symbols $\{a_k\}_{k=-\infty}^{\infty}$, $a_k = 0, 1$. The elements of the sequence are emitted at a rate of B symbols per second. The probability of occurrence of either of the two symbols is 1/2, independent of the value of any other symbol in the sequence. The encoder is included in order that differentially coherent modems could be included in this model along with other schemes. Thus with DPSK the b_i's are formed according to the following rule:

$$b_{k+1} = \bar{a}_k \oplus b_k \quad , \quad \text{all } k \tag{1-1}$$

where $\oplus$ denotes addition modulo two and $\bar{a}$ is the binary complement of a. In FSK the encoder would set $b_k=a_k$ for all k.

The transmitter is assumed to be representable as an ideal waveform generator which selects one of two anticorrelated waveforms, $s_0(t)$ or $s_1(t)$, and applies it to the input of the channel filter. The selection of the waveform to be applied is determined by the symbol having been emitted by the encoder. Thus the waveforms are applied to the channel filter at a rate of B waveforms per second.

The channel filter is assumed to be a time-variant linear system completely specified by an associated time-variant impulse response $h(\tau,t)$, defined to be the complex envelope of the filter's response at time t to an impulse forcing function applied τ seconds earlier. We further assume that $h(\tau,t)$ is a sample function from a complex-valued Gaussian random process. Throughout this work it will be assumed that the rate of variation of $h(\tau,t)$ with t, that is, the rate of time variation of the channel, is much slower than the signaling rate of the transmitter. Thus we can replace the time-variant impulse response $h(\tau,t)$ by a random but time-invariant filter whose impulse response is $h(\tau)$. Further descriptions of the channel filter are discussed in the following section.

After the transmitted waveforms are passed through the channel filter, additive noise is introduced. This noise is assumed to be zero-mean, white Gaussian noise with double-sided spectral density N_0 watts/cps. It is also assumed to be statistically independent of the random effects of the

channel filter. We can now visualize two distinct effects of the channel on the communication system. The first effect, the noise, adds a random process to the signal causing unwanted fluctuations at the detector output. Second, the channel filter distorts the transmitted signal causing pulse-shape mismatch and loss of signal power, both of which tend to increase the error probability.

These two independent effects can be seen by examining a typical curve of error probability versus signaling rate, assuming signal energy per bit is held constant. Such a curve is shown in Figure 2. This curve is characterized by a horizontal asymptote to the left which is the error probability for the system with flat Rayleigh fading and additive noise. On the right the error probability curve is asymptotic to a line of increasing error probability as data rate increases. This line represents the lowest probability which can be achieved no matter how much the signal-to-noise ratio is increased. This irreducible error probability is caused by distortion and intersymbol interference effects which result from the selective fading of the channel. Thus, since the selective fading phenomenon is related to the width of the data transmission bandwidth, the irreducible error probability is a function of the data rate. The presence of the horizontal asymptote indicates the effect of additive noise and the varying received signal amplitude. That is, it represents the error probability of such a system under the assumption of additive Gaussian noise and flat Rayleigh

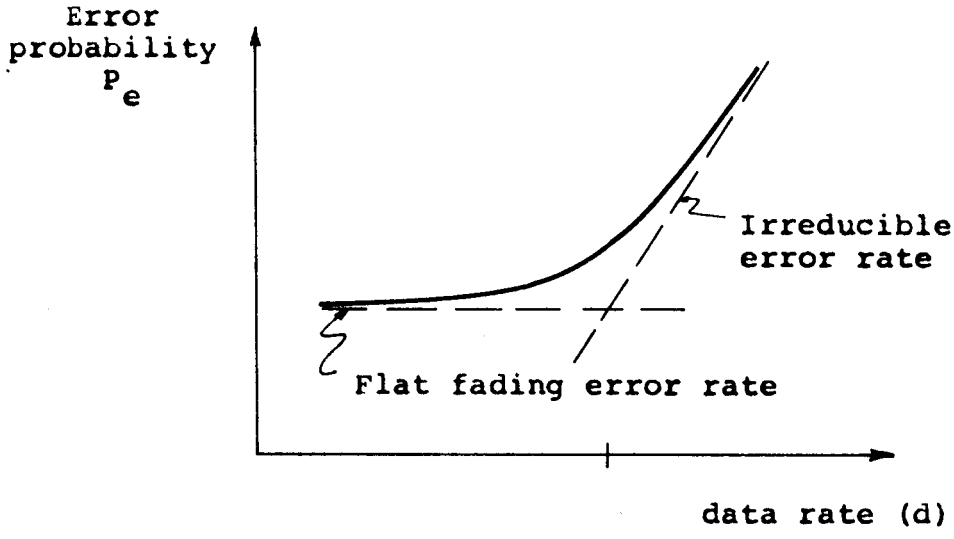

Figure 2. Typical Curve of Error Probability vs Data Rate.

fading. The flat fading error probability, of course, is independent of the signaling rate, which is the reason that the left asymptote is a constant.

The curve of Figure 2 leads to an interesting interpretation of the problem of communication through selective fading channels. For very slow data rates, the signaling bandwidth is so small that the frequency-dependent properties of the channel filter are unimportant - the channel filter transmittance is essentially a constant across the entire signaling band. In this case, only the additive noise and the varying magnitude of the channel transmittance at the carrier frequency are of importance. Thus the error probability is only dependent on the average signal-to-noise ratio at the detector input. For larger data rates, the signal bandwidth becomes larger, and the fact that the channel filter possesses a frequency-dependent transmittance causes distortion and intersymbol effects to become important. As the data rate is further increased, these effects ultimately predominate. The purpose of this report is to investigate a method of reducing the irreducible error probability in such systems and to investigate some methods of calculating the error rate expressions for these systems.

1.5 Channel Representation

As discussed in the previous section, we will assume that the channel filter is a linear time-variant system, and is therefore completely specified by its time-varying

equivalent low-pass impulse response $h(\tau,t)$[1]. We further assume that $h(\tau,t)$ is a sample function from a complex zero-mean Gaussian random process which is wide-sense stationary in the variable t. Thus, the statistical characteristics of the channel filter can be completely specified by the correlation function $P(\tau,\mu,\alpha) \equiv E[h(\tau,t)h^*(\tau+\mu,t+\alpha)]$. In order to examine the frequency domain properties of the channel, we can define an equivalent low-pass time-variant transfer function as

$$H(f,t) = \int_{-\infty}^{\infty} h(\tau,t)e^{-j2\pi f\tau}d\tau \qquad (1\text{-}2)$$

Justification for naming $H(f,t)$ the time-variant transfer function comes from the fact that $H(f,t)$ is simply the complex amplitude of the channel filter's response at time t to the sinusoidal input $e^{j2\pi ft}$. Since $H(f,t)$ is defined as a linear transformation on a sample function from a zero-mean Gaussian random process, then it too is a sample function from a zero-mean Gaussian random process. Therefore its statistical characteristics are completely described by its correlation function defined by

$$R(f_0,f,t) = E[H(f_0,t_0)H^*(f_0+f,t_0+t)] \qquad (1\text{-}3)$$

---

[1] In all communication systems there is some delay between the time of transmission to the time of reception of the signals. In the systems we are considering, we may separate this delay into a constant average delay and a randomly variant delay whose average value is zero. Throughout this work, $h(\tau,t)$ is assumed to be the true impulse response of the physical channel filter with the unimportant constant delay component removed.

We now assume that H(f,t) is wide-sense stationary in the variable f. Thus the correlation function R is no longer a function of f_0 and can be written R(f,t). This stationary assumption on H(f,t) implies that the correlation function P has a special form (23). We can write

$$P(\tau,\mu,\alpha) = p(\tau,\alpha)\cdot\delta(\mu) \tag{1-4}$$

where $\delta(\mu)$ is the Dirac delta function. We will call R and p the frequency correlation function and the delay spread correlation function respectively. It can be shown that R and p possess the following Fourier transform relationship

$$R(f,t) = \int_{-\infty}^{\infty} p(\tau,t)e^{-j2\pi f\tau}d\tau \tag{1-5}$$

The frequency correlation function is quite important since it provides information about the nature of the frequency selective fading that takes place in the channel. This is true because R(f,t) indicates the degree of decorrelation to be expected in the channel response at the two frequencies f_0 and $f_0 + f$ at time t. Thus if R(f,t) is small, then if a signal is transmitted through the channel which possesses significant spectral components at the two frequencies f_0 and $f_0 + f$, we may expect it to undergo significant frequency selective distortion. For this reason, it is convenient to determine some measure of "width" of this correlation function to indicate the range of f-values over which R(f,t) remains reasonably large. This width is usually called the

coherence bandwidth of the channel and is assumed to be related to the maximum bandwidth which a signal can occupy if it is to be reliably transmitted through the channel. Several measures of coherence bandwidth are discussed and compared in Section 2.5.

Under the assumption that the channel varies slowly enough that time-invariant analysis of the filter is valid, we can write

$$\begin{aligned} h(\tau,t) &\longrightarrow h(\tau) \\ H(f,t) &\longrightarrow H(f) \\ R(f,t) &\longrightarrow R(f) \\ P(\tau,\mu,\alpha) &\longrightarrow P(\tau,\mu) \\ p(\tau,\alpha) &\longrightarrow p(\tau) \end{aligned} \qquad (1\text{-}6)$$

Throughout this report, this quasi time-invariant, or "slowly-varying" assumption will be used in the channel models considered.

1.6 Summary of the Report

The major part of this report is devoted to an evaluation of the performance of an adaptive receiver scheme which reduces the intersymbol effects introduced by a frequency selective channel. The adaptive receiver considers the frequency selective channel filter to be approximately modeled by only its delay and delay distortion components. In order to compare the adaptive systems investigated with equivalent systems containing no adaptive features, and also to check

the operation of the computer simulation programs used in this study, a detailed study of the theoretical performance of non-adaptive systems was undertaken. First, the technique of Bello and Nelin was used to determine the exact theoretical performance of non-adaptive systems under study. This work appears in Chapter II. Chapter III contains a comparison of Sunde's approximation to the error probability in a frequency selective fading system with the exact error probabilities calculated in Chapter II. In Chapter IV the computer simulation program developed for this work is discussed. Then experimental verification of an error rate expression given in Chapter II is shown, along with some other experimental results on non-adaptive fading channel communication systems which cannot be evaluated analytically. Chapter V contains a description of a novel adaptive communication scheme for use with frequency selective fading channels and presents experimental performance curves for the proposed system. In Chapter VI the major conclusions of this report are summarized and some suggestions for further work in the area are given.

CHAPTER II: EXACT ERROR PROBABILITIES FOR SELECTIVE FADING SYSTEMS

2.1 Method of Computation of Error Probabilities

This report is devoted to investigation of the accuracy of the Sunde approximate error expression and to an investigation of the usefulness of linear delay distortion correction for fading channel communication systems. Fundamental to both of these investigations is a comprehensive knowledge of the exact error rate behavior of such communication systems. For this reason this chapter presents a method of calculating such error probabilities and the application of this method to three specific cases. There are:

1. Square pulse signal and channel with Gaussian frequency correlation function,
2. Square pulse signal and channel with sin(f)/f frequency correlation function, and
3. Raised cosine signal and channel with sin(f)/f frequency correlation function.

All three cases are for differentially coherent phase shift keying systems. The techniques to be employed in these error calculations were first presented by Bello and Nelin (5), in which case one above was investigated. However, in their

paper and in the subsequent corrections, some of the expressions are in error. To the author's knowledge, the error probabilities for cases two and three above have not been calculated before.

Since the DPSK case is being considered, we can for simplicity redraw the canonic receiver of Figure 1 in the form of a differentially coherent matched filter receiver as shown in Figure 3.

Now the error probabilities are computed by computing the probability that $Z_i > 0$ given that $a_i = 0$ and the probability that $Z_i < 0$ given that $a_i = 1$. Since we are assuming that a sequence of binary digits is being transmitted, the intersymbol interference effects of adjacent pulses must be included in the probability computations. Thus we must compute several error probabilities, each conditioned on one of the possible transmitted sequences of pulses.

At this point we must restrict our consideration to include only the intersymbol interference arising from pulses transmitted either immediately before or after the binary digit of interest. Since two pulses are required to transmit one binary digit, we will need to compute error probabilities conditioned on various sequences of four transmitted pulses. This restriction to consideration of only adjacent pulses implies that we are restricting ourselves to situations where the selective fading is mild enough to warrant this assumption. This in turn can be related to a restriction on d - i.e., that the final expression will be

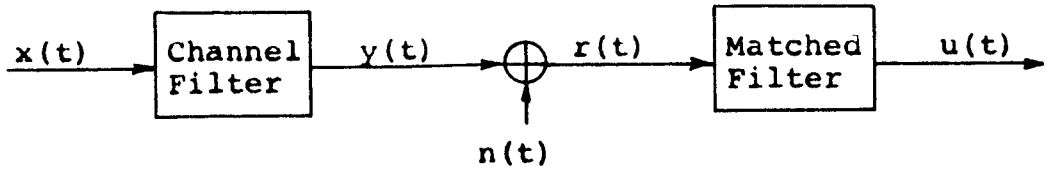

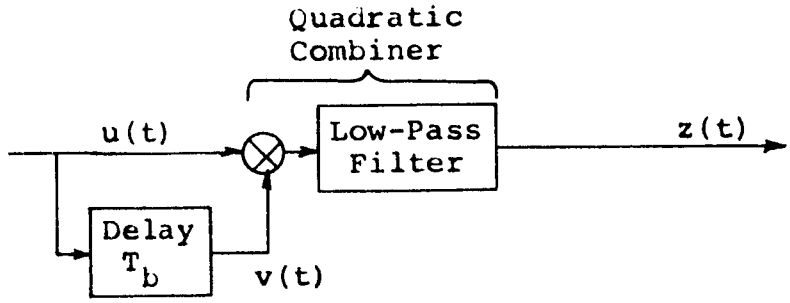

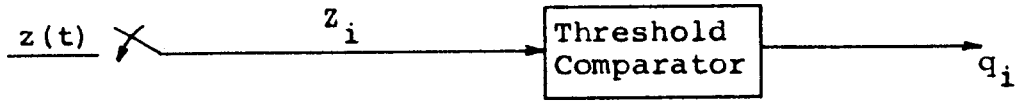

$$q_i = 0, \quad Z_i \leq 0$$

$$q_i = 1, \quad Z_i > 0$$

Figure 3. DPSK Receiver.

considered valid only for values of d below some maximum. This maximum value of d is either estimated or computed exactly in Appendices A, B, and C for each of the three cases considered. In each of these three cases, it will be seen that all values of d which are of practical interest satisfy this restriction.

Since we have assumed that the probabilities associated with the a_i's are time-invariant and the channel impulse response together with the additive white noise are stationary, we can compute the error probabilities for our system by computing the error probability associated with the transmission of binary digit a_1. Thus, we must concern ourselves with the detection of the sequence b_0, b_1. The assumption made above that only adjacent pulse intersymbol interference need be taken into account means that it will be necessary to take into account the transmitted sequence b_{-1}, b_0, b_1, b_2. It will be convenient to define this subset of the modulation sequence as S. Figure 4 illustrates a possible received waveform (in the absence of noise) for a particular sequence S.[1]

We now define

$$p_{abcd} = \Pr[\text{error occurs} \mid S = (a,b,c,d)]$$

---

[1] We will define b_k to be the modulation symbol corresponding to the pulse whose peak value occurs at $(k - \frac{1}{2})T_b$ sec. or, in the case of a square signaling pulse, b_k corresponds to the pulse transmitted during the time interval $[(k - 1)T_b, kT_b]$.

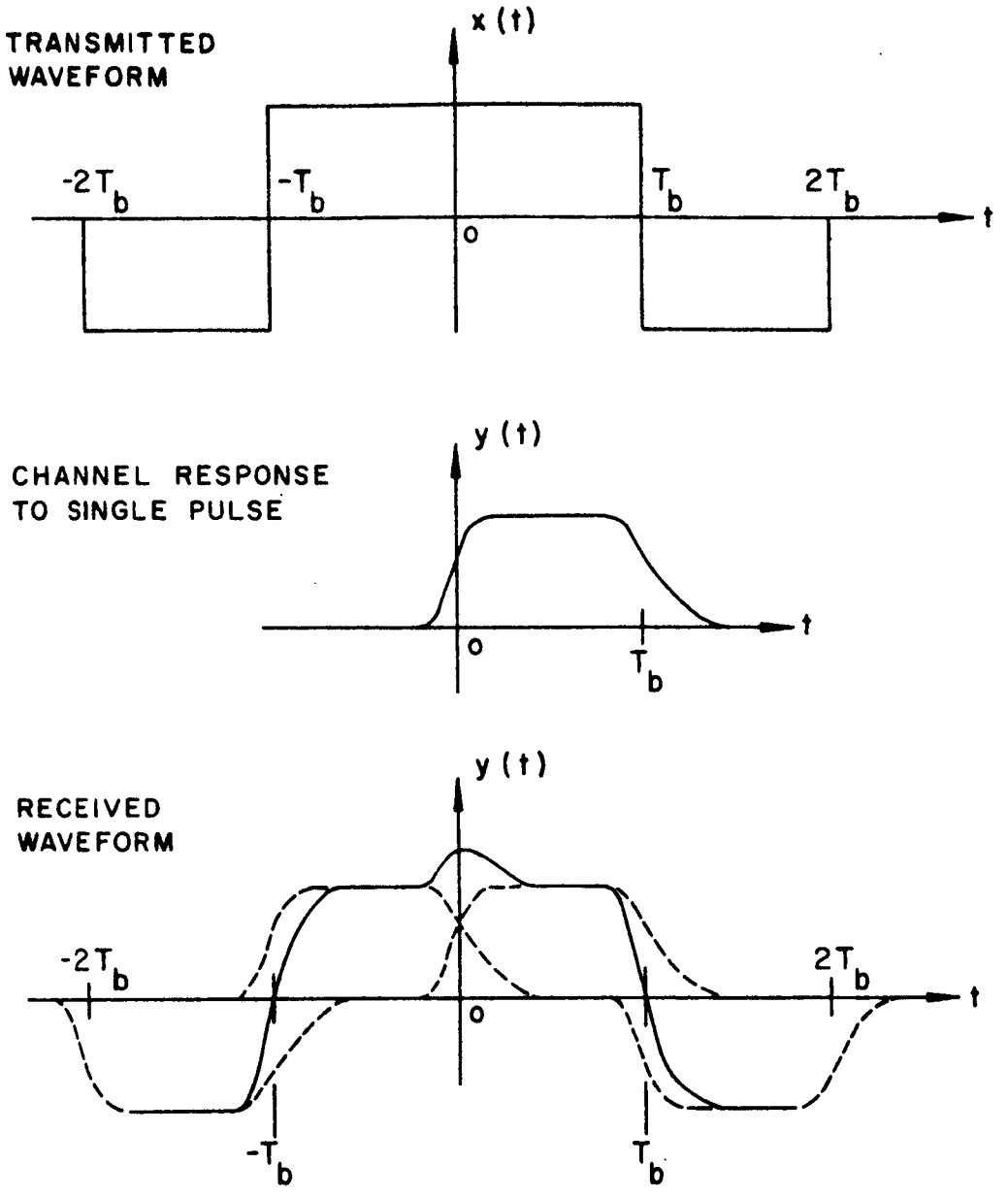

Figure 4. Transmitted and Received Waveforms Corresponding to S = (0,1,1,0) Showing Possible Effects of Intersymbol Interference.

Defining $\bar{b}$ to be the binary compliment of b, we then have

$$p_{ab\bar{b}c} = Pr[Z_1 > 0 | S = (a,b,\bar{b},c)]$$
$$p_{abbc} = Pr[Z_1 < 0 | S = (a,b,b,c)] \qquad (2\text{-}1)$$

We also define

$$p_0 = Pr[q_1 = 1 | a_1 = 0]$$
$$p_1 = Pr[q_1 = 0 | a_1 = 1] \qquad (2\text{-}2)$$

Bello and Nelin have shown that two forms of symmetry exist in the conditional probabilities above. These are

$$p_{abcd} = p_{\overline{abcd}}$$
$$p_{abcd} = p_{dcba} \qquad (2\text{-}3)$$

Thus, recalling that we have assumed that each a_i can be a "1" or a "0" with equal probability and that the a_i's are statistically independent, we can write

$$p_0 = \frac{1}{4}[p_{0101} + p_{1100} + 2p_{0100}]$$
$$p_1 = \frac{1}{4}[p_{0110} + p_{1111} + 2p_{0111}] \qquad (2\text{-}4)$$

Finally, the system probability of error can be written

$$P_e = \frac{1}{2}(p_0 + p_1) \qquad (2\text{-}5)$$

Now using the fact that the signals u(t) and v(t) are Gaussian, we can write the probability required to evaluate the above expressions as follows (24):

$$\Pr(q_i \leq 0) = \frac{1}{2 + R}$$

$$\Pr(q_i > 0) = 1 - \frac{1}{2 + R} = \frac{1}{2 + R'} \qquad (2\text{-}6)$$

where

$$R' = \frac{-R}{1 + R}$$

R and R' can be considered to be "equivalent" signal-to-noise ratios in the given system, since they enter into the probability expressions in a manner analogous to the way the SNR enters into the error probability expressions in the flat fading case. Thus, we may write

$$P_{abbc} = \frac{1}{2 + R_{abbc}}$$

$$P_{ab\bar{b}c} = \frac{1}{2 + R'_{ab\bar{b}c}} \qquad (2\text{-}7)$$

where R_{abbc} is the value of R given that S = (a,b,b,c).

The R's are related to the moments of u and v as follows (24):

$$R = \frac{2(\overline{u^*v} + \overline{v^*u})}{[(\overline{u^*v} + \overline{v^*u})^2 + 4(\overline{|u|^2} \cdot \overline{|v|^2} - |\overline{u^*v}|^2)]^{\frac{1}{2}} - (\overline{u^*v} + \overline{v^*u})} \qquad (2\text{-}8)$$

To compute R_{abcd} using this equation, the values of $\overline{|u|^2}$, $\overline{|v|^2}$, and $\overline{u^*v}$ given that S = (a,b,c,d) are inserted in the expression. The moments of u and v are functions of the channel frequency correlation function R(f), the additive noise spectral density N_0, the transmitted signal energy E, the ratio of the signaling rate to the coherence bandwidth of the channel d, and the shape of the transmitted signal. For convenience in later expressions we define a detector input signal-to-noise ratio as

$$r = \frac{\text{average signal energy per pulse at detector input}}{\text{additive noise spectral density}}$$

We will consider two different frequency correlation functions - the Gaussian-function (G-F) frequency correlation function and the sinc-function (S-F) frequency correlation function.

1. G-F frequency correlation function

   For this case, R(f) is defined by

$$R(f) = 2\sigma_0^2 \exp(-4f^2/B_c^2) \qquad (2\text{-}9)$$

   The corresponding delay spread correlation function is

$$p(\tau) = \sigma_0^2 \sqrt{\pi} B_c \exp[-(\pi B_c \tau/2)^2] \qquad (2\text{-}10)$$

   We therefore have $r = \sigma_0^2 E/N_0$, and it is convenient to define $d = (T_b B_c)^{-1}$. B_c is the channel bandwidth at the e^{-1} points on R(f).

We shall call this the coherence bandwidth of the G-F channel.

2. S-F frequency correlation function

In this case we have

$$R(f) = 2R_0T_m \operatorname{sinc}(2fT_m) \tag{2-11}$$

where $\operatorname{sinc}(x) = \sin(\pi x)/(\pi x)$.

Therefore $r = \frac{R_0T_mE}{N_0}$, and it is convenient to define $d = T_m/T_b$. $\frac{2}{T_m}$ is the channel bandwidth at the first zeros of R(f). We shall call this the coherence bandwidth of the S-F channel. The sinc-function frequency correlation function was suggested by Sunde (6) who showed it to be the frequency correlation function associated with a simplified model of a radio scatter channel.

In this work, two pulse shapes will be considered for the signal s(t). These are the square pulse signal and the raised cosine spectrum signal.

1. Square Pulse Signal

The square pulse signal is specified by the equation

$$s(t) = \begin{cases} \sqrt{\frac{2E}{T_b}} & , 0 < t < T_b \\ 0 & , \text{otherwise} \end{cases} \tag{2-12}$$

2. Raised Cosine Signal

The raised cosine signal obtains its name from the fact that the spectrum of its pulse transfer characteristic has the shape of a raised or "offset" cosine function, i.e.

$$|S(f)|^2 = \begin{cases} \frac{2E}{B}\cos^2(\pi f/2B) & , \ |f| < B \\ 0 & , \ \text{otherwise} \end{cases} \tag{2-13}$$

The time domain expression for this signal is given by

$$s(t) = \sqrt{2BE}\ [\text{sinc}(2Bt - \tfrac{1}{2}) + \text{sinc}(2Bt - 3/2)] \tag{2-14}$$

2.2 Error Probabilities for G-F Channel, Square Pulse Signaling

For the G-F channel with square pulse signaling, exact expressions for the six required equivalent SNR's are given in Appendix A. In this appendix it is also shown that for small d, say d < .1, the R's can be closely approximated by

$$R_{1111} = 2r$$

$$R_{0110} = \frac{2r(1 - 4c_1 d)}{1 + r(4c_2 d^2)}$$

$$R_{0111} = \frac{2r(1 - 2c_1 d)}{(1 + r)\{1 - 2c_1 g(r) d + 2d^2[c_2 g(r) - c_1^2 g(r)]\} - (1 - 2c_1 d)}$$

$$R'_{0101} = 2r(1 - 8c_1 d + 8c_2 d^2)$$

$$R'_{1100} = R_{0110}$$

$$R'_{0100} = \frac{2r(1 - 6c_1 d + 4c_2 d^2)}{(1+r)\{1-6c_1 g(r)d+2d^2[3c_2 g(r)-c_1^2 g^2(r)]\}-r(1-6c_1 d+4c_2 d^2)} \qquad (2\text{-}15)$$

where

$$c_1 = 1/\pi\sqrt{\pi}\ ,\ c_2 = 1/\pi^2,\ \text{and}\ g(r) = r/(1 + r).$$

All of these expressions except the one for R_{1111} are in disagreement with those of Bello and Nelin. The effect that their errors have on the resulting error probability is shown in Appendix A.

It is important to note that for each of the R's above we have

$$\lim_{d\to 0} R = 2r, \text{ giving } \quad \lim_{d\to 0} P_e = [2(1+r)]^{-1}$$

which agrees with the well known expression for DPSK signaling through a flat Rayleigh fading channel.

When we examine the limits of the six conditional probabilities as $r \to \infty$, we have

$$p_{1111} \to 0$$

$$p_{0110} \to \frac{2c_2 d^2}{1 - 4c_1 d + 4c_2 d^2}$$

$$p_{0111} \to \frac{(c_2 - c_1^2)d^2}{1 - 2c_1 d + 2(c_2 - c_1^2)d^2}$$

$$P_{0101} \to 0$$

$$P_{1100} \to \frac{2c_2 d^2}{1 - 4c_1 d + 4c_2 d^2}$$

$$P_{0100} \to \frac{(c_2 - c_1^2) d^2}{1 - 6c_1 d + 2(3c_2 - c_1^2) d^2} \qquad (2\text{-}16)$$

Thus we can write

$$\lim_{r \to \infty} P_e = P_e^i = \frac{d^2}{4} \left[\frac{2c_2}{1-4c_1 d+4c_2 d^2} + (c_2 - c_1^2) \cdot \right. \qquad (2\text{-}17)$$

$$\left. \left(\frac{1}{1-2c_1 d+2(c_2-c_1^2) d^2} + \frac{1}{1-6c_1 d+2(3c_2-c_1^2) d^2} \right) \right]$$

This is the expression for the so-called irreducible error probability in a selective fading system. This is because for a given relative data rate d, the system probability of error cannot be reduced below this value no matter how much the signal-to-noise ratio is increased. We note that for small d, say d<.05, we can write an asymptotic approximation for P_e^i as

$$P_e^i = \frac{d^2}{4} [2c_2 + 2(c_2 - c_1^2)] = d^2 \left(\frac{1}{\pi^2} - \frac{1}{2\pi^3} \right) = 0.085 d^2 \qquad (2\text{-}18)$$

which indicates that P_e^i decreases as d^2 as $d \to 0$.

Figure 5 is a plot of the system probability of error for this case wherein curves are given indicating P_e as a

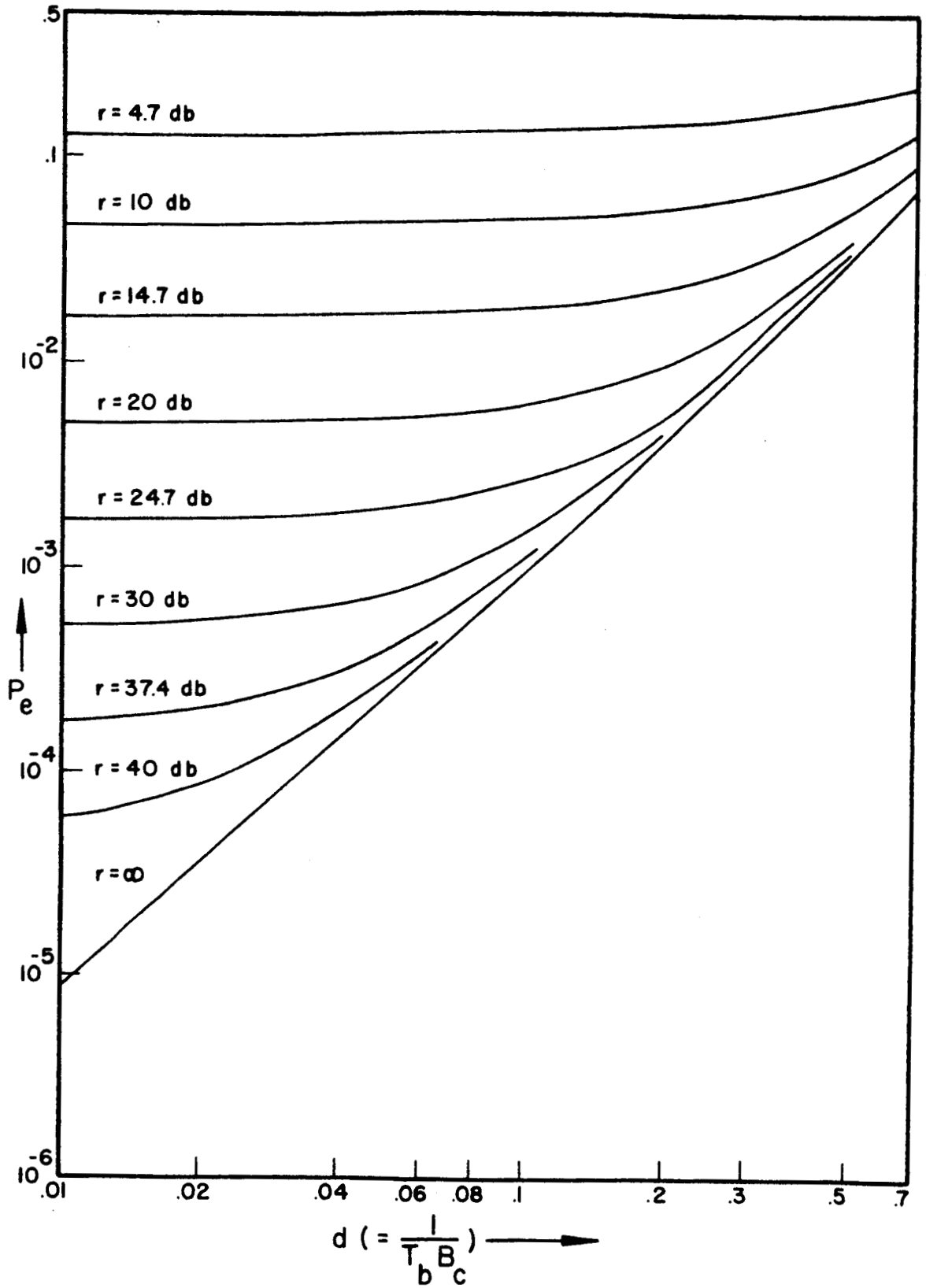

Figure 5. Error Probabilities for G-F Channel, Square Pulse Signaling.

function of the data rate d for fixed values of r. Notice that holding r fixed implies that the energy E per transmitted bit is being held constant while the data rate is being varied. This accounts for horizontal asymptotes on the left which are the values of P_e for flat nonselective fading. The line labeled $r = \infty$ shows $P_e{}^i$.

2.3 Error Probabilities for the S-F Channel, Square Pulse Signaling

For the S-F channel with square pulse signaling, exact expressions for the six required equivalent SNR's are given in Appendix B. In this appendix, it is also shown that for small d, say d<.1, the R's can be closely approximated by

$$R_{1111} = 2r$$

$$R_{0110} = \frac{2r(1 - 4c_3 d)}{1 + r(4c_4 d^2)}$$

$$R_{0111} = \frac{2r(1 - 2c_3 d)}{(1 + r)\{1 + 2c_3 g(r) d + 2d^2[c_4 g(r) - c_3{}^2 g^2(r)]\} - r(1 - 2c_3 d)}$$

$$R'_{0101} = 2r(1 - 8c_3 d + 8c_4 d^2)$$

$$R'_{1100} = R_{0110}$$

$$R'_{0100} = \frac{2r(1 - 6c_3 d + 4c_4 d^2)}{(1+r)\{1 - 6c_3 g(r) d + 2d^2[3c_4 g(r) - c_3{}^2 g^2(r)]\} - r(1 - 6c_3 d + 4c_4 d^2)}$$

(2-19)

where

$$c_3 = 1/4$$

$$c_4 = 1/6$$

We again note that each of the R's above approaches 2r as a limit when d→0, giving $\lim_{d\to 0} P_e = [2(1 + r)]^{-1}$, the flat fading result.

Examining the limits of the six conditional probabilities as r→∞, we have

$$\begin{aligned}
p_{1111} &\to 0 \\
p_{0110} &\to \frac{d^2/3}{1 - d + 2d^2/3} \\
p_{0111} &\to \frac{5d^2/24}{1 - d/2 + 5d^2/24} \\
p_{0101} &\to 0 \\
p_{1100} &\to \frac{d^2/3}{1 - d + 2d^2/3} \\
p_{0100} &\to \frac{5d^2/48}{1 - 3d/2 + 7d^2/8}
\end{aligned} \tag{2-20}$$

Thus the irreducible probability of error is

$$P_e^{\,i} = \frac{d^2}{4}\left[\frac{1/3}{1-d+2d^2/3} + \frac{5}{48}\left(\frac{1}{1-d/2+5d^2/24} + \frac{1}{1-3d/2+7d^2/8}\right)\right] \tag{2-21}$$

As before, for small d, say d<.05, we can write

$$P_e{}^i = \frac{d^2}{4}\left(\frac{1}{3} + \frac{10}{48}\right) = .135d^2 \qquad (2\text{-}22)$$

and we again see that $P_e{}^i$ decreases as d^2 as $d \to 0$.

Figure 6 is a plot of the system probability of error for this case wherein curves are given indicating P_e as a function of d for fixed values of P_{ave}, the average power (on a one-ohm basis) dissipated at the output of the transmitter. This type of curve is shown to indicate the differences in the performance curves which occur when a restriction which may be physically more meaningful is imposed. Here we consider that many communication transmitters are designed with a fixed average transmitted power rather than a fixed energy per transmitted bit. In this curve, we see that the asymptotes on the left are now sloping. This is due to the fact that as the data rate is increased while average transmitted power is held constant, the energy per transmitted bit decreases, causing the error probability to increase. The asymptote to the right (the line of irreducible probability of error) is the same line that would appear in a graph of P_e with r held fixed. This is because $P_e{}^i$ is only a function of d and not of r or P_{ave}.[1] It is interesting to note from this graph that for finite average

---

[1] Recall that $P_e{}^i = \lim_{r \to \infty} P_e = \lim_{P_{ave} \to \infty} P_e$

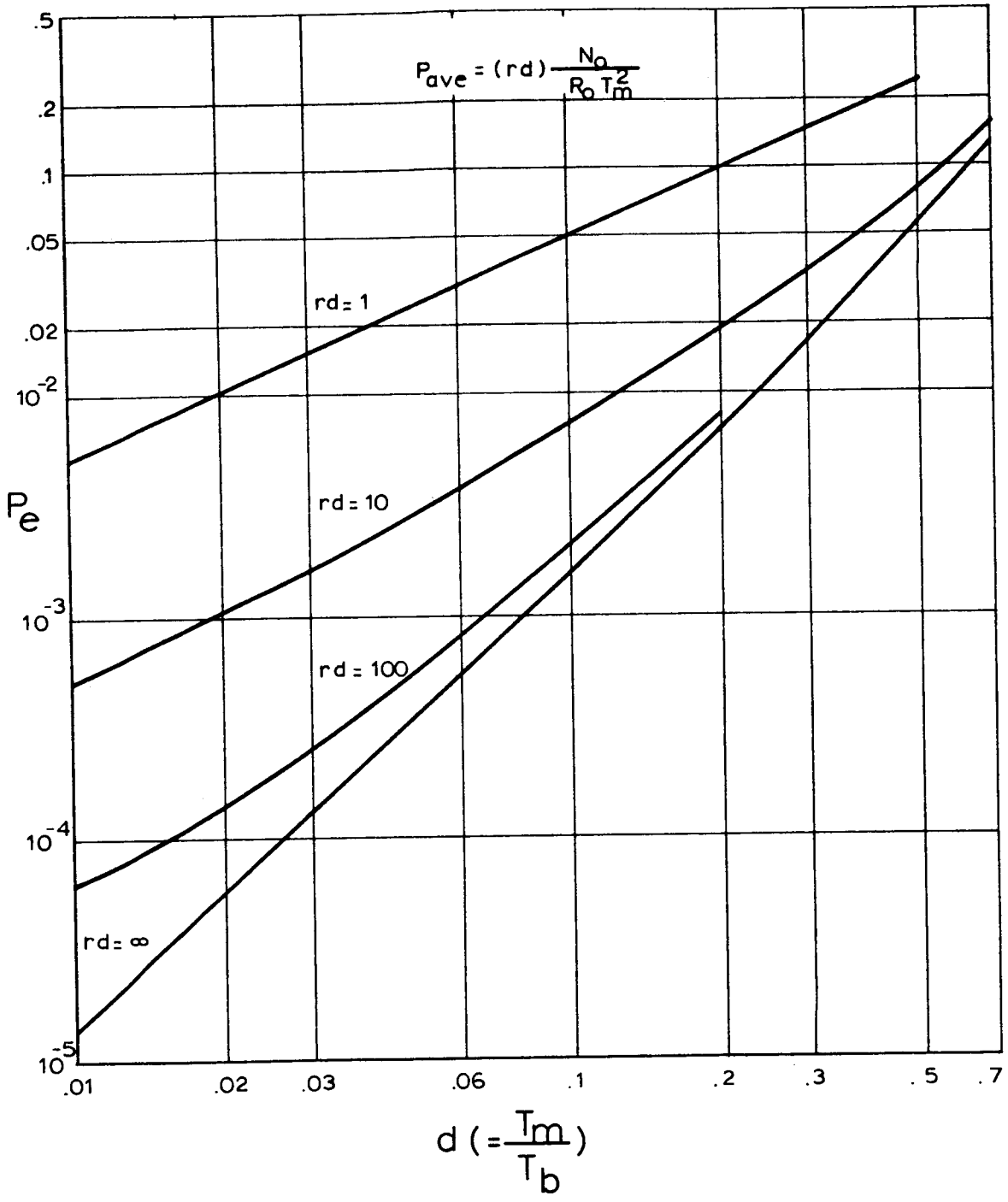

Figure 6. Error Probabilities for S-F Channel, Square Pulse Signaling.

SNR's, the mechanism of a frequency selective fading channel yields an error probability which is proportional to d for small d and which is proportional to d^2 for large d.

In order to plot a curve of the type shown in Figure 5, we compute the average transmitted power as follows. By definition

$$P_{ave} = E/T_b$$

$$r = 2\sigma_0^2 E/N_0$$

$$d = \frac{1}{T_b B_c}$$

Thus

$$P_{ave} = \frac{rN_0}{2\sigma_0^2 T_b} = (rd)\,\frac{N_0 B_c}{2\sigma_0^2}$$

Now N_0, B_c, and σ_0^2 are all constants associated with the channel and are assumed to be fixed. Thus P_{ave} is fixed if the product rd is held constant. Therefore, in order to prepare one curve of the type of Figure 6 from a graph like Figure 5, the value of rd is first determined and then the points on Figure 5 are found whose r and d correspond to the desired value of d and fixed value of rd. The values of P_e which are read are then plotted versus d on the new graph.

2.4 Error Probabilities for S-F Channel, Raised Cosine Signaling

For the S-F channel with raised cosine signaling, the computations required to evaluate the required signal-to-noise ratios become much more formidable than for the two cases discussed above. For this reason it is impossible to write reasonably compact expressions for the required R's. We will therefore write the moments of u and v, realizing that these are used with Equation (2-8) to yield the R's. It is convenient to make the following definitions:

$$m_{11}^{abcd} \equiv \overline{|u|^2} \text{ given } S = (a,b,c,d)$$

$$m_{00}^{abcd} \equiv \overline{|v|^2} \text{ given } S = (a,b,c,d) \qquad (2\text{-}24)$$

$$m_{10}^{abcd} \equiv \overline{u^* v} \text{ given } S = (a,b,c,d)$$

$$\begin{aligned} s_1 &= 2a - 1 \\ s_2 &= 2b - 1 \\ s_3 &= 2c - 1 \\ s_4 &= 2d - 1 \end{aligned} \qquad (2\text{-}25)$$

It is shown in Appendix C that

$$m_{rs}^{abcd} = \frac{8R_0E^2}{B} \sum_{i=1}^{4} \sum_{k=1}^{4} s_i s_k \sum_{j=-1}^{1} \sum_{n=-1}^{1} (1 - \tfrac{1}{2}|j|)(1 - \tfrac{1}{2}|n|) \cdot$$

$$\cdot K[j-2(3-i-r),\ n-2(3-k-s),\ 2d] + 32EN_0\delta_{rs} \qquad (2\text{-}26)$$

where

$$K(p,q,M) \equiv \int_{-M}^{M} \text{sinc}(x + p)\ \text{sinc}(x + q)dx \qquad (2\text{-}27)$$

The evaluation of K(p,q,M) in terms of the sine and cosine integrals Si(x) and Cin(x) is given in Appendix C.

In order to examine the behavior of $P_e^{\,i}$ for this case, we must resort to examination of the graphical results obtained from numerical evaluation of the above expressions. Figure 8, which will be discussed in detail in the next section, contains these graphical results. It shows that for this case, as with the previous two cases, $P_e^{\,i}$ is proportional to d^2 as $d \to 0$. From the graph, we find that the proportionality factor is .047, allowing us to write

$$P_e^{\,i} = .047d^2 \qquad (2\text{-}28)$$

for small d.

Figure 7 is a plot of the error probabilities computed from combining equations (2-26) and (2-27) with (2-4) - (2-8). In this plot, values of P_e are plotted versus r for fixed values of relative data rate d. The effect of the irreducible probability of error can be seen in the horizontal asymptotes on the right. These asymptotes show that increasing r indefinitely results only in reducing P_e to a non-zero value which depends on the relative data rate. The asymptote on the left represents the error probability for the flat

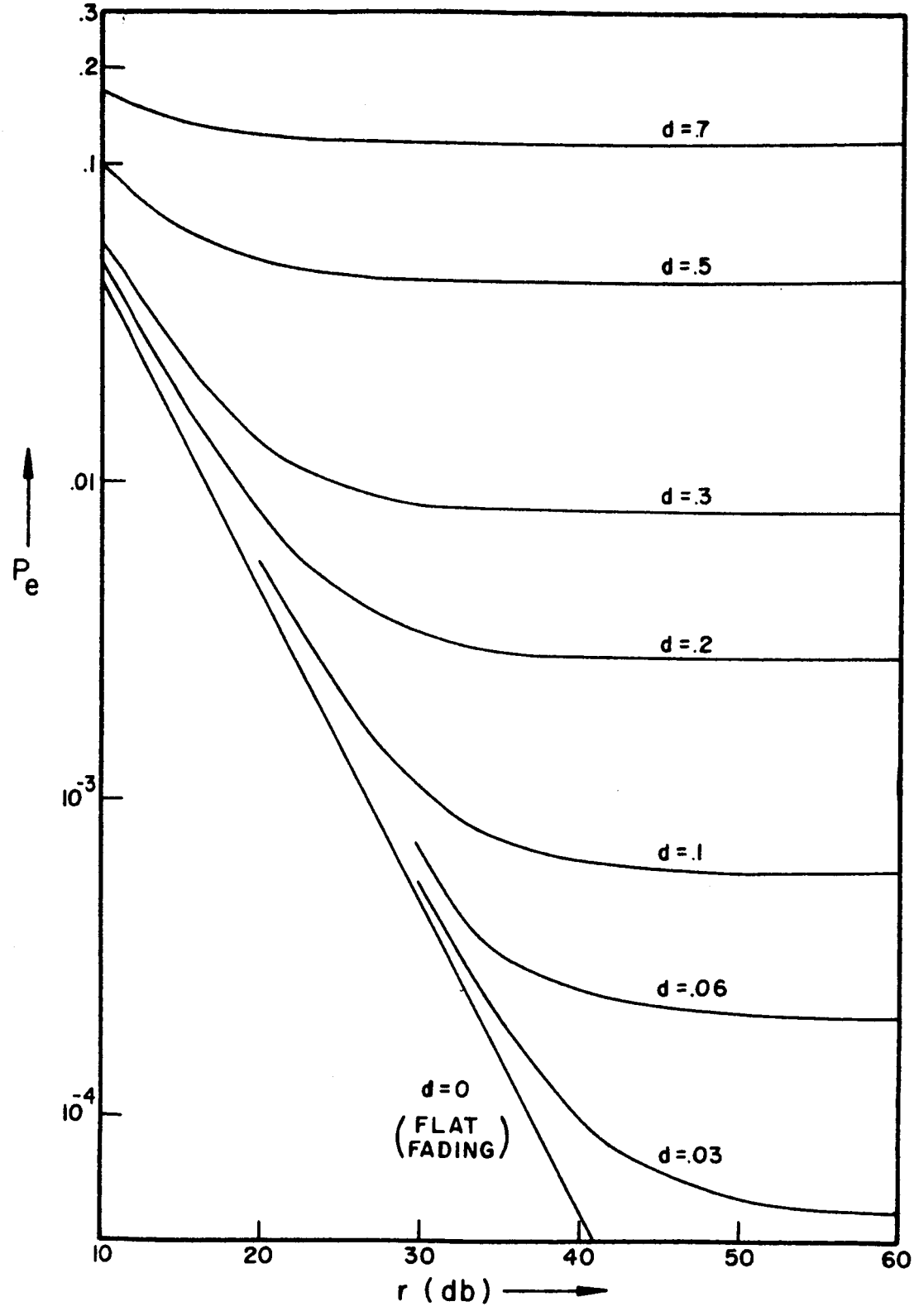

Figure 7. Error Probabilities for S-F Channel, Raised Cosine Signaling.

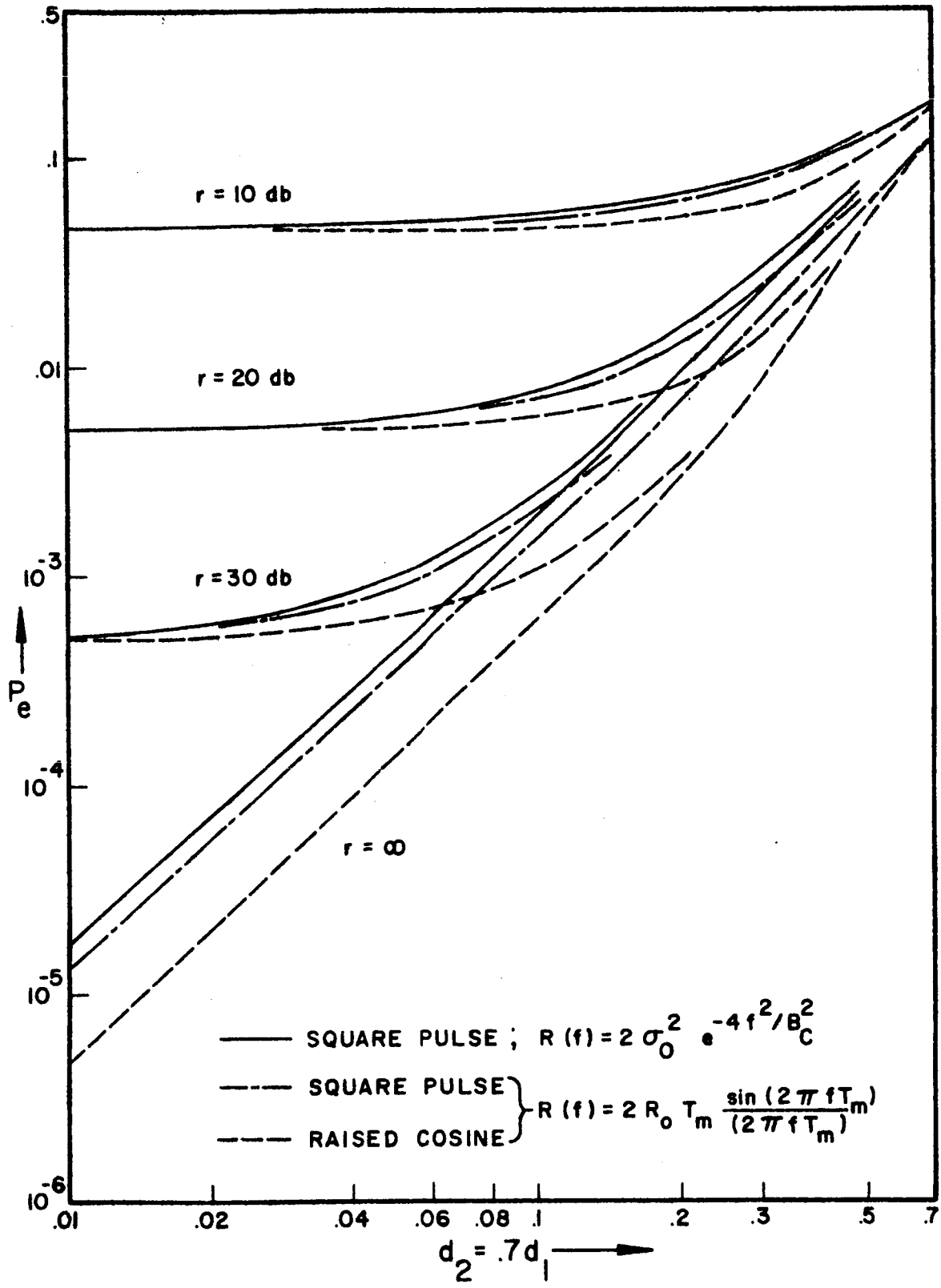

Figure 8. Comparison of Error Probabilities - Curves of Constant SNR.

Rayleigh fading case. This is also the d=0 curve since all our P_e expressions approach the flat Rayleigh fading expression as d→0. This flat fading asymptote shows that for low average SNR's the error probability is controlled by the effects of the additive noise and the variable received signal amplitude, while the distortion and intersymbol interference effects are negligible. The horizontal asymptotes indicate that even if the additive noise and variation in received signal amplitude are removed, distortion and intersymbol interference will still cause errors to occur.

2.5 Comparison of Results

In this section graphs are presented which compare the results of each of the above three sections. These three comparisons are made in the three graphical forms which were presented in those sections, namely

1. curves of P_e versus d with average SNR held constant,
2. curves of P_e versus d with average transmitted power held constant, and
3. P_e versus SNR with relative data rate, d, held constant.

Before any comparison can be made between digital communication systems operating over different selective fading channels, the question must be asked: "How can the relative data rates for each system be defined in an equivalent manner?" The motivation for asking this question can be seen by considering the two channel models investigated above.

For the G-F channel we defined the relative data rate, say d_1, as

$$d_1 = \frac{1}{B_c T_b} \tag{2-29}$$

That is, it is the ratio of the nominal signaling bandwidth $1/T_b$ to the coherence bandwidth of the channel. For the S-F channel we defined the relative data rate, say d_2, as

$$d_2 = \frac{T_m}{T_b} \tag{2-30}$$

This can be interpreted as the ratio of the nominal signaling bandwidth $1/T_b$ to one-half the coherence bandwidth of the channel, $2/T_m$. Furthermore, it should be noted that for the G-F channel, the coherence bandwidth B_c was defined as the distance between e^{-1} points on the frequency correlation function of the channel, while for the S-F channel the coherence bandwidth was defined as the distance between the first zeros of the frequency correlation function. This means that d_1 and d_2 do not really represent equivalent measures of data rate in the two different channels.

The above suggests that in order to compare digital systems operating over frequency selective channels, one must

a. choose an equivalent definition of signaling bandwidth for each system ($1/T_b$ in each case for the systems considered here),

b. choose an equivalent definition of coherence bandwidth for each channel, and

c. use the same definition of relative data rate for each system.

In this work we have defined relative data rate to be proportional to the ratio of signaling bandwidth to coherence bandwidth in each case. Therefore, we are left with the problem of deciding on a meaningful definition of coherence bandwidth and applying it to the two channels under investigation.

At least four definitions of coherence bandwidth are possible. These are:

1. "RMS" Coherence Bandwidth

$$B^{(1)} = 2\left[\frac{\int_{-\infty}^{\infty} f^2 R(f)\,df}{\int_{-\infty}^{\infty} R(f)\,df}\right]^{\frac{1}{2}} \qquad (2\text{-}31)$$

This definition of coherence bandwidth was suggested by Bello (25), who also suggested some practical techniques for measuring it.

2. "Equivalent" Coherence Bandwidth

This definition is suggested by the equivalent noise bandwidth definition which is used in analysis of linear systems. We have

$$B^{(2)} = \frac{1}{R(0)} \int_{-\infty}^{\infty} R(f)\,df \qquad (2\text{-}32)$$

3. "e^{-1}" Coherence Bandwidth

   Here we define the coherence bandwidth of the channel as the difference between the two frequencies f_1 and f_2 which satisfy $R(f_1) = R(f_2) = R(0)e^{-1}$. Thus

$$B^{(3)} = f_2 - f_1$$

4. Reciprocal Delay Spread Coherence Bandwidth

   Here we define the coherence bandwidth as the reciprocal of the normalized rms width of the delay spread correlation function. The rms width of the delay spread correlation function is given by

$$\tau_0 = \frac{2\int_{-\infty}^{\infty} \tau^2 p(\tau)d\tau}{\int_{-\infty}^{\infty} p(\tau)d\tau} \qquad (2\text{-}33)$$

   The coherence bandwidth is then defined by

$$B^{(4)} = \frac{1}{\tau_0} \qquad (2\text{-}34)$$

It can be shown that τ_0^2 is proportional to the spread of the density function associated with the second derivative of the phase response function of the channel transfer function H(f). This means that it is related to the average strength of the linear delay distortion being introduced by the channel. Equating $B^{(4)}$ for two different channels is the

equivalent to equating the average strengths of the linear delay distortion being introduced by the channels. This method of equating the coherence bandwidths of random channels was suggested by Sunde (6, page 208).

Unfortunately, coherence bandwidth $B^{(1)}$ does not exist for the S-F channel. We can, however, use the other three bandwidth definitions to provide a normalization between the relative data rates of the systems we are considering.

Applying definition 2, we find for the G-F channel:[1]

$$B_1^{(2)} = \frac{1}{2\sigma_0^2} \int_{-\infty}^{\infty} 2\sigma_0^2 \exp(-4f^2/B_c^2)\,df = B_c\sqrt{\pi}/2$$

For the S-F channel, we obtian

$$B_2^{(2)} = \frac{1}{2R_0T_m} \int_{-\infty}^{\infty} 2R_0T_m \operatorname{sinc}(2fT_m)\,df = \frac{1}{2T_m} \qquad (2\text{-}35)$$

Equating these two bandwidths, we obtain

$$B_c = \frac{1}{\sqrt{\pi}T_m} \qquad (2\text{-}36)$$

and

$$d_2 = T_m/T_b = d_1/\sqrt{\pi} = .565d_1 \qquad (2\text{-}37)$$

---

[1] Throughout this section bracketed superscripts correspond to the various coherence bandwidth definitions while subscripts correspond to the specific frequency correlation functions being investigated, e.g., $B_1^{(2)}$ is the bandwidth defined by definition 2 for the G-F channel correlation function.

Applying definition 3, the coherence bandwidth for the G-F channel is

$$B_1^{(3)} = B_c,$$

while for the S-F channel, we obtain

$$B_2^{(3)} = \frac{.7}{T_m}$$

Equating these two bandwidths, we obtain

$$B_c = \frac{.7}{T_m} \tag{2-38}$$

and

$$d_2 = .7d_1 \tag{2-39}$$

Applying definition 4, we find for the G-F channel:

$$B_1^{(4)} = \left[\frac{\int_{-\infty}^{\infty} \tau^2 (\sqrt{\pi} B_c \sigma_0^2) \exp[-(\pi B_c \tau/2)^2] d\tau}{\int_{-\infty}^{\infty} (\sqrt{\pi} B_c \sigma_0^2) \exp[-(\pi B_c \tau/2)^2] d\tau} \right]^{-\frac{1}{2}}$$

$$= \left(\frac{2}{\pi^2 B_c^2} \right)^{-\frac{1}{2}} = \frac{\pi}{\sqrt{2}} B_c$$

For the S-F channel, we obtain

$$B_2^{(4)} = \left[\frac{\int_{-T_m}^{T_m} R_0 \tau^2 d\tau}{\int_{-T_m}^{T_m} R_0 d\tau} \right]^{-\frac{1}{2}} = \tfrac{1}{2}(T_m^2/3)^{-\frac{1}{2}} = \frac{\sqrt{3}}{2T_m}$$

Equating these two bandwidths, we find

$$B_c = \frac{\sqrt{6}}{\pi T_m} \tag{2-40}$$

and

$$d_2 = \frac{\sqrt{6}}{\pi} d_1 = .78 d_1 \tag{2-41}$$

We note that definitions 3 and 4 result in ratios of d_1 to d_2 which are fairly close to each other. Definition 2 gives a result somewhat different from the other two. A possible explanation for this difference is that definition 2 is based on the area under the curve of R(f). For the S-F channel, R(f) becomes negative for some values of f, and these regions subtract from the total contribution to $B_2^{(2)}$. Thus, the different ratio of d_2 to d_1 which we find in this case can be linked to a basic deficiency of the bandwidth definition used. It appears that in such cases modifying definition 2 to $B^{(2)} = \frac{1}{R(0)} \int_{-\infty}^{\infty} |R(f)| df$ would be advisable, but for the S-F channel, this bandwidth does not exist. Since definitions 3 and 4 resulted in nearly the same ratio of d_2 to d_1 while definition 2 appears to give somewhat unreliable results in this case, a ratio of d_2 to d_1 of .7 was

chosen for the graphical comparisons of Figures 8, 9, and 10. These graphs are all plotted with d_2 as the indicated parameter.

In Figure 8 the three systems which have been investigated are compared with curves of P_e versus d_2 with average SNR held constant. The most important fact which this graph points out is that for a given relative data rate the irreducible error probability is different for each system. We note that raised cosine signaling in the S-F channel results in the lowest P_e^i, with square pulse signaling in the S-F channel and square pulse signaling in the G-F channel providing respectively poorer performance. This difference in performance of the systems leads us to two conclusions. First, it appears that for a given random channel, a bandlimited signal or a signal whose spectral energy is heavily concentrated near the center frequency is preferable to a signal whose spectrum has tails which fall off slowly. Second, for a given waveform, it appears that the differences which result from the use of channels with different frequency correlation functions is relatively small. From the figure we see that the change in performance which results from changing signals with the S-F channel is much greater than that resulting from changing channels with square pulse signaling. This fact is encouraging for designers of systems similar to the one under consideration here. It indicates that if one designs a system using the assumption that the channel to be used possesses a specified frequency correlation function, then even if the

Figure 9. Comparison of Error Probabilities - Curves of Constant Power.

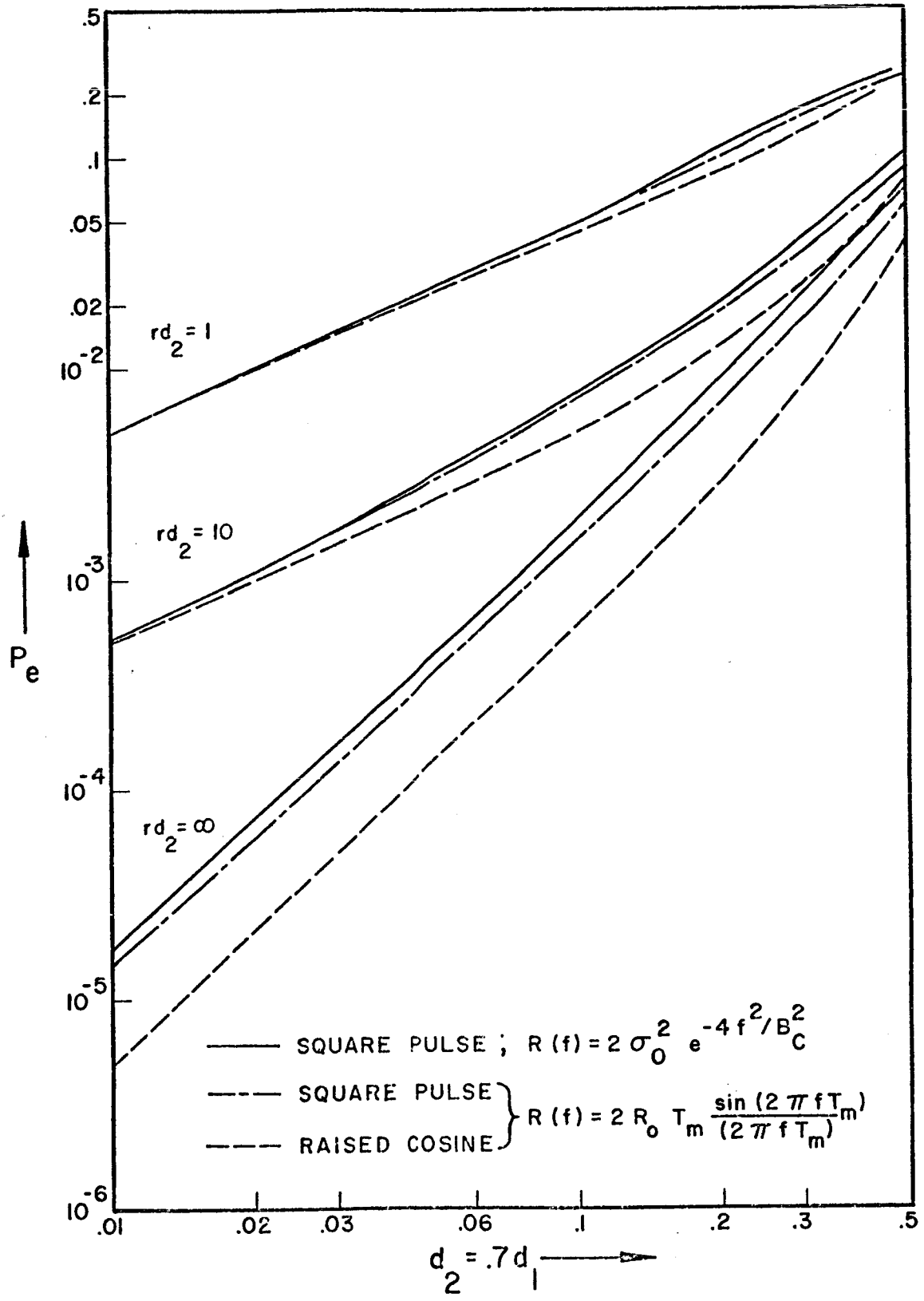
.5
.2
.1
.05
.02
10^{-2}
10^{-3}
10^{-4}
10^{-5}
10^{-6}
P_e
$rd_2 = 1$
$rd_2 = 10$
$rd_2 = \infty$
SQUARE PULSE ; $R(f) = 2\sigma_0^2 e^{-4f^2/B_C^2}$
SQUARE PULSE
RAISED COSINE
$R(f) = 2R_o T_m \frac{\sin(2\pi f T_m)}{(2\pi f T_m)}$
.01
.02
.03
.06
.1
.2
.3
.5
$d_2 = .7d_1$

Figure 9

given correlation does not exactly correspond to that of the channel, the predicted performance of the designed system will probably not differ significantly from the actual performance it realizes. For instance, if one can show that a certain signal shape is the optimum one to use in a given fading channel, then it could well result in nearly optimum performance for a wide variety of channels.

Other facts which can be observed in Figure 8 are that P_e^i decreases as d^2 for small values of d for each of the three systems and that for any finite average SNR, the error probability approaches the same value for each system as d becomes small.

In Figure 9 curves of P_e versus d with average transmitted power held constant are shown for each of the systems investigated. In this graph, we again note the difference in irreducible error probability for the three cases, as well as the fact that this probability decreases as d^2 for small d. We again see that for finite average SNR, the error probability approaches an asymptote as d becomes small. In this case, however, the asymptote is proportional to d.

In Figure 10, curves of P_e versus average SNR for fixed d are shown for each of the three cases. In this graph we see that each system approaches the performance of a flat-fading, Gaussian noise system for low average SNR. The difference in irreducible error probabilities for the three systems can be seen in these curves also for specific values of d.

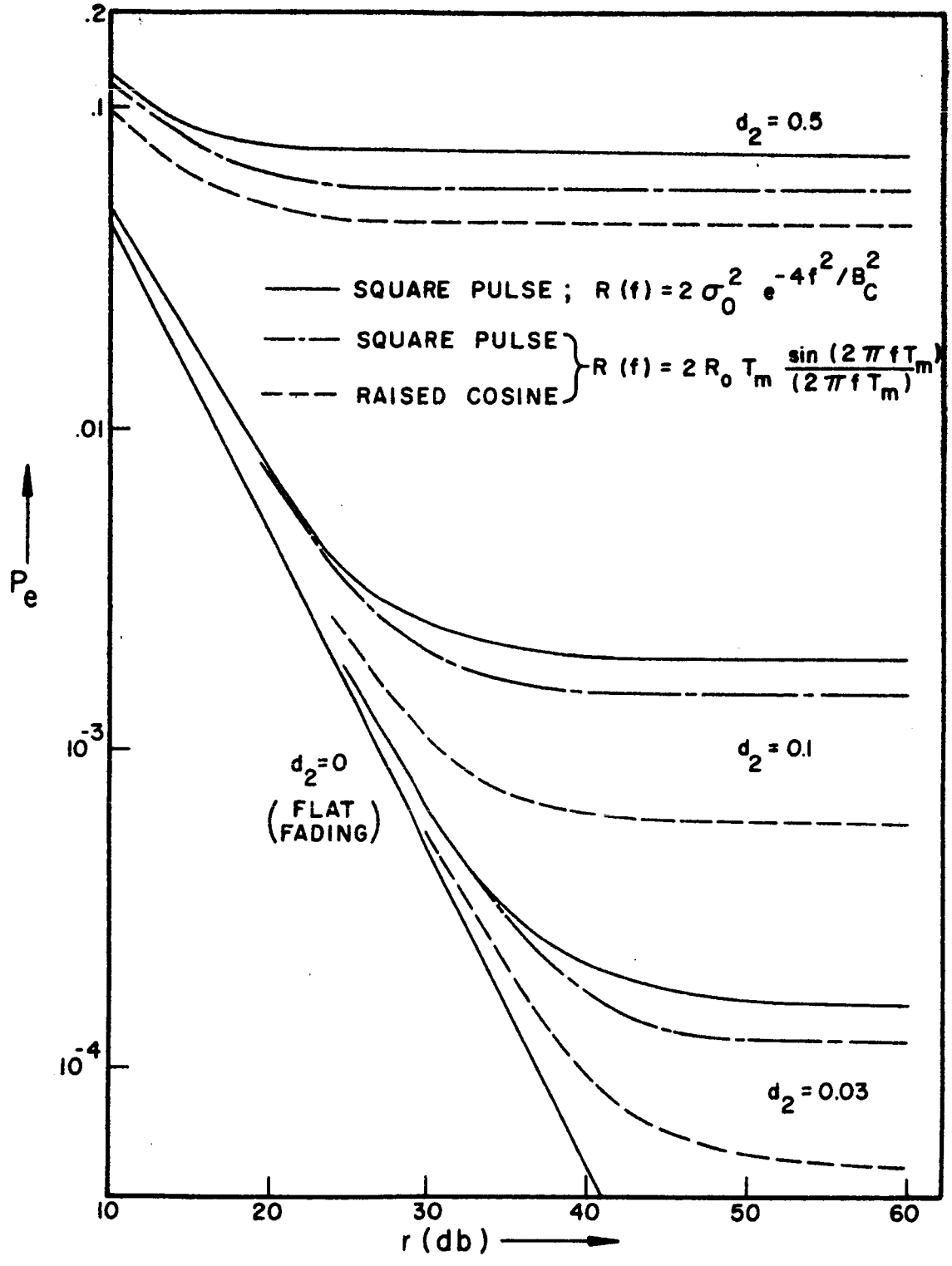

Figure 10. Comparison of Error Probabilities - Curves of Constant Relative Data Rate.

2.6 Summary

In this chapter we have shown that it is possible, although somewhat tedious, to compute error probabilities for matched-filter communication systems employing Gaussian fading channels by using the techniques of Bello and Nelin. These calculations verify that:

1. For very low data rates, the system performance approaches that of a flat Rayleigh fading system.
2. An irreducible error probability exists in such systems in the sense that the error probability cannot be reduced by increasing the average SNR.
3. The irreducible error probability always decreases as d^2 for small values of d.

Comparisons made between the three cases investigated show that:

1. A bandlimited or compact signal spectrum should be preferable to one whose spectrum is "spread out" when using a random channel communication system near its irreducible error probability.
2. The system's performance is not as sensitive to the shape of the channel frequency correlation function as it is to the shape of the transmitted signal.

The results of this chapter gives us some insight into the nature of the performance of some random channel communication systems. In the next chapter, a technique for approximating these error probabilities will be examined. With the results of this chapter, it will be possible to make a quantitative comparison between the approximate and exact system error rates. Furthermore, we will use these results in Chapter IV to check the computer simulation program for selective fading communication systems which was developed for this work. Finally, in Chapter V the error rates found herein will be compared with the performance of a proposed adaptive scheme to reduce the effects of distortion and intersymbol interference due to frequency selective fading.

CHAPTER III: THE SUNDE APPROXIMATION TO ERROR PROBABILITY

3.1 Introduction

In this chapter, we review a method of approximating the error probability of a communication system subject to frequency selective fading. This method was first employed by Sunde (6), and involves the approximation of the channel's phase response function by a truncated Taylor's series. After a brief explanation of the approximation, it is applied to the specific examples which were investigated in Chapter II, namely the G-F channel with square pulse signaling, the S-F channel with square pulse signaling, and the S-F channel with raised cosine signaling. For these three cases, the irreducible probability of error as computed from the Sunde approximation and the irreducible error probability as computed in Chapter II are compared. It is shown that the Sunde expression compares poorly to the exact results in several respects, and that it does not provide a good estimate of the error probability when the frequency selective fading is of importance.

3.2 The Sunde Approximation Method

The Sunde approximation to error probability is based on considering the channel filter effects on a transmitted signal as being divided into two parts - those due to the amplitude

and phase response functions respectively. Mathematically, these are defined by

$$H(f) = M(f)\ \exp[jG(f)]$$

or

$$\begin{aligned} M(f) &= |H(f)| \\ G(f) &= \tan^{-1}\{\mathrm{Im}[H(f)]/\mathrm{Re}[H(f)]\} \end{aligned} \tag{3-1}$$

Here M(f) is the amplitude response function and G(f) is the phase response function associated with H(f). We note that since H(f) is a sample function from a complex random process, M(f) and G(f) are sample functions from real random processes. Therefore, they have associated density functions, correlation functions, etc. Sunde assumes that we can write Taylor's series expansions for M(f) and G(f) as follows:

$$M(f) = m_0 + m_1 f + \frac{m_2}{2!} f^2 + \ldots$$

$$G(f) = g_0 + g_1 f + \frac{g_2}{2!} f^2 + \ldots$$

where

$$\begin{aligned} m_i &= \frac{d^i}{df^i} M(f)\Big|_{f=0} \\ g_i &= \frac{d^i}{df^i} G(f)\Big|_{f=0} \end{aligned} \tag{3-2}$$

Now for values of f near to zero,[1] it should be permissible to truncate these series and write

$$M(f) = m_0 + m_1 f \tag{3-3}$$

$$G(f) = g_0 + g_1 f + \frac{g_2}{2!} f^2 \tag{3-4}$$

Here we have retained in each series the first term which can be related to distortion introduced on the transmitted signal. That is, we retain the term involving m_1 since an amplitude response function which varies linearly with frequency will introduce distortion in a pulse transmitted through the system. In the phase response function the term involving g_1 introduces a delay into the received pulse but does not distort the shape of the received waveform. However, the quadratic function in f, the series term involving g_2, does result in distortion of the transmitted pulse, so this term is retained in the approximation. Distortion caused by a quadratic phase response function is called linear delay distortion, since this corresponds to an envelope delay function which varies linearly with frequency. We will therefore call the Taylor's series term involving g_2 the linear delay distortion term.

Because H(f) has been assumed to be a sample function from a Gaussian random process, the probability distributions associated with the random variables m_1 and g_2 can be determined. Based on these statistics and a study of the effects

---

[1]Here the term "near to" implies that f is small with respect to the coherence bandwidth of the channel.

of the values of m_1 and g_2 on raised cosine pulse distortion, Sunde (6, page 174) concluded that the effects of linear amplitude distortion (i.e., the value of m_1) were negligible when compared to the effects of linear delay distortion (the value of g_2). An experiment which will be described in Section 4.4 of this report has demonstrated the validity of this conclusion. Thus, assuming the term involving g_1 has negligible effect on the system, we should be able to study the behavior of a small-bandwidth system by studying the properties of the linear delay distortion parameter associated with the random channel filter. Specifically, we can attempt to find a value of g_2, say $\hat{g}_2$, with the property that for $|g_2| > \hat{g}_2$ pulse distortion will be so bad that some detection errors will result even in the absence of noise. With $\hat{g}_2$ specified and with the distribution function of g_2 available, we can then associate the channel's effects on the error rate of the system with the function $Pr[|g_2| > \hat{g}_2]$. In particular, using an argument concerning the polarity combinations of the adjacent bits, Sunde (6, page 179) concluded that the error probability is $\frac{1}{4}$ when $|g_2| > \hat{g}_2$. Thus, the approximation to the system probability of error in the absence of noise is

$$P_e^{\,i} = \tfrac{1}{4} Pr[|g_2| > \hat{g}_2]. \qquad (3\text{-}5)$$

In order to take into acocunt the effect of additive noise in the system, Sunde assumed that for small error probabilities (that is, small $P_e^{\,i}$ and high average SNR), one can write

$$P_e(r,d) = P_e^{f}(r) + P_e^{i}(d). \qquad (3\text{-}6)$$

where P_e^{f} is the flat-fading error probability which is dependent only on the average signal-to-additive-noise ratio r. P_e^{i}, being the irreducible error probability, is only a function of the relative data rate d. It can be seen that this experession does possess two properties which we know that all such expressions must have. These are

1. $\lim_{r\to\infty} P_e = P_e^{i}(d)$ and

2. $\lim_{d\to 0} P_e = P_e^{f}(r)$.

Sunde (6, page 164) found that for small probabilities, the required probability function of g_2 is given by[1]

$$\Pr[|g_2| \geq \hat{g}_2] = \frac{2\pi\tau_0^2}{\hat{g}_2}\left[1+\ln(1+\hat{g}_2/2\pi^2\tau_0^2)\right] \qquad (3\text{-}7)$$

where τ_0 is the rms delay spread defined by Equation (2-33). This approximation is valid for values of $\hat{g}_2$ which are greater than $100\pi^2\tau_0^2$, that is, when the probability is below .03.

It should be noted that as the signaling bandwidth changes in the transmission system, the value of $\hat{g}_2$ changes proportionally. This is associated with the fact that g_2 is the coefficient of the term in (3-2) which produces a delay

---

[1] Identify $\tau_0^2/4$ with b_2/b_0 in Sunde's Equation (45).

function which varies linearly with frequency. Because of this, if a filter has a constant value of g_2 and the bandwidth of the signal passing through the filter is doubled, then the delay undergone by signal spectrum components at the edge of the signaling band will be doubled. It can be shown that this changing of the delay undergone at each point of the signal spectrum, changes the shape of the received pulse. Thus $\hat{g}_2$ varies with changes in the signaling bandwidth. However, g_2 can be related to a normalized parameter which has the advantage that the pulse shape remains invariant as the signal bandwidth is changed. This parameter, L, is defined by

$$L \equiv D/T_b \tag{3-8}$$

where D is the filter delay at the edge of the signal transmission band and T_b is the baud length associated with the signaling pulse. g_2 can be related to L as follows:

$$g_2 = 2\pi T_b^2 L \tag{3-9}$$

The probability distribution function associated with L can be easily determined from that of g by the use of this equation. Thus for $\hat{L} > 50\pi\tau_0^2/T_b^2$, we have

$$Pr[|L| \geq \hat{L}] = \frac{\tau_0^2}{\hat{L}T_b^2}\left[1+\ln\left(1+\frac{\hat{L}T_b^2}{\pi\tau_0^2}\right)\right] \tag{3-10}$$

In order to write the approximate error probability function in terms of the relative data rate, the value of τ_0^2 must be evaluated for each of the channel models being investigated. From the work of section 2.5, it can be seen that for the G-F channel

$$\tau_0^2 = \frac{8}{\pi^2 B_c^2}$$

while for the S-F channel

$$\tau_0^2 = \frac{4}{3} T_m^2$$

Substituting these values of τ_0^2 into (3-10) and recalling that $d_1 = \frac{1}{T_b B_c}$ and $d_2 = T_m/T_b$, the complete approximate error probability can now be written as

$$P_e(r,d_1) = \frac{1}{2(1+r)} + \frac{1}{4}\left\{\frac{8d_1^2}{\pi^2\hat{L}}\left[1 + \ln\left(1 + \frac{\pi\hat{L}}{8d_1^2}\right)\right]\right\} \qquad (3\text{-}11)$$

for the G-F channel, and

$$P_e(r,d_2) = \frac{1}{2(1+r)} + \frac{1}{4}\left\{\frac{4d_2^2}{3\hat{L}}\left[1 + \ln\left(1 + \frac{3\hat{L}}{4\pi d_2^2}\right)\right]\right\} \qquad (3\text{-}12)$$

for the S-F channel. In the following section, the choice of a value of $\hat{L}$ is discussed and Equations (3-11) and (3-12) are compared with the exact expressions of Chapter II.

3.3 The Sunde Error Probability Approximation for DPSK

In order to determine precisely the value of $\hat{L}$ required for Equations (3-11) and (3-12), and also to investigate the validity of some of the assumptions made in the development of the Sunde approximation, a computer simulation program of an idealized communication system was developed. The system simulated is identical to the one we have been concerned with in this work (see Figure 3) except that the channel filter is replaced by a time-invariant filter which exhibits only linear delay distortion. That is, the channel transfer function is given by

$$H(f) = \exp(jg_2 f^2/2)$$
$$= \exp(j\pi T_b^2 L f^2)$$

where L is the normalized linear delay distortion parameter defined above. We still allow additive white Gaussian noise to remain, so there are now two constants which completely specify the channel - the normalized linear delay distortion parameter L and the additive noise spectral density N_0. The digital computer program was used to determine the system probability of error as a function of the two system parameters L and r, the average SNR. The program was written to take into account any intersymbol interference contributed from pulses up to two bauds removed from the pulses being detected [i.e., all possible combinations of the six-element modulation sequence $S' = (b_{-2}, b_{-1}, b_0, b_1, b_2, b_3)$ were

considered]. Details of the computer program are given in Appendix D.

The results of the computer calculations are shown in Figures 11, 12, and 13. Figures 11 and 12 show results for the raised cosine spectrum, while Figure 13 is for the square pulse signaling case. The same results are shown in both Figures 11 and 12, but they are plotted in different forms. In Figure 11, curves are given for error probability versus SNR with the normalized linear delay distortion parameter L being held constant. Figure 12 shows the error probability for the same system, but plotted versus L for fixed values of the average SNR. Figure 13 shows the results for the square pulse signal plotted in the same manner as Figure 12.

Several interesting facts can be seen from these graphs. In Figure 11, the curve labeled L = 0 is the well-known exponential curve of error probability for a DPSK system in additive white noise (no fading). To the right of this are curves indicating the degradation resulting from addition of various amounts of linear delay distortion. For example, we can determine the penalty in increased SNR required to maintain a given error probability by drawing a horizontal line corresponding to the desired P_e on this graph. The intersections of this line with the curves shown will indicate the SNR's required to maintain the desired P_e for various amounts of linear delay distortion. These curves show that degradation due to linear delay distortion does not occur uniformly. Almost no degradation occurs from L = 0 to L = 1, while over

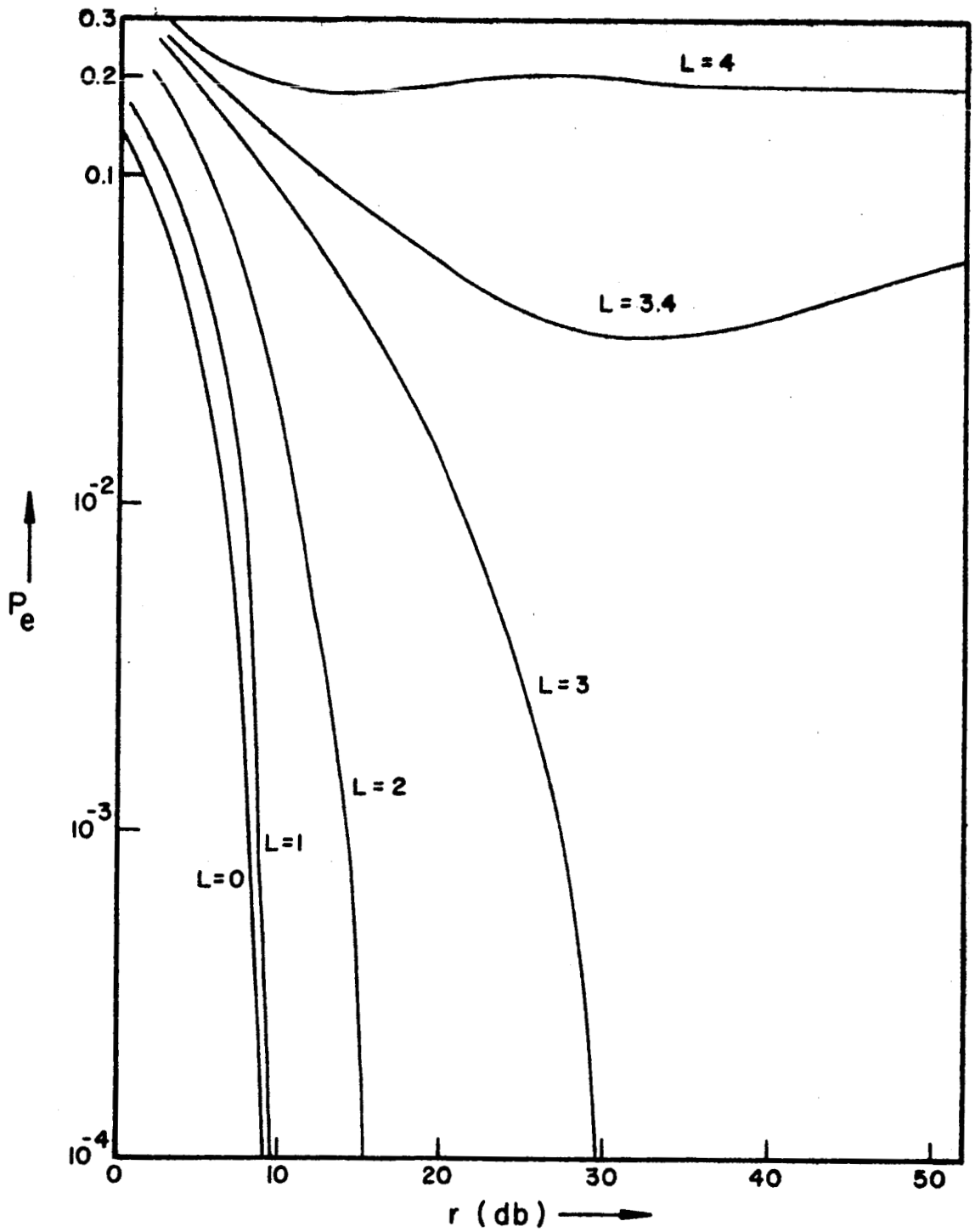

Figure 11. Error Probability vs SNR for Pure Linear Delay Distortion Filter and Raised Cosine Signaling.

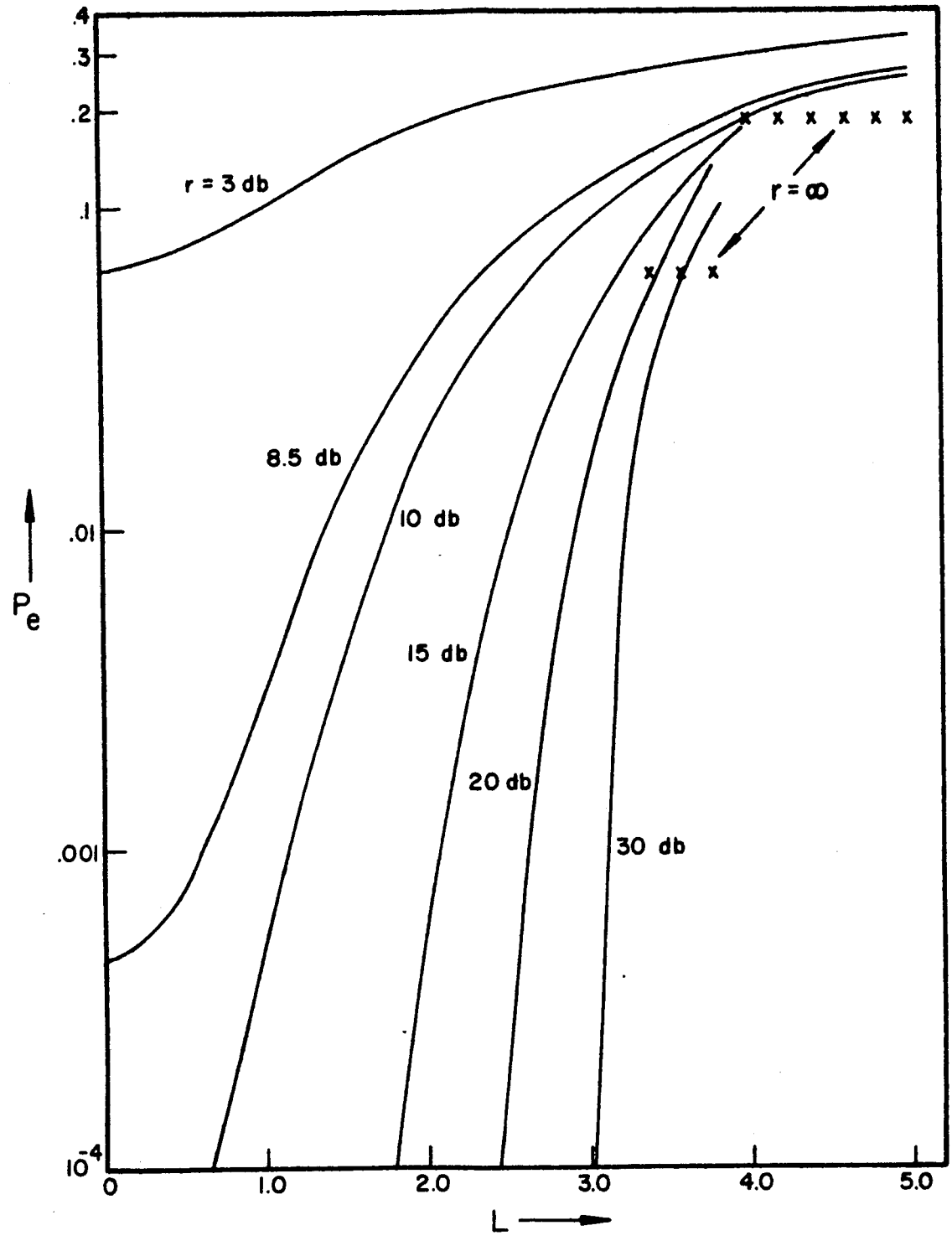

Figure 12. Error Probability vs L for Pure Linear Delay Distortion Channel Filter and Raised Cosine Signaling.

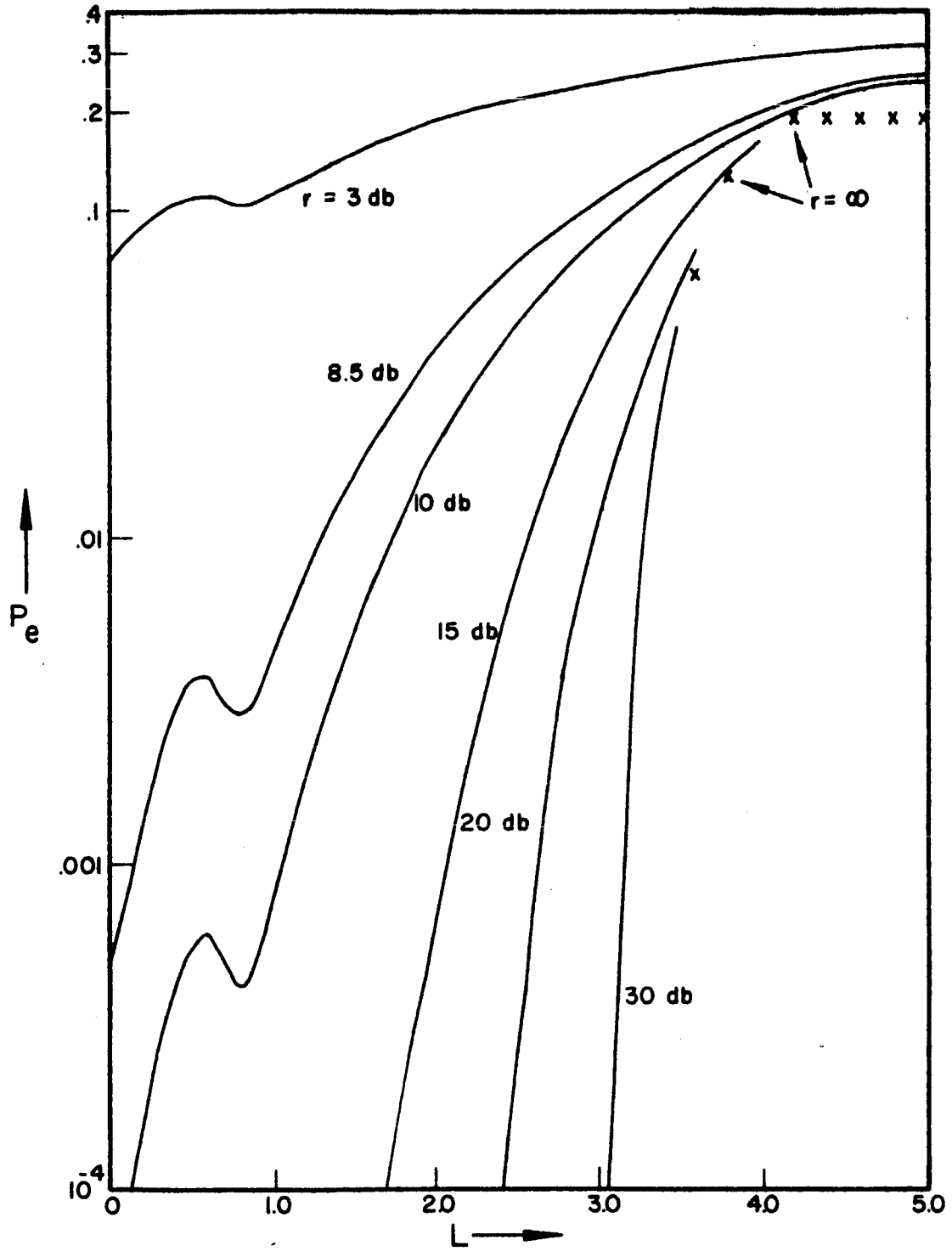

Figure 13. Error Probabilities vs L for Pure Linear Delay Distortion Channel Filter and Square Pulse Signaling.

10db of SNR degradation occurs from L = 2 to L = 3 for most practical error rates. We also see that infinite degradation occurs for error rates below .03 when L is increased from 3 to 3.4. This shows that pulse distortion is so severe at L = 3.4 that an irreducible error probability results. The curve of L = 3.4 also points out the interesting fact that for some severely distorted pulses, the error probability is actually lower for certain finite SNR's than it is at r = ∞. The reason for this can be seen by realizing that if an irreducible error probability exists, then some pulse combinations will cause the detector sampler to sample a voltage of the wrong polarity even when no noise is present. When moderate amounts of noise are inserted into the system in such a case, the probability of the sampled voltage crossing over to the correct polarity increases. Thus the conditional error probability can be smaller for some finite SNR's than it is for r = ∞.

In Figures 12 and 13, we note a very important property of our linear delay distortion system. This is the fact that there is a much higher rate of degradation for high SNR's than for low SNR's. For example, for an SNR of 30 db, the error probability rises from about $3 \cdot 10^{-5}$ to above 0.1 for an increase of L from 3 to 3.8, while at an SNR of 10 db, an equivalent rise in error probability occurs from L = 0 to L = 3.2. The extreme of this behavior is evident for the infinite SNR case, where an almost "instantaneous" jump from zero error probability to $P_e = .1875$ occurs at about L = 4.

It should be pointed out that although the graphical results of Figures 11-13 are being used here as part of a study of the Sunde approximation, they may well have important practical applications in themselves. For instance, the designer of a communication system employing a time-invariant channel (such as a telephone line or transmission cable) whose response function can be approximated by that of a pure linear delay distortion filter could use these graphs to estimate the error probability for his system as a function of data rate and average SNR. Such information could, for example, be of use in specifying the accuracy to which delay distortion equalizers must be adjusted in such systems to guarantee desired levels of performance. Also, these graphical results can be extended to other signals and other channel filters with only minor modifications to the computer program used for these results (see Appendix D).

From the above results we can immediately note two facts relative to the assumptions involved in the development of the Sunde approximation. First, we see that the assumption that an $\hat{L}$ exists for which $|L|>\hat{L}$ results in a very high error probability and for which $|L|<\hat{L}$ results in an extremely low probability is indeed valid. For both the raised cosine and square pulse signaling cases, we see that $P_e^i = .1875$ for $L>4$ while $P_e^i = 0$ for $L<3.4$. Thus it appears that we can reasonably set $\hat{L} = 4$ for both signals. Second, we see that Sunde's assumption that $P_e^i = .25$ given $|L|>\hat{L}$ is somewhat inaccurate. As mentioned above, we find a value of $P_e^i = .1875$ for $|L|>\hat{L}$.

For simplicity in calculation, and to take into account a possible increase in P_e^i due to inclusion of intersymbol interference beyond two bauds away from the detection interval, we will assign a value of $P_e^i = .2$ for $|L| > \hat{L}$.

Substituting the value $\hat{L} = 4$ and changing the conditional value of P_e^i from .25 to .2 in Equations (3-11) and (3-12), we obtain

$$P_e(r,d_1) \approx \frac{1}{2(1+r)} + \frac{.4d_1^2}{2\pi^2}\left[1 + \ln\left(1 + \frac{\pi}{2d_1^2}\right)\right] \qquad (3\text{-}13)$$

for the G-F channel, and

$$P_e(r,d_2) \approx \frac{1}{2(1+r)} + \frac{d_2^2}{12}\left[1 + \ln\left(1 + \frac{3}{\pi d_2^2}\right)\right] \qquad (3\text{-}14)$$

for the S-F channel. Since $\hat{L}$ was found to be 4 for both the square pulse and raised cosine signals, these expressions apply to both cases.

Figure 14 shows a comparison of the exact and approximate irreducible error probabilities which we have found. Three curves of exact P_e^i are shown for the three cases investigated in Chapter II. Two curves are shown for the approximate irreducible error probabilities - the second terms of (3-13) and (3-14). The normalization $d_2 = .7d_1$ between the data rates for the two different channel models has been used in this graph, as was done for the graphs of Section 2.5.

Three important facts can be noted from these plots. First, the Sunde approximation gives higher error probabilities

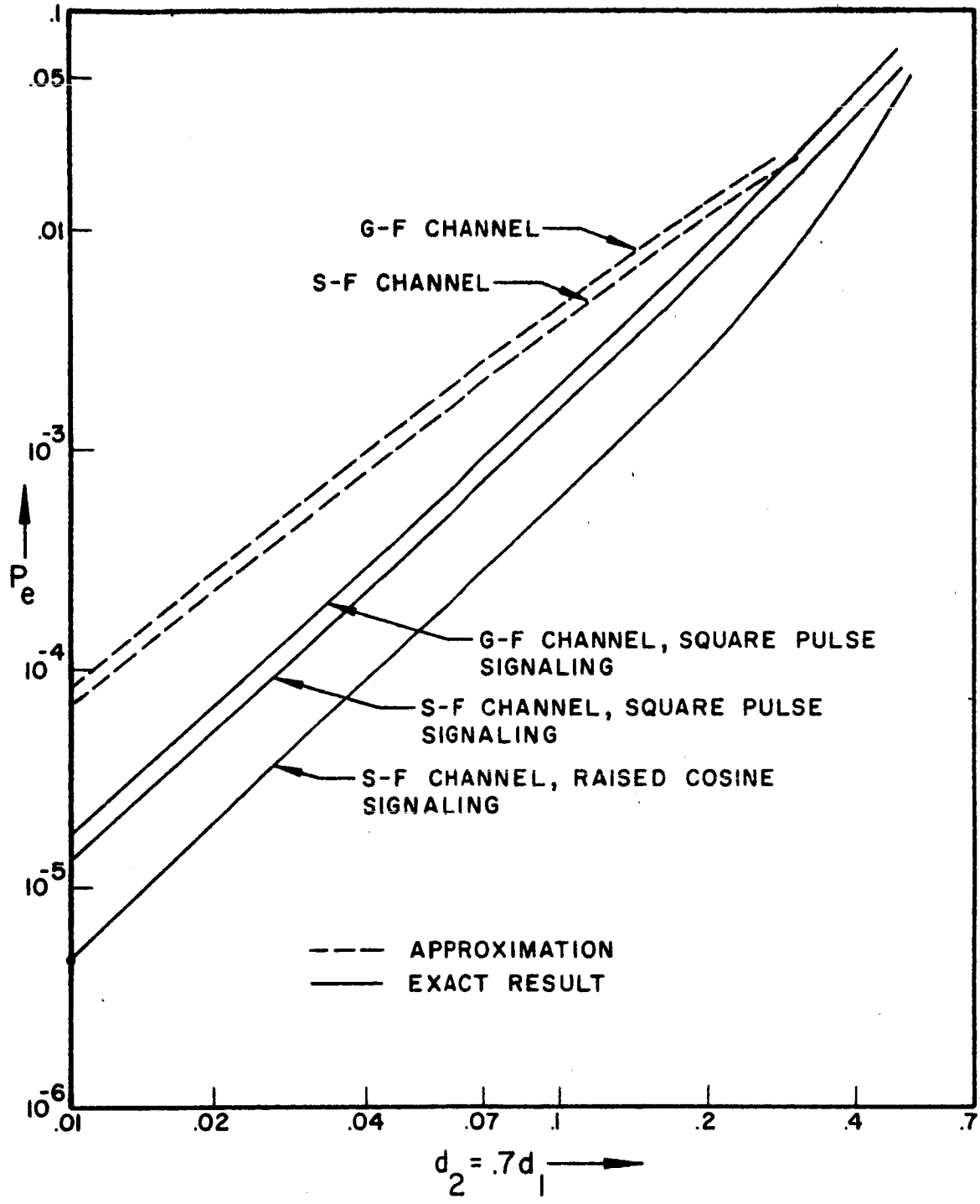

Figure 14. Comparison of Exact and Approximate Irreducible Error Probabilities.

than the exact results. Approximately one-half to one order of magnitude difference exists between the exact results and the approximation for the ranges of d considered. Second, the approximation fails to provide indication of the relative difference in error probability which was found for the two signals investigated. That is, the approximation provides no indication of the relative difference in performance between square pulse and raised cosine signaling which was found in Chapter II.

Third, it can be seen on the left side of the graph that the limiting behavior of the exact and approximate probabilities is not the same as $d \to 0$. As was shown in Chapter II, the exact irreducible error rate expressions are all of the form $P_e^{\,i}(d) = Kd^2$ for small d. Expressing this another way,

$$\lim_{d \to 0} \frac{P_e^{\,i}(d)}{d^2} = K \qquad (3\text{-}15)$$

where K is a constant satisfying $0<K<\infty$ which depends on the specific channel-signal combination under consideration. For the approximate irreducible error rate, which we will write as $\tilde{P}_e^{\,i}$, it can be shown that

$$\lim_{d \to 0} \frac{\tilde{P}_e^{\,i}(d)}{d^q} = \begin{cases} 0 & , q<2 \\ \infty & , q \geq 2 \end{cases} \qquad (3\text{-}16)$$

This means that if the relative error between the approximation and the exact results is defined as

$$E(d) = \frac{\left| P_e^{\,i}(d) - \hat{P}_e^{\,i}(d) \right|}{P_e^{\,i}(d)} = \left| 1 - \frac{\hat{P}_e^{\,i}(d)}{P_e^{\,i}(d)} \right| \qquad (3\text{-}17)$$

then this error becomes infinite as $d \to 0$ for all the cases investigated.

3.4 Summary and Comments

The Sunde error rate approximation has been shown to possess the basic properties which we would expect of such an expression. Specifically, for small d the approximate expression approaches the constant flat fading probability while an irreducible error probability is accounted for as the relative data rate increases. The results of this chapter also show that for error rates of practical interest, the Sunde expression for the irreducible error probability is within an order of magnitude of the exact value. However, it was found that the approximation does not reflect the difference in performance which was noted for different signaling pulse shapes. Also, it was found that the relative error between the Sunde approximation and the exact results will become infinite as $d \to 0$ for all cases investigated.

The fact that the Sunde approximation for irreducible error probability does not possess the same limiting form for very small signaling bandwidths as do the exact results is a particularly disturbing result. This is because much of the development of the approximation was based on the use of a truncated Taylor's series expression for the phase response

function, the justification for this being that such an approximation becomes increasingly better as the bandwidth of interest becomes smaller. In spite of this, we find that the error probability based on this expression becomes a worse approximation to the exact probability as the bandwidth diminishes. The answer to this apparent dilemma lies in the fact that the phase response function, G(f), of the random channel filter, when considered as a sample function from a random process, cannot be represented in a mean square sense by a Taylor's series expansion. We are led to this conclusion from the fact that the random variable g_2 of Equation (3-2) does not possess a finite variance.[1] This implies that the autocorrelation function of g_2 cannot be analytic, and from this it follows that a mean square convergent Taylor's series for G(f) does not exist (26). Furthermore, the lack of a finite variance for g_2 means that a random process, $g_2(f)$, which we call the second derivative of G(f) does not exist. Therefore there is no assurance that Equation (3-4) will become a good approximation to G(f) even for very small bandwidths. This

---

[1]This follows from noting that for $g_2' > 0$, the probability density function of g_2 (which is symmetric) is given by

$$p(g_2') = -\frac{1}{2}\frac{d}{dg_2'}\Pr[|g_2| \geq g_2'].$$

After inserting (3-7) into this expression, it is found that $p(g_2')$ does not decrease as fast as $(g_2')^{-2}$ for $g_2' \to \infty$, and thus $\overline{g_2^2}$ does not exist.

lack of an adequate representation for the phase response function is probably the major cause for the discrepancies between the exact results we have found and the approximations.

It should also be noted that the assumptions required to develop the Sunde approximation differ somewhat from the assumptions which we have made for the system under investigation in this work. This refers to Sunde's assumption that the pure delay term in Equation (3-4) will have no effect on the performance of the receiving system. The delay term in Equation (3-4) is the small change in delay which occurs due to the random fluctuations in the channel filter. In a physical communication system, it represents the small random delay which the fluctuations in the medium superimpose on the constant propagation delay of the channel. In the system which we have analyzed, it was assumed that the constant average propagation delay was known and that the detector system employs a sampler which has been adjusted to take this delay into account. However, any additional random delays introduced by the channel filter in our model (see Figure 3) are not known and are therefore not taken into account in the detector design. This means that the additional random delays can possibly degrade the system performance.

In Sunde's model, the analyses of the signal distortion properties (such as those resulting in Figures 11, 12, and 13 of this chapter) have assumed ideal sampling of the received

signal at all times. This means that no degradation due to delay is assumed to take place.

It can be seen that this assumption correctly models only those communication systems in which a scheme has been implemented for adaptively changing the detector syncronization in order to counteract the random delay changes. There are some systems in existence in which such schemes have been implemented, e.g., systems with "syncronizers" to extract timing information from the low-pass data signal itself. In other systems, e.g., systems where timing information is obtained from a separate channel of an FDM system or where the integration time in the receiver syncronization system is very long compared to the channel's "coherence time," the assumption of perfect bit syncronization may not be valid. Because of this, we might feel that the Sunde error rate approximation would be better suited to systems with perfect adaptive syncronization. This appears dispelled by the fact that in Figure 14 the approximation gives consistently high approximations to the error probability especially for small d. We intuitively feel that a system with perfect adaptive syncronization should perform no worse than the same system without such a feature at all SNR's. Thus it appears that the Sunde approximation would not be valid for this case either. We therefore conclude in this case also that the inability of the channel phase response function to be adequately represented on the basis of point measurements (the derivatives) has made the Sunde approximation invalid. Thus, on the basis

of the results of this chapter, we are forced to conclude that at least for the DPSK case, the Sunde error rate approximation does not provide a good estimate of the error probability when the frequency selective fading is of importance.

CHAPTER IV: EXPERIMENTAL RESULTS FOR NONADAPTIVE SELECTIVE FADING SYSTEMS

4.1 Introduction

In Chapter V we will investigate the performance of a receiver which attempts to adaptively correct for the effects of phase distortion caused by a selectively fading communication channel. Since the mathematical analysis of this system is intractable, its performance was investigated by digital computer simulation. In order to check the operation of the simulation program which was developed for this purpose, some computer simulations of the system which was analyzed in Chapter II were carried out. In addition, several experiments which investigated the relative effects of phase and amplitude distortion in such a system were performed. In each of these cases the receiver structure considered was that shown in Figure 3 of Chapter II. This receiver consists of a matched filter, multiplier, low-pass filter, and threshold detector. In contrast to the "adaptive" receiver of Chapter V which attempts to change its character in accordance with measurements made on the channel, we will refer to the receiver of Chapter II as the "nonadaptive" DPSK receiver.

In this chapter we begin with a general discussion of the computer simulation programs which were developed for this

research. Next the results of the simulation of the non-adaptive selective fading system are shown and compared with the theoretical results of Chapter II. Finally, the experimental results on the relative effects of amplitude and phase distortion are given.

4.2 The Computer Simulation Programs

The purpose of the computer simulation programs used for this research was to evaluate the error probability for certain special receiver systems used in conjunction with a Gaussian frequency selective fading channel. Although the program design was general in nature, all the results shown in this report are for the case of DPSK signaling and an S-F channel model. The method employed to obtain these error probabilities consisted of using a subprogram which computed the average error probability for a given channel transfer function and then using this program in a Monte Carlo scheme which generated a sequence of pseudo-random channel transfer functions and evaluated the average performance over the entire set of channels. Thus, for each given channel, the subprogram computed a conditional probability of error by effectively averaging over the randomness of the additive noise and over the possible message sequence combinations. This subprogram was then used as a part of the main program which averaged over the ensemble of random channels. Details of the operation of this subprogram are presented in Appendix D. From the standpoint of the main program, the operation

required was that of determing the sample means of an infinite population of random variables. The selection of the particular random variable is controlled by the pseudo-random channel generated, and the resulting value of P_e is then one of the independent random variables selected from the population. The independence of the random variable P_e from one selection (experiment) to the next is insured by the fact that each new channel sample generated is effectively independent of all the other channel samples.

From the above discussion it is obvious that the procedure required to arrive at an estimate of the system probability of error is to compute the sample mean of the various conditional error probabilities as they are determined in the computer. Thus, writing the sequence of conditional error probabilities as P_n, n = 1,2 ...N, we have as our estimate of the system error probability

$$\hat{P}_e = \frac{1}{N} \sum_{n=1}^{N} P_n \qquad (4\text{-}1)$$

where N is the number of conditional error probabilities generated, i.e., the number of random channel samples investigated. In order to obtain an idea of the accuracy of the error probability estimate computed in these programs, an estimate of the standard deviation of $\hat{P}_e$ was also computed for each estimate.

4.3 Comparison of Theoretical Results and Experimental Computer Results

In this section the results of two computer simulation experiments are described. These experiments both involve simulation of communication systems for which theoretical analysis is available, enabling the results of these experiments to be compared with the theoretical predictions.

The first experiment performed was the simulation of the nonadaptive communication system of Figure 3 for the S-F channel with raised cosine signaling. Thus the analysis of Chapter II is applicable to predict the error rate performance of the system. The experiment was performed for two different relative data rates - .56 and .28. For d = .56, 500 channel samples were used for the experiment while 1,500 samples were used for the d = .28 case. Figure 15 shows the theoretical predictions and experimental results for both cases. Intervals extending one estimated standard deviation above and below the error probability estimate are shown in this graph for each experimental point. For the d = .56 case, the estimated standard deviation of the error probability estimate ranged from 4.27% of the probability estimate at the 7db point to 11.7% at infinite SNR. The error of the estimate relative to the theoretical predictions was about 1.5% at the 7db point, 6.45% at infinite SNR point, and reached a maximum of 8.6% at the 20db point. For the d = .28 case, the ratio of the estimated standard deviation to the error probability estimate was 3.48% at r = 7db and 21.8% for infinite SNR. The error of the

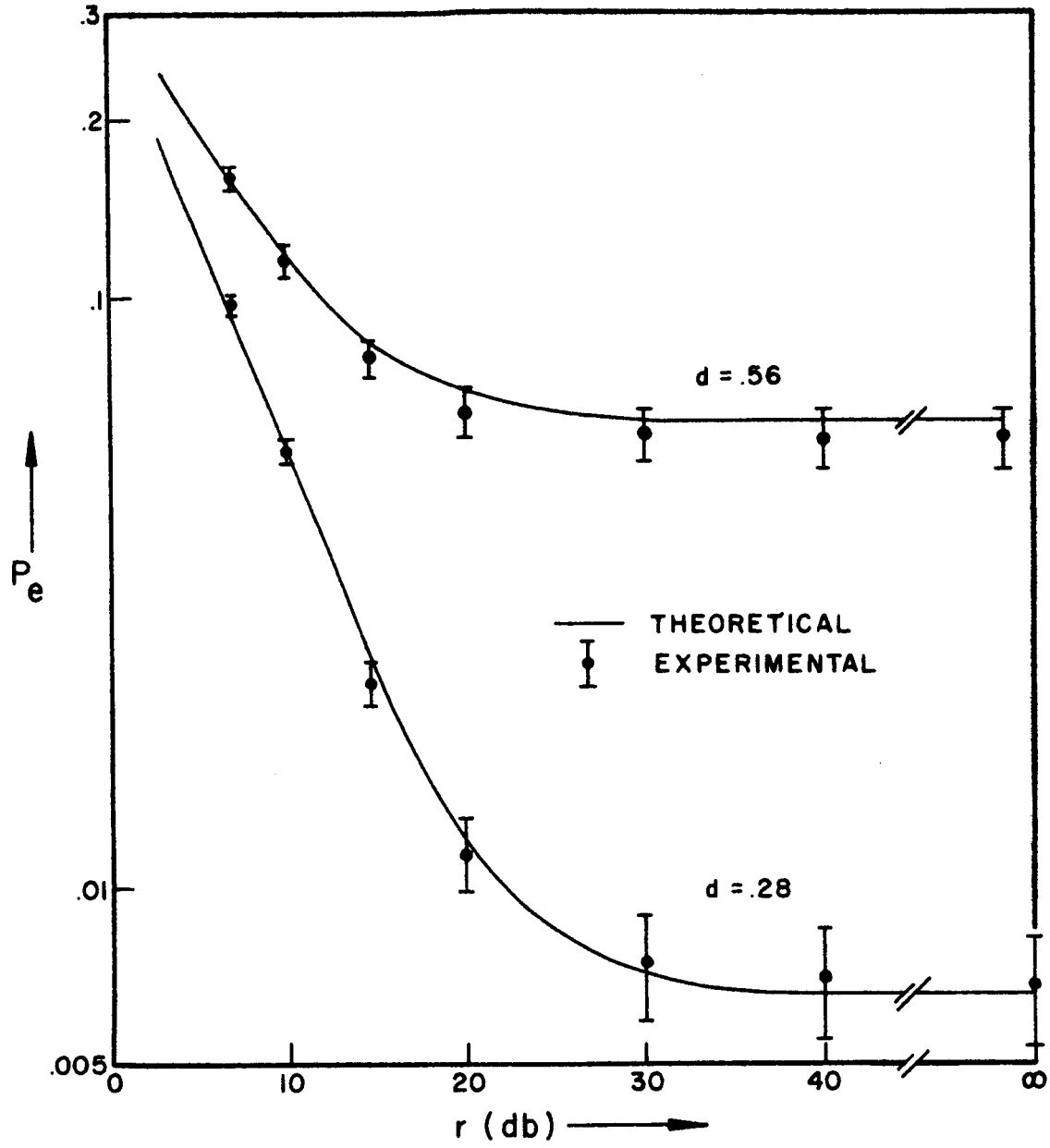

Figure 15. Comparison of Experimental and Theoretical Error Rates for the Nonadaptive System.

estimate relative to the theoretical prediction was 3.6% at r = 7db, 3.48% for infinite SNR, and reached a maximum of 10.3% at r = 14.7db.

These results clearly point out the fact that as the error probability being estimated decreases, much longer experiments are required to obtain good experimental results. In the two cases investigated here, the relative error of the experimental results compared to the theoretical predictions was roughly the same. The estimated standard deviation expressed as a fraction of the error probability estimate was almost twice as large for the d - .56 case as for the d = .28 case. However, to achieve even these results, three times as many channel samples were required for the d = .56 case as for the d = .28 case.

The standard deviation limits shown about the probability estimates on this graph can also be interpreted as confidence intervals associated with the estimates. As discussed by Cochran (27), it can be assumed that the ensemble of probability estimates possesses a normal distribution. Thus, from normal probability tables, we can determine that the intervals drawn about the estimate points can be considered to be 68% confidence intervals. Similarly, if one were to extend the indicated intervals by 50% in each direction, 87% confidence intervals would result, while 95% confidence intervals correspond to intervals extending two standard deviations in each direction. These comments also apply to all the other plots of experimental points which are given in this report.

The second experiment to be described in this section is a simulation of a communication system subject to nonselective flat Rayleigh fading. Since this system has been analyzed mathematically, it is again possible to compare the experimental error probabilities from the computer simulation with theoretically predicted ones. These results are presented here because they will be used in the next section for comparison with experimentally determined error rates for two other systems. This system was simulated on the computer by simply replacing the pseudo-random, frequency-dependent channel transfer functions generated by the computer with a constant transfer function whose value was equal to the value of the original transfer function at the center frequency. Writing $H_m(f)$ for the new transfer function and H(f) for the originally generated transfer function, the simulation simply implemented the equation

$$H_m(f) = H(o) \quad \text{for } |f| < B. \tag{4-2}$$

As shown in Chapter II, this system can be considered to be the limit of our general frequency selective system for the special case of very small signaling bandwidths.

Figure 16 shows a comparison of the experimental and theoretical results for this experiment. The experimental points were all obtained by using 1,000 pseudo-random channel samples in the simulation program. As before the experimental points are plotted with bars indicating the $\pm$ 1 standard

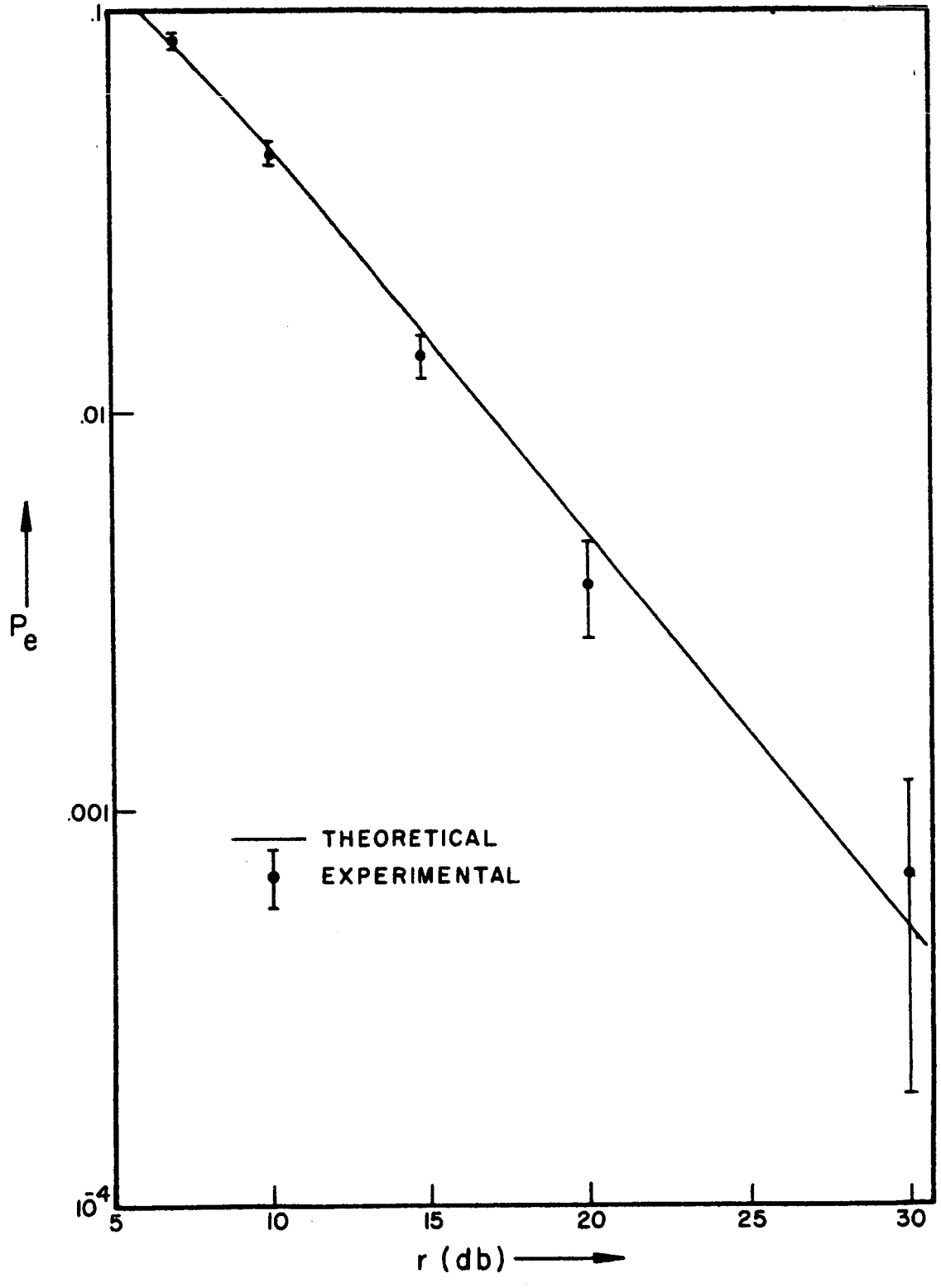

Figure 16. Experimental and Theoretical Flat Fading Error Probabilities.

deviation interval about the probability estimate. These estimated standard deviations range from 4.6% of the error probability estimate at the 7db point to 27.6% at the 20db point to 72.1% at the 30db point. The actual experimental error relative to the theoretical error probabilities ranges from a minimum of .084% at the 7db point to a maximum of 36% at the 40db point. This experiment again points out the difficulty of accurately estimating error probabilities of the order of 10^{-3} and below as compared to estimating those near 10^{-2} and above. However, we do find that the experimental points virtually always remain within one estimated standard deviation of the theoretical value. In both of the experiments described above, the experimentally measured error probabilities and the theoretically predicted ones generally agree quite well. From this we conclude that the computer simulation model has closely approximated the mathematical model used in Chapter II. As mentioned above, these experiments provide a relative accuracy in the error probability estimate which is much better at high average probabilities than it is at low ones.

4.4 The Separate Effects of Amplitude and Phase Selective Fading

In this section, an experiment is described which was designed to indicate the relative severity of amplitude and phase distortion in the Gaussian frequency selective fading channels which we have studied. One motive for carrying out this experiment is to determine the accuracy of Sunde's

for all f in the bandwidth of interest. Thus the channel transfer function used in the experiment possesses all the variations in magnitude that H(f) does, but it is a pure real function. To determine the effect of phase distortion alone, the original channel transfer function is replaced by a transfer function with constant magnitude and phase response function equal to that of the original transfer function. The magnitude of the modified transfer function was set equal to the value of the magnitude of the original transfer function at the center frequency. Mathematically, we can express this operation as

$$H_m(f) = |H(0)|[H(f)/|H(f)|] \qquad (4\text{-}4)$$

Figure 17 shows the result of the first set of experiments. This figure plots probability of error versus SNR for a fixed value of relative data rate d. For this experiment d was 0.28. Five sets of points are plotted on this graph. These are:

1. Theoretical Flat Fading
2. Theoretical Selective Fading - d = .28
3. Experimental - Amplitude Distortion Only
4. Experimental - Phase Distortion Only
5. Experimental - Flat Fading

The three sets of experimental points all were obtained by performing the respective experiments using the same set of 1,000 pseudo-random channel samples. The use of identical

conjecture that phase distortion is the dominating factor in determining the error probability in such systems. Further, we would like to deepen our understanding of the Gaussian channel by obtaining quantitative data on the relative severity of the two types of distortion. If Sunde's conjecture is true, we wish to know to what extent it is true and how the system parameters such as relative data rate and SNR effect this. In the results to follow, it will be shown that the Sunde conjecture is indeed true for ranges of r and d where intersymbol interference and distortion effects outweigh the effects of additive noise. This result will lead, in Chapter V, to the formulation of a simple adaptive scheme which is capable of providing significant improvement in the operation of digital systems over Gaussian fading channels.

In order to compare the relative effects of amplitude and phase distortion, two experiments were performed. Each experiment consisted of using the computer simulation scheme described previously with one modification. This modification consisted of changing the pseudo-random channel sample before it was used in the signal processing portion of the program. To determine the effect of amplitude distortion above, the complex-valued transfer function was simply replaced by its magnitude at each frequency. Writing $H_m(f)$ for the transfer function after modification, the program implemented

$$H_m(f) = |H(f)| \tag{4-3}$$

sets of channel samples, allows us to make meaningful comparisons between the results obtained for each experiment.

The first and most important fact that this graph shows is that the error rates due to phase distortion are significantly greater than those for amplitude distortion at all SNR's. Indeed, the results of this simulation indicate that an irreducible error rate due to phase distortion exists while no indication of an irreducible error rate due to amplitude selective fading was found. For the entire set of 1,000 channel samples examined the error probability at infinite signal-to-noise ratio was zero for the amplitude distortion case. It is thus apparent that if an irreducible error rate due to amplitude-selective fading exists this error rate must be several orders of magnitude below that due to phase distortion.

A second fact of great importance which can be seen from this graph is that the error rates due to amplitude selective fading are actually lower than those for the identical system subject to flat fading only. In order to show this, both the theoretical flat fading error probability and the experimentally determined rate are shown in the figure. This result is somewhat startling since it indicates that the average error rate for a system which introduces frequency selective amplitude distortion is lower than for such a system with no distortion introduced at all. After a careful investigation of many individual channels which were used in this experiment, it was determined that the reason for this phenomenon

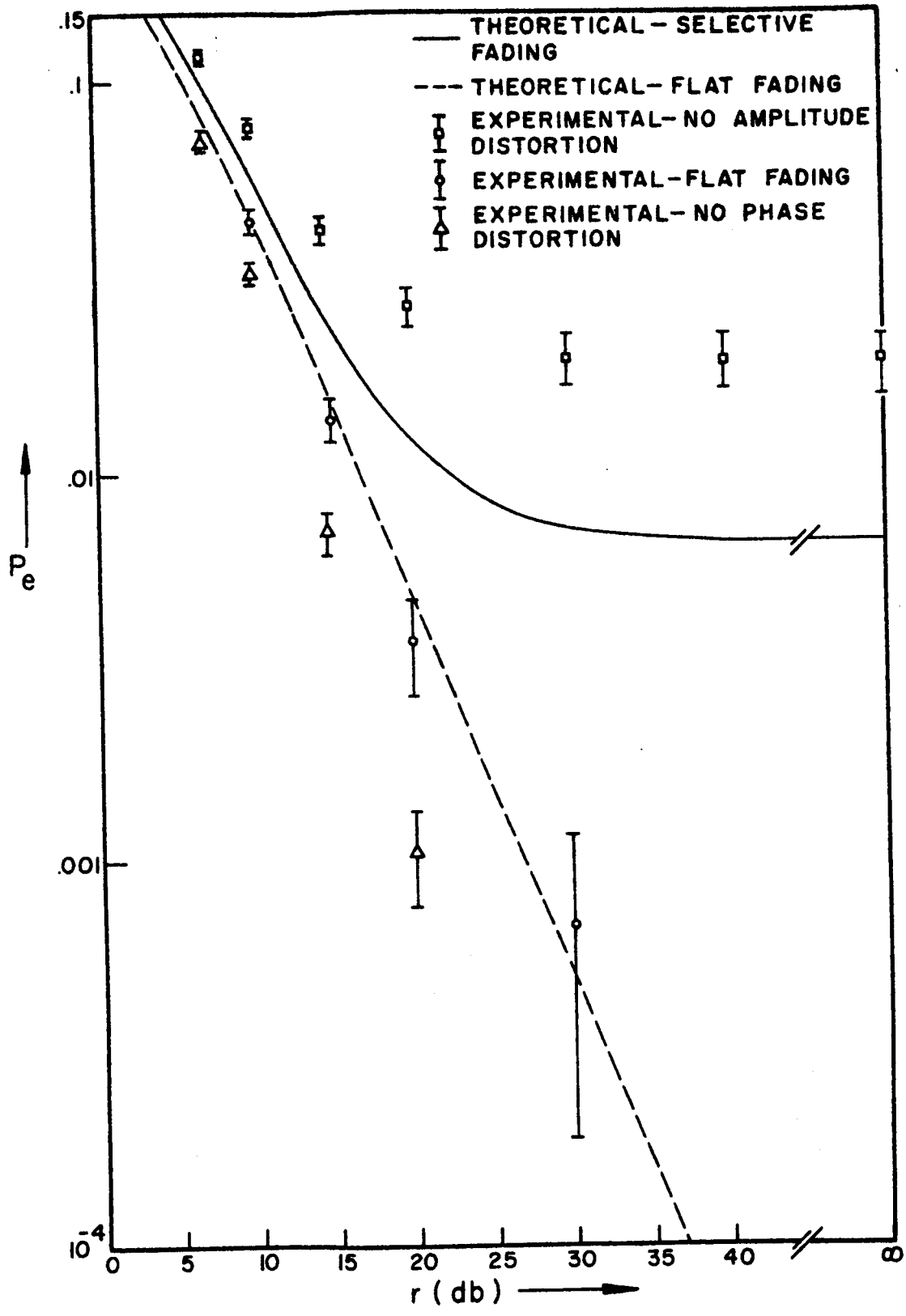

Figure 17. Comparison of Amplitude and Phase Distortion Effects - d = 0.28.

is that in many cases where deep fading occurs at one frequency in the transmission band other frequencies in the band are not undergoing such severe fading. This means that the total energy available for detection is greater than if the channel were undergoing a deep flat fade across the entire band, as in the case of flat fading. Thus another way of looking at this phenomenon is that we are taking advantage of a diversity effect in the channel. Multi-channel diversity communication systems rely on the fact that the probability of a deep fade occurring simultaneously in several fading channels is much lower than the probability of a deep fade in one channel. Similarly, our results show that when the phase distortion in the Gaussian frequency selective channel is removed, we can take advantage of the same effect in a single transmission band.

It is interesting to note that the experimental points for the pure amplitude distortion case all fall on a straight line for SNR's greater than 10db. The relationship between error probability and SNR corresponding to this line was found to be

$$P_e^a = .946r^{-1.463} \tag{4-5}$$

where we have written P_e^a for the probability of error due to amplitude distortion. This can be compared to the asymptotic flat fading result for large r which is

$$P_e = .5r^{-1} . \tag{4-6}$$

The smaller exponent for the pure amplitude distortion case indicates the fact that the error probability is falling faster as a function of r for this case than for the flat fading case.

In Figure 17 the theoretical error probability for the frequency selective Gaussian fading channel (both amplitude and phase distortion) is also plotted. Comparing this curve with the experimental points for the pure phase distortion channel shows us that the irreducible error rate due to phase distortion only is actually higher than the irreducible error probability due to combined phase and amplitude distortion. It appears from this that the diversity effect associated with amplitude selective fading which was mentioned above has the effect of reducing the irreducible error rate due to phase distortion when the two effects are combined.

Figure 18 is a plot of experimental and theoretical data plotted in an identical manner as that of Figure 17. In this case all the results are for a lower relative data rate - d = 0.14. This graph confirms that for d = 0.14 the nature of our results is identical to the case shown in Figure 17 where the relative data rate was 0.28. We see again that the error rates due to pure phase distortion are higher than those due to amplitude distortion alone for all SNR's. Further, while an irreducible error probability definitely exists for the phase distortion case, no irreducible error rate was experimentally found for the pure amplitude distortion case. We also note that again the error rate due to amplitude

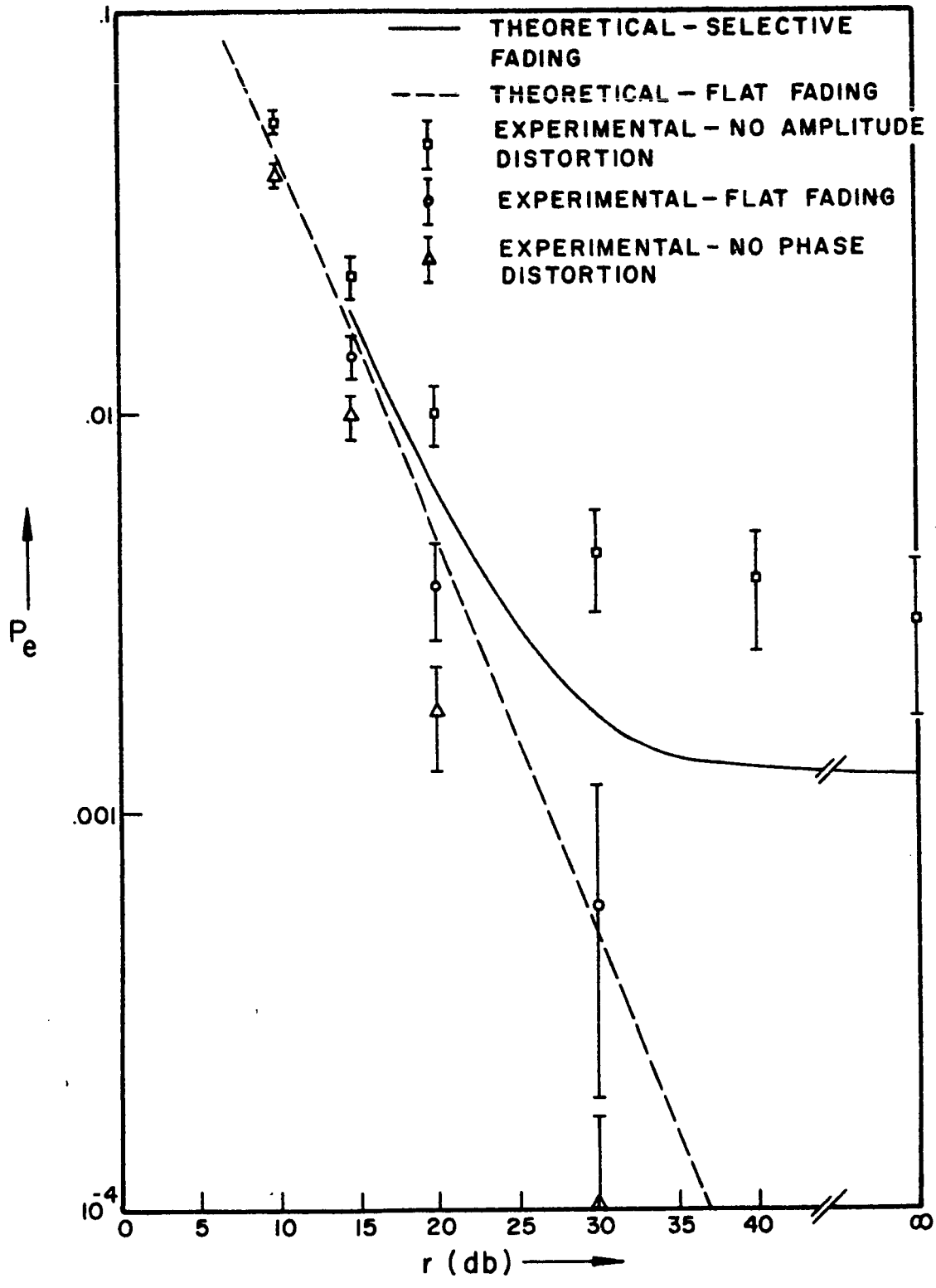

Figure 18. Comparison of Amplitude and Phase Distortion Effects - d = .14.

distortion alone is lower than the flat fading error rate, indicating that the diversity effect is again present. Finally we note that the irreducible error rate due to phase distortion alone is again greater than that for combined amplitude and phase distortion.

We again note that the experimental points for the pure amplitude distortion case fall very nearly on a straight line for SNR's above 10db. In this case the equation of error probability to SNR was determined to be

$$P_e^a = .794r^{-1.3} \qquad (d = .14) \qquad (4\text{-}7)$$

This can be compared with the result from Figure 17,

$$P_e^a = .946r^{-1.463} \qquad (d = .28) \qquad (4\text{-}8)$$

and with the flat fading result

$$P_e = .5r^{-1} \qquad (4\text{-}9)$$

The different exponents in the two amplitude distortion expressions support a fact which we know must be true about the pure amplitude distortion results for our system. This is that for small relative data rates, the pure amplitude fading error rates must approach the flat fading error rates. This can be seen by first recalling that the reason for the particular behavior we have found for the pure amplitude distortion system was that the transmission band was wide enough so that a deep fade at one frequency in the band would not

necessarily indicate a deep fade throughout the entire band. In other words, the signaling bandwidth is wide enough compared to the width of the channel's frequency correlation function that a significant difference in the amplitude of the channel's transmittance can occur within the signaling bandwidth. From this viewpoint, it is obvious that as the signal bandwidth gets smaller, the probability of a significant change in the channel transfer function's amplitude within the signaling bandwidth becomes smaller. In the limit, we approach the case of a flat transfer function whose amplitude must, of course, possess a Rayleigh distribution. Thus we see that for small relative data rates the pure amplitude distortion error rates must approach the Rayleigh flat fading error rates. The fact that the exponent in the expressions for the pure amplitude distortion error rates seem to approach -1 as d becomes smaller shows that the results are in accordance with the predicted behavior.

In order to show graphically that the experimental amplitude distortion results are in accordance with the predicted limiting behavior described above, Figure 19 has been prepared which contains the following error probability plots:

1. Theoretical Flat Fading
2. Experimental Flat Fading
3. Experimental Pure Amplitude Distortion - d = .280
4. Experimental Pure Amplitude Distortion - d = .140
5. Experimental Pure Amplitude Distortion - d = .0933

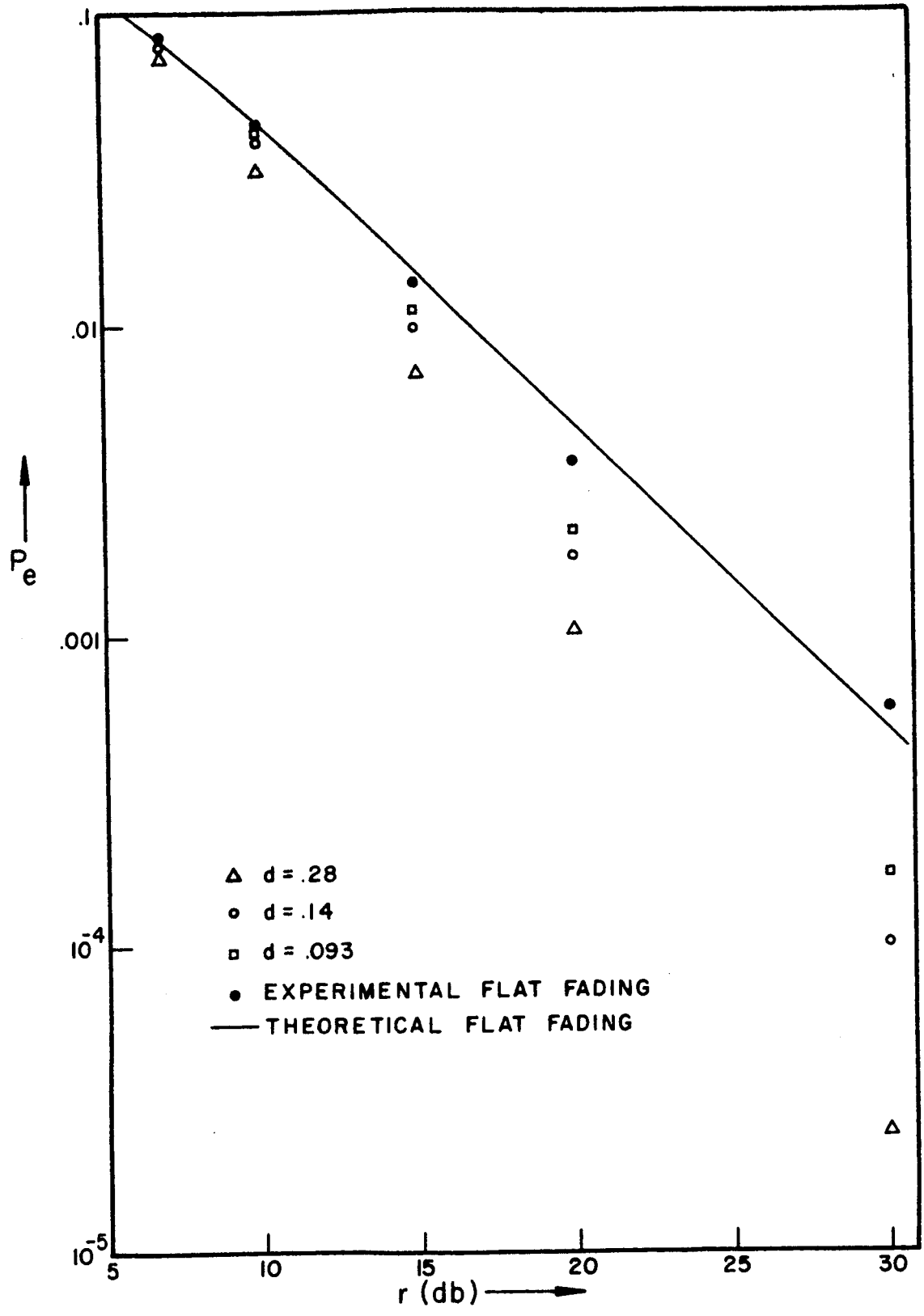

Figure 19. Comparison of Flat Fading and Pure Amplitude Distortion Systems.

Each of the experimental curves was obtained by using an identical set of 1,000 channel samples. For clarity, the estimated standard deviation limits have not been included in this graph. The results shown in this graph indicate clearly that for each value of r considered, the error rate approaches the flat fading case as d becomes smaller. From these results, we conclude that our experimental results do agree with the predicted limiting behavior for the pure amplitude distortion case.

4.5 Summary

In this chapter the results of several computer simulations of systems containing the nonadaptive DPSK receiver are given. First, the frequency selective fading system examined in Chapter II was considered. It was shown that the simulation results for this system are in good agreement with the theoretical predictions, from which it is concluded that the computer simulation accurately models the communication system of interest. As expected, it was also found that the accuracy obtainable with a simulation experiment of any given length becomes poorer as the error probability being estimated decreases. Next, the results of the simulation of a pure flat Rayleigh fading system were shown. As in the first experiment, the experimental and theoretical rates were in agreement. Finally, communication systems subject only to the phase distortion or amplitude distortion components of the Gaussian fading channel were simulated. The results of

these experiments revealed that in the presence of phase distortion alone the system performs worse than in the presence of amplitude and phase distortion combined; while in the presence of amplitude distortion alone, it performs better than the same system in the presence of flat fading. Thus, Sunde's conjecture that phase distortion is responsible for virtually all of the degradation which occurs in the frequency selective fading channel was found to be true. It was found that the improvement which the amplitude distortion case affords over flat fading can be interpreted as being due to a diversity effect.

CHAPTER V: EXPERIMENTAL RESULTS FOR ADAPTIVE SELECTIVE FADING SYSTEMS

5.1 Introduction

The experimental results of the previous chapter have shown that phase distortion can be considered to be the basic influence in causing errors due to intersymbol interference and pulse shape distortion in selective fading communication systems. This fact is important because it indicates that if one is operating a system whose probability of error is controlled by distortion effects (i.e., the effect of P_e^i), then he may be able to significantly reduce the system error rate with the use of some form of phase distortion equalization. Of course, for a random fading channel, this implies an adaptively time-varying equalization scheme. In general such a scheme would involve a system for measurement at the receiver to determine the distortion characteristics, a feedback scheme to transmit the measurement data to the signal generator, and an adaptive control on the signal generator which would change the signal's shape so as to optimally combat the channel effects. However, in the present case the fact that phase distortion is the primary cause of the signal distortion is extremely important in that it allows elimination of the requirement for a feedback system. This is because phase

correction is ideally performed with a network which possesses a constant amplitude response function and phase response function designed to compensate for the given channel phase characteristic. Such a network, when placed between the channel output and the matched filter input does not change the additive noise spectral density. Because of this, the system's performance is the same whether this filter is placed at the transmitter output or at the detector input. Thus, since measurement and correction can both take place at the receiver, no feedback channel is necessary.

It should be pointed out that some of the results of Chapter IV are of direct interest in relation to the performance of an adaptive system such as is described above. This is because, in the light of the above discussion, we can interpret the results of the experiment with only amplitude-selective fading as an indication of the ultimate performance which could be achieved by a phase-correcting adaptive system. That is, if an adaptive system could be constructed to measure the phase distortion of a channel and perfectly correct for such phase distortion, the resulting performance would be simply that of the amplitude-selective system shown in Chapter IV. This shows us that for systems which are subject to the effects of a Gaussian fading channel, significant reductions in error rate may be possible if an adaptive receiver system is implemented which attempts to measure the channel phase characteristic and to compensate for it. We naturally realize that such a system could not achieve the

performance levels of the pure amplitude-selective fading system since neither the measurement nor the compensation could be perfect, but this does not preclude the possibility of significant error probability reductions for such a system.

We thus conclude that it is of interest to attempt to formulate an adaptive system for phase measurement and correction and to attempt to evaluate its performance. In this chapter two such systems are investigated - one designed to compensate for the residual delay introduced by the channel and the other designed to combat residual delay and linear delay distortion. In each case, measurements are assumed to be made with pilot tone measurement systems which consist of two pilot tone generators at the transmitter and two corresponding pilot tone receivers at the receiver. In addition, the effects of additive noise in the pilot tone measurement system and of using a physically realizable equalization filter in the adaptive system are investigated.

5.2 Measurement and Representation of Channel Phase Distortion

In considering an approximate representation for the phase response function of a random channel, the work of Sunde provides an intuitively attractive approach. That is, we feel that for bandwidths which are reasonably small with respect to the channel's coherence bandwidth, we should be able to approximate the phase response function by some combination of pure phase shift, pure delay, and pure delay distortion (i.e., by some quadratic expression in f). Of course,

the results of Chapter III show us that intuition must be combined with good mathematical understanding in this situation, since we have seen that the use of a Taylor's series approximation is invalid in this case.

In essence, the reason that the Taylor's series representation fails to adequately represent the phase response function of the Gaussian fading channel is that in this case measurements made at a point fail to represent the true nature of the phase response function over an interval - the transmission band. Thus, it is obvious that a method of representation should be sought which takes into account the properties of the phase response function over an interval. This representation over an interval can be accomplished while retaining the delay and linear delay distortion approximation features described above by using a polynomial fit approach to the representation. Specifically, if the phase response function is G(f) and the bandwidth is $2\Delta f$, then letting[1]

$$G_0 = G(0)$$

$$G_1 = G(\Delta f)$$

$$G_2 = G(-\Delta f) \ ,$$

we can approximate G(f) by

$$G(f) \approx Af^2 + Bf + C \qquad (5\text{-}1)$$

[1]It is assumed that G(f) is represented as a continuous function of f and is not expressed in modulo 2π form.

where

$$A = \frac{G_1 + G_2 - 2G_0}{2(\Delta f)^2} \tag{5-2}$$

$$B = \frac{G_1 - G_2}{2\Delta f} \tag{5-3}$$

$$C = G_0 \tag{5-4}$$

We note that this polynomial fit representation insures that the error in representation of the phase response function will be zero at the three points 0, Δf, and $-\Delta f$. Thus, we have reason to believe that this representation may provide an adequate interval representation for the phase response function even though the first three terms of the Taylor's series may fail to do this.

The polynomial fit approach to the representation of the phase response function is naturally associated with a physically realizable method of channel measurement. In this method, pilot tones are transmitted to the receiver at frequencies $f_0 + \Delta f$ and $f_0 - \Delta f$. Phase detectors at the receiver are tuned to each of these two frequencies, providing estimates of the quantities G_1 and G_2. In addition, a phase detector can be used to obtain an estimate of G_0 from the data signal. When phase modulation is being used, a signal suitable for processing by the phase detector can be derived by either squaring the incoming message signal or by a decision directed measurement phase reversal scheme. Both

of these methods are discussed by Proakis, et al. (28), in connection with a different problem

5.3 Performance of the Adaptive Systems

In this section we show the results of computer simulation experiments which were conducted in order to determine the error probability of the adaptive receiver scheme formulated above. Two adaptive systems were investigated. The first of these employs a simple straight-line approximation to the channel filter's phase response function. This means that only the residual delay of the channel filter is compensated for. The estimate of the filter delay is made by using Equation (5-3) in conjunction with the pilot-tone measurement system which was described above. This means that only two phase detectors are required at the detector and no measurement is made on the data signal (i.e., G_0 is not measured).

The second adaptive system which was simulated attempts to compensate both for the delay and linear delay distortion introduced by the channel filter. Again the pilot-tone measurement scheme is employed, but now both Equations (5-2) and (5-3) are used to estimate the two required parameters.

In the simulation of each of the above adaptive systems an ideal equalization filter was assumed to be placed in the receiver system ahead of the matched filter. This filter provides perfect delay and linear delay distortion compensation corresponding to the parameters measured by the pilot-tone measurement system. In both of the systems investigated

the value of the constant phase shift, given by C in Equation (5-4) was ignored and was not compensated for by the equalization filter. The reason for this is that in a DPSK system, a constant phase shift in the channel filter will have no effect on the operations at the receiver as far as information processing is concerned. This is because an identical phase shift is introduced in both the delayed "reference" signal and in the non-delayed "information" signal and this phase shift will not effect the output of the multiplier and low pass filter combination.

Figures 20, 21, and 22 are graphs showing a comparison of the error probability performance of the nonadaptive and the two adaptive systems. Each graph is a plot of error probability versus SNR for a fixed relative data rate. In Figure 20 the relative data rate for each set of points is .56. Four curves are included in this graph:

1. Nonadaptive system, theoretical error probability (results from Chapter II).
2. Nonadaptive system, experimental error rates (results from Chapter III).
3. Adaptive system, delay correction only, experimental error rates.
4. Adaptive system, delay and delay distortion correction, experimental error rates.

The three experimental curves shown were each obtained from a set of 1,000 channel samples. The same set was used for

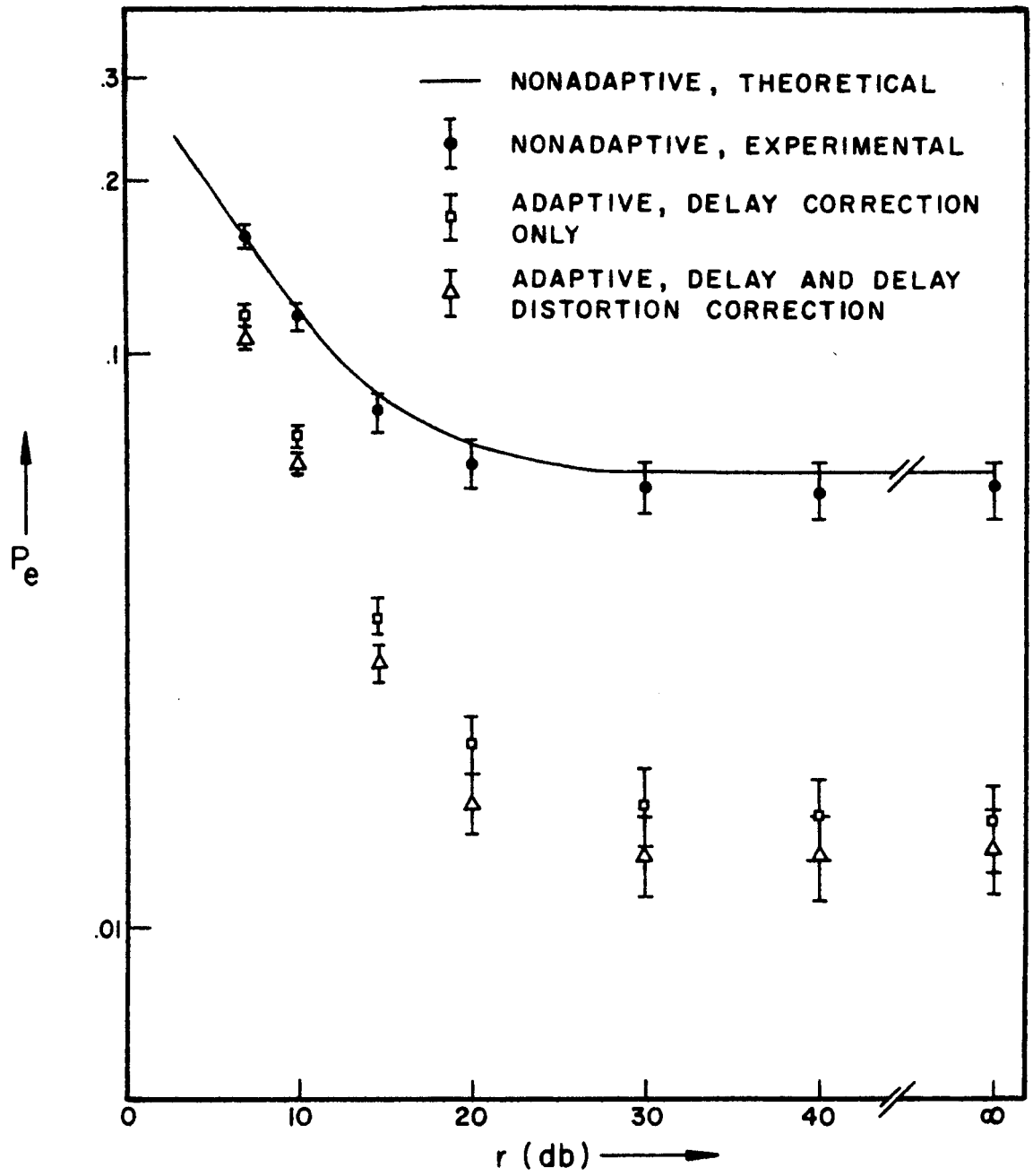

Figure 20. Performance of Nonadaptive and Adaptive Systems - d = 0.56.

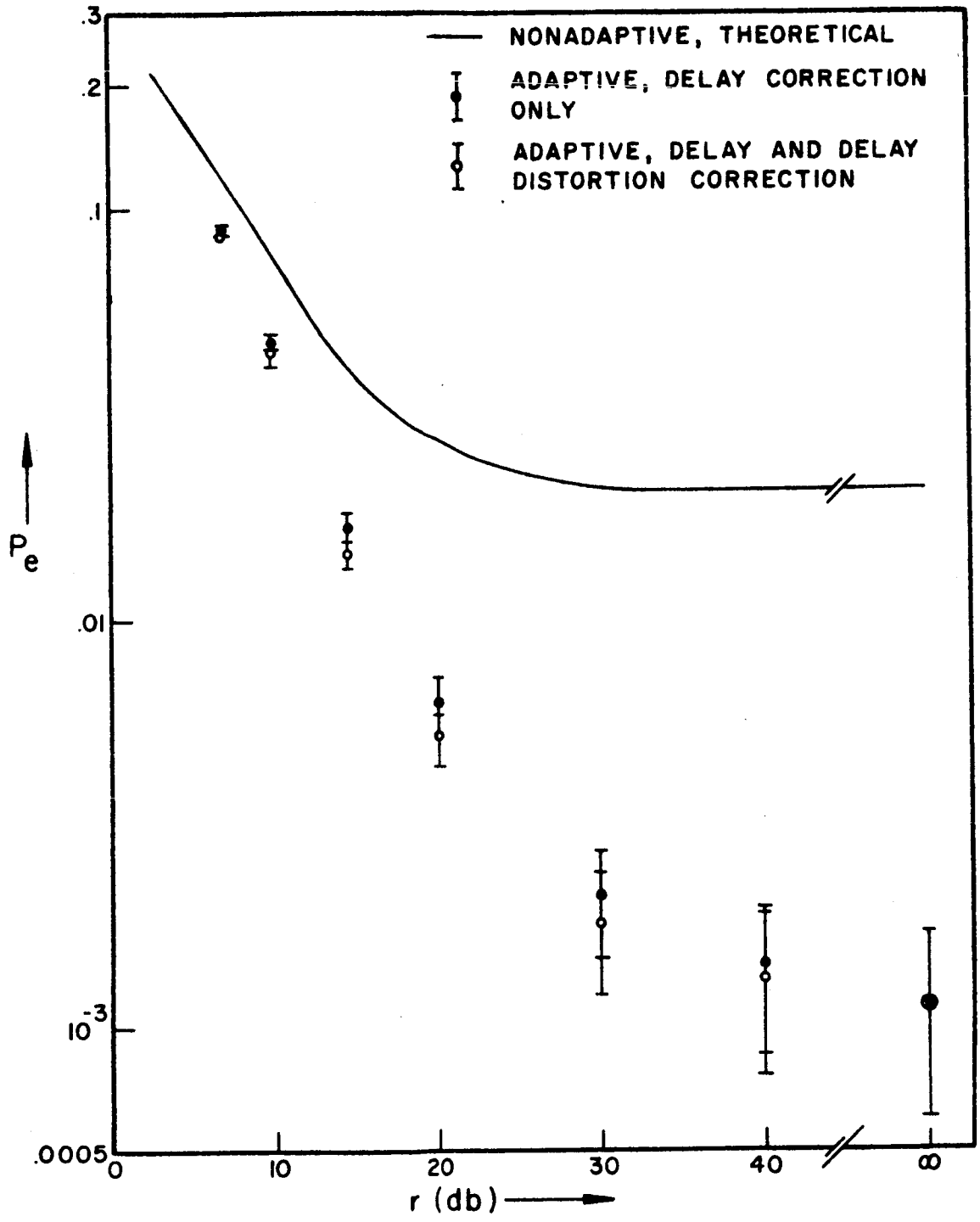

Figure 21. Performance of Nonadaptive and Adaptive Systems - d = 0.4.

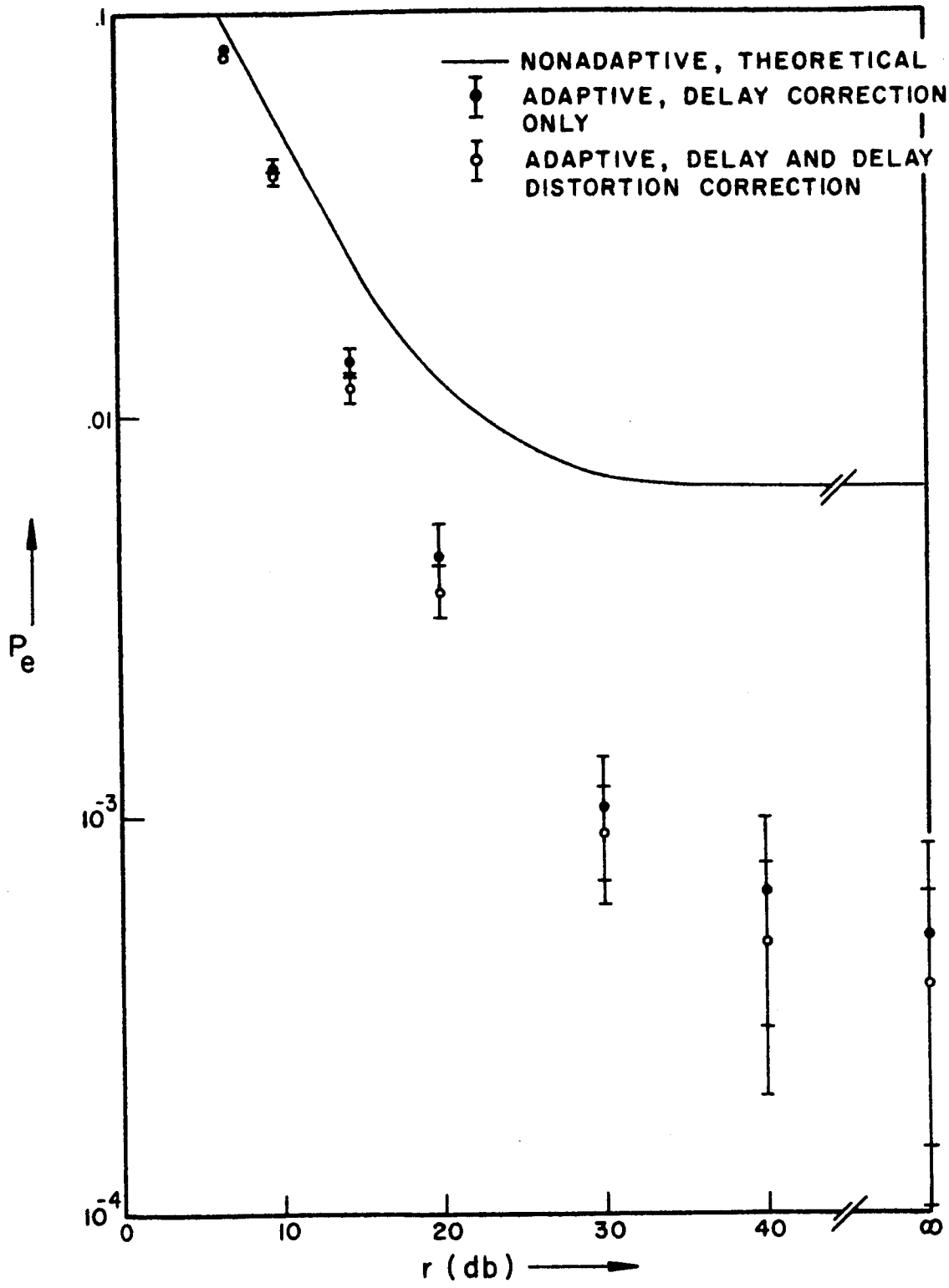

Figure 22. Performance of Nonadaptive and Adaptive Systems - d = 0.28.

each experiment, thus allowing a comparison to be made between them. Figure 20 shows us that the adaptive phase-correction systems do provide significant, measurable improvement in the error rate performance of our communication system at all SNR's. The relative improvement provided by these systems varies significantly from the low SNR region, where there is very little improvement, to the high SNR region, where a large improvement is apparent. The reason for this is that the adaptive systems being investigated here combat the effects of pulse distortion and intersymbol interference but do not change the effects of additive noise on the system. Thus, at lower SNR's where the additive noise effects are prevalent, very little improvement is noted. However, at high SNR's where distortion effects are most important, much greater improvement is noted. The relative improvement (ratio of adaptive error rate to nonadaptive error rate) at infinite SNR is about one-fourth for both systems.

Figure 20 also indicates that the improvement provided by correcting for linear delay distortion and delay is only slightly greater than that provided by correcting for delay alone. Compared to the improvement provided by the delay-correction system, the further improvement provided by the delay and delay distortion correction system is virtually insignificant. This indicates that the effect of the channel filter delay is much more important in the degrading of the

system's performance than the effect of linear delay distortion.

Figure 21 is a plot of the experimental performance of the two phase-adaptive systems along with the theoretical error probability of the nonadaptive system for d = 0.4. For each of the experimental curves in this graph, 1,500 channel samples were used. In general, the results shown by this graph are quite similar to those of Figure 20. We again note that both adaptive systems provide significant reductions in error rate at all SNR's when compared to the performance of the nonadaptive system. However, for this relative data rate, the irreducible error probability of the adaptive systems is roughly one-twentieth of the nonadaptive system's while it was only one-fourth of the nonadaptive error probability for d = 0.56. This means that the relative improvement of the adaptive system is far greater for d = .4 than for d = .56. We also note from this graph that the relative improvement of the delay and delay distortion correction system is only slightly greater than that of the delay-only correction system. As in the d = .56 case, the relative difference between the two systems compared to the improvement they show over the nonadaptive system is nearly insignificant. We do note, however, that for all SNR's except $r = \infty$, the estimated error rate of the delay and delay distortion correction system is lower than that for the delay correction system. This is, of course, the expected behavior

since we expect a greater degree of correction to yield a lower error rate.

Figure 22 is a graph of the same type of information as is shown in Figures 20 and 21, but in this plot the relative data rate is 0.28. For each of the experimental curves on this graph, 2,000 channel samples were used. The results shown in this graph indicate that the same basic behavior is occurring at this data rate as occurred at the other two data rates discussed above. We again notice a significant improvement in error probability performance of the adaptive systems compared to the non-adaptive one, the relative improvement being much greater for SNR's where signal distortion and intersymbol interference are of most importance. As before, only a small difference in performance exists between the two adaptive systems, with the delay and delay distortion correction system exhibiting consistently lower error rates than the system for delay correction only.

In this case we find that the relative improvement of the irreducible error probabilities for the two adaptive systems is only slightly smaller than it was in the d = .4 case, still being approximately one-twentieth. Thus the change in relative improvement at r = ∞ is not as great when comparing the d = .28 case with the d = .4 case as it is when the d = .4 and d = .56 cases are compared. However, when one considers the method we are using for representation of the channel's phase response function (approximation by the delay and linear delay distortion components only), it is

apparent that the representation, and therefore the correction, should improve as the signaling bandwidth becomes smaller. For this reason it is felt that the improvement afforded by the phase-correction schemes examined above should become greater as the relative data rate becomes smaller. As discussed above this conjecture does seem to be supported by the results of this section. From this reasoning, it is felt that the relative improvement of the adaptive systems at the data rates investigated here should represent the minimum relative improvement which should be attainable at lower relative data rates.

The information we have obtained in this section on the performance of the adaptive systems can be used to formulate some design examples which indicate the improvement which such systems can provide. We consider first the case of a system for which the SNR available at the receiver is constant and which must perform at or below some given error rate. In this case we can show that if r = 30 db, the maximum relative data rate for which $P_e \leq 10^{-3}$ is 0.09 for the nonadaptive system, while it is about .28 for either of the adaptive systems. Thus the data rate can be tripled without increasing the error rate. Similarly, if $r \geq 40$ db, the maximum relative data rate for $P_e \leq 10^{-3}$ is .125 for the nonadaptive system and about .37 for the adaptive systems. Again we see that the data rate can be nearly tripled.

If the transmitted power must be held constant and the error probability is required to be below some given value,

then a somewhat different situation arises since the product rd must be held constant. In this case we can show that for $P_e \leq 10^{-3}$ and for rd = 100, the maximum relative data rate for the nonadaptive system is .095, while it is 0.2 for the adaptive systems. If rd = 200 and the same error probability is desired, the maximum relative data rates become 0.125 and 0.24 respectively. Thus the data rate can be doubled in each of these cases with no increase in error probability. Finally, if rd > 500 and $P_e \leq 10^{-3}$, the maximum relative data rates become .125 for the nonadaptive system and .4 for the adaptive system. Thus the data rate can be more than tripled in this case.

5.4 Performance of a Physically Realizable Adaptive System

In Section 5.3, we considered an idealized adaptive receiver system for combating the effects of frequency selective fading. The idealizations involved in examining the system were:

1. The phase response function of the channel filter was measured perfectly at the frequencies of interest.
2. A perfect equalizer filter was available for delay and delay distortion correction.

In this section we will determine the effect of relaxing these idealizations so that the mathematical model becomes one which could be implemented with physical components. To do this, we will consider the effects on the system

performance of introducing additive noise in the phase measurement system and of employing a physically realizable phase equalization filter.

To obtain an understanding of the possible effects of additive noise in the measurement system, let us consider the SNR's which might be required for the phase detectors of this system. It is reasonable to assume that if the SNR at the input of a phase detector is greater than 20db, then virtually perfect measurement of the channel filter's phase shift can be achieved. In this case signal-to-noise ratio must be interpreted as the ratio of the power in the sinusoidal pilot tone to the average noise power at the detector input. Now the bandwidth of the predetection filtering system required for the pilot tone phase detectors should be set equal to the fading bandwidth of the medium. This allows the fluctuations of the pilot tone to pass through the filter but prevents all unnecessary additive noise from reaching the detector input. Since the additive noise is assumed to be white, it can be seen that the ratio of noise powers at the pilot tone and data channel detectors is just the ratio of the channel's fading bandwidth to the signaling bandwidth of the system. Now, if the data channel is operating at a SNR of 20-30db, very good phase response measurements can be obtained if the phase detector input SNR is equal to this. Therefore, good phase measurements could be obtained with each pilot tone having a power of $\frac{B_f}{B}$ times the data channel

power, where B_f is the channel's fading bandwidth. For a troposcatter system, the following values might apply

$$B_f = 10\text{Hz}$$

$$B_c = 1\ \text{MHz}$$

$$d = .2$$

In this case, the ratio of power required for both pilot tones to data channel power would be

$$\frac{2(10)}{.2(10^6)} = 10^{-4} = .1\%$$

Thus even if 10db more SNR were required for the pilot tone phase detectors than for the data channel, only 1% of the total transmitted power would be needed for the pilot tones. From the above discussion it is apparent that for many systems of practical interest, excellent measurement of the channel filter's phase response function can be obtained by using only a very small portion of the total transmitted power for pilot tone sounding of the channel. Thus, the additive noise in the channel measurement scheme will have negligible significance on the performance of the adaptive system we have studied.

We next investigate the effect of employing a physically realizable filter for the phase equalizer in the adaptive receiver. Although there are many possible schemes for implementing such an equalizer, we will consider only one. It is felt, however, that this scheme is representative of

the various possibilities which exist. We will assume that a bank of variable single-pole all-pass networks are to be used as the phase distortion equalizer. A single-pole (band-pass) all-pass network is specified by two poles and two zeros in its s-plane plot. The two poles are located at $s = -\alpha \pm j\omega_r$ and the two zeros at $s = \alpha \pm j\omega_r$. Because of the symmetrical nature of these pole-zero positions, the amplitude response function of the all-pass network is constant for all frequencies. Its phase response function, however, is given by

$$P_c(\omega) = -2\left[\tan^{-1}\left(\frac{\omega - \omega_r}{\alpha}\right) + \tan^{-1}\left(\frac{\omega + \omega_r}{\alpha}\right)\right] \qquad (5\text{-}5)$$

Thus the envelope delay function of N such networks in cascade is given by

$$\beta_c(\omega) = -\frac{d}{d\omega}\left[N \cdot P_c(\omega)\right] = 2N\alpha\left[\frac{1}{\alpha^2 + (\omega - \omega_r)^2} + \frac{1}{\alpha^2 + (\omega + \omega_r^2)}\right] \qquad (5\text{-}6)$$

It can be shown that if $\omega_r >> \alpha$, the envelope delay of the one-pole all-pass filter is a maximum at $\omega = \omega_r$ and that the value of the envelope delay at this point is $2/\alpha$ seconds.

Using the above facts, an algorithm for compensation of a channel's residual delay characteristics by N identical cascaded all-pass networks may be constructed as follows. Let ω_0 be the center frequency of the data channel and D be the measured residual delay. Then we adjust each filter so

that its center frequency equals ω_0 and its delay at ω_0 is exactly -D/N. Thus each filter is specified by the two equations

$$\omega_r = \omega_0 \tag{5-7}$$

$$\alpha = -2N/D \tag{5-8}$$

In order to determine how well the above filtering scheme would compare to the ideal adaptive filtering investigated in the previous section, the computer simulation program was modified to simulate the presence of the physically realizable all-pass networks in the receiver. The algorithm of Equations (5-7) and (5-8) was employed in the program. Tables 1 and 2 give the results of these simulations. In each of these tables, the estimated standard deviation of the error probability estimates is shown in parentheses next to the estimate. Table 1 shows the results of two simulations of the physically realizable systems along with the performance of the ideal delay correction receiver. The two physically realizable systems which were simulated contained one and three single-pole all-pass networks respectively. All of these experiments were performed with d = .4 and used the same set of 1,500 channel samples.

In this table, it can be seen that for both the three-network and the one-network equalizers, the performance is nearly identical to that of the ideal equalizer. Indeed, for low SNR's the error probability is slightly lower than that of the ideal system.

Table 1. Error Probabilities for Physically Realizable and Ideal Adaptive Systems - d = .4.

SNR	Ideal Delay Correction	Physically Realizable Delay Correction: One All-Pass Network	Physically Realizable Delay Correction: Three All-Pass Networks
10db	.0475(.00205)	.0464(.00214)	.0472(.00216)
20db	.00626(.00099)	.00593(.00086)	.00618(.00087)
30db	.00210(.00062)	.00202(.00055)	.00207(.00061)
40db	.00142(.00056)	.00135(.00055)	.00141(.00055)
∞	.00117(.00055)	.00117(.00055)	.00117(.00055)

Table 2. Error Probabilities for Physically Realizable and Ideal Adaptive Systems - d = .56.

SNR	Ideal Delay Correction	Physically Realizable Delay Correction - One All-Pass Network
10db	.0717(.0032)	.0689(.0026)
20db	.0209(.0023)	.0204(.0019)
30db	.0163(.0024)	.0153(.0019)
40db	.0156(.0025)	.0148(.0019)
∞	.0153(.0025)	.0148(.0020)

In Table 2 the results of computer simulations of the realizable system with one all-pass filter and of the ideal delay correction system are compared for $\bar{d} = 0.56$. Again we see that the performance of the two systems is almost identical. Thus we see that it is possible to construct physical networks of reasonable size which will serve quite well as the equalization filters in the adaptive systems proposed above. In fact, practically no difference in performance from the ideal performance shown here should be expected.

5.5 Summary

In this chapter it is shown that the experimental results of Chapter IV on the performance of the Gaussian fading system with amplitude distortion only can be interpreted as the performance of an ideal adaptive system which corrects perfectly for channel-induced phase distortion. The potential performance gains of such a system provided the motivation to develop a pilot tone measurement system and an approximate phase equalization technique - equalization for delay and linear delay distortion - to improve the performance of the nonadaptive selective fading system. Performance results were then obtained by computer simulation for the pilot tone adaptive system with ideal phase equalization filters for delay and delay distortion. It was shown that reductions in error rate by factors of five to twenty could be obtained with such a system operating between $d = 0.28$ and $d = 0.56$. Finally it was shown that a

physically realizable implementation of such a system can be expected to perform at virtually the same levels as the idealized pilot tone system.

CHAPTER VI: CONCLUDING REMARKS

6.1 Summary and Conclusions

This report has been directed toward a study of certain adaptive phase compensation receiver systems for selective fading channels. The evaluation of the error rate performance of such systems required experimental simulation techniques. For this reason, the research began with an exact analysis of the error rate properties of nonadaptive receiver systems in the presence of selective fading channels. This analysis was carried out for three different combinations of channel correlation function and transmitted pulse shape. The results of this analysis showed that significant differences in error rate performance can occur for different pulse shapes employed on the same fading channel while little difference in performance seems to occur when the same pulse shape is used with different channels.

The work of Sunde has important connections with the research carried out for this report. First, a basic assumption of Sunde's work - that the effect of phase distortion is much more important in Gaussian fading channels than that of amplitude distortion - is a basic idea in the formulation of the adaptive system presented herein. Second, Sunde's approximation to the error probability in a selective fading

communication system represents a great computational simplification over the more precise technique of Bello and Nelin. For these reasons, a careful formulation of the Sunde error rate approximation was carried out for this research. It was found that the Sunde approximation does not provide a good estimate of the error probability when the frequency selective fading is of importance.

The experimental phase of this work consisted of computer simulation of a communication system operating over a frequency selective channel. The simulation system was designed in such a way that extensive modifications of the channel structure or the receiver filter system could be implemented. The first experimental results showed that such a computer simulation provides good agreement with theoretically predicted error rates for nonadaptive systems operating over the Gaussian selective fading channel. Next experimental results were presented which show conclusively that the Sunde conjecture concerning the importance of phase distortion effects compared to amplitude distortion effects is true. This allowed the formulation of adaptive receiver systems which attempt to measure the instantaneous phase deviation present in a fading channel and to compensate for it. Two such systems were formulated - one which compensated only for delays introduced in the random channel filter and another which compensated for delays and linear delay distortion introduced in the channel filter. The computer simulation of these systems showed that for relative data rates

near 0.3, more than one order of magnitude improvement in error probability can be realized; while for relative data rates near 0.5, a factor of five in improvement of the error rate can be achieved. These results also showed that such systems provide an increase of two to three times in allowable data rate for fixed error probability when the system SNR is reasonably high. It was found that correction for delay and delay distortion offered little more improvement than correction for delay alone. It was also shown that a physically realizable implementation of the adaptive delay-correction system can be expected to perform at virtually the same levels as the idealized pilot tone system.

In conclusion, this research has contributed to the general understanding of the performance of communication systems in the presence of selective fading channels, pointed out some errors which have been made in previous analysis attempts for such systems, and has indicated a practical method which is capable of rendering significant improvement to the irreducible error rate performance of some such systems.

6.2 Recommendations for Future Investigation

The results of this research have suggested several investigations which would be of interest. The first of these is an investigation of the design problems which would be associated with the implementation of a phase correction receiver system for selective fading channels. One of the

most important of these problems concerns the implementation of a variable filter system to compensate for the phase distortion. An interesting aspect of this problem is that integrated circuit technology may provide an easily-implementable method of constructing such a phase correction system. It may be possible to design and economically mass produce a single phase correction circuit with the property that a number of such circuits could be cascaded to compensate for a given degree of phase distortion. In this case a switching system could then be constructed to "switch in" the proper number of such circuits in order to effectively cancel the measured phase distortion.

Another question which naturally arises from the results of this research concerns the usefulness of representation of the channel phase response function in terms of cubic or higher-order polynomials. Using the measurement techniques presented in this report, this would require more than two pilot tones for the channel measurement systems, but it is possible that in FDM systems it would be natural to place one pilot tone in the guard band between each data channel - thus easily allowing the extension to higher order polynomials for representation.

The results of Chapter II provide two interesting topics of investigation. The first of these arises from the fact that a significant difference was noted in the irreducible error rates for two different signal shapes when used with the same fading channel. This indicates that the problem of

choosing an optimum pulse shape for digital signaling over selective fading channels may be a fruitful one.

In connection with this problem, it is encouraging to note that our results have indicated that the performance of a given signal over different channels may not vary greatly. Thus there is some reason to believe that a signal which is optimum for one channel model may yield very good performance with other channels.

The second topic of investigation is related to the fact that the conditional probabilities (the p_{abcd}'s) were found to approach unequal limits as the SNR becomes infinite. Indeed, p_{1111} and p_{0101} approach zero while the other four conditional probabilities approach nonzero limits. From this, it appears that if one were constructing an encoding scheme to encode multilevel data (such as the output of a PCM quantizer) into binary data, it would be highly desirable to encode the most significant data digits in such a way that they result in the sequences with the lowest total error probability. It would be of interest to determine the performance of a system using such a coding scheme and compare this to the performance resulting from the use of the conventional methods.

Finally, it is necessary to point out that all the research described in this report has been based on the assumption of a Gaussian fading channel model. Therefore the usefulness of our results is probably in direct proportion to the degree to which the Gaussian fading channel model

approximates the effects of physical channels. It is felt that analysis work such as that in this report must procede hand-in-hand with channel characterization investigations designed to indicate the usefulness and weak points of such analysis. Among the channel characterization problems which should be investigated are:

1. Can any of the common scatter/multipath channels be assumed to possess Gaussian fading statistics?
2. If so, then what is a good frequency correlation function to use in mathematically representing such channels?
3. If such channels do not possess Gaussian statistics, is it still possible to predict system performance over such channels (such as error probabilities) by approximating the channel as Gaussian?
4. Is it possible that a relatively simple channel model, such as a two-path model, can predict the performance of a selective fading communication system as well as or better than a more complicated one?
5. For engineering applications, is it possible to characterize a fading channel by a few parameters (such as coherence bandwidth) in order to roughly predict a system's performance?

It is felt that there are a large number of such problems in channel characterization whose results should have definite bearing on the research being done on selective fading communication systems, and that similarly, the results of such analytical investigations will help to point out the significant areas of channel characterization research.

LIST OF REFERENCES

LIST OF REFERENCES

1. Schwartz, M., W. R. Bennet, and S. Stein. Communication Systems and Techniques, McGraw-Hill Book Co., Inc., New York, Ch. 9, 1966.

2. Lebow, I. L., P. R. Drouilhet, N. L. Daggett, J. N. Harris, and F. Nagy. "The West Ford Belt as a Communications Medium," Proceedings of the IEEE, Vol. 52, pp. 543-563, May, 1964.

3. Anderson, R. E. "Sideband Correlation of Lunar and Echo Satellite Reflection Signals in the 900-Mc. Range," Proceedings of the IRE, Vol. 49, pp. 1081-1082, June, 1961.

4. Watterson, C. C., J. R. Juroshek, and L. J. Demmer. "SHF Bandwidth Study - Phase III," NBS Report 8842, National Bureau of Standards, Boulder Colorado, July 22, 1965.

5. Bello, P. A. and B. D. Nelin. "The Effect of Frequency Selective Fading on the Binary Error Probabilities of Incoherent and Differentially Coherent Matched Filter Receivers," IEEE Transactions on Comm. Systems, Vol. CS-11, pp. 170-186, June, 1963. See also Corrections, IEEE Transactions on Comm. Systems, Vol. COM-12, p. 230, Dec., 1964.

6. Sunde, E. D. "Digital Troposcatter Transmission and Modulation Theory," Bell System Tech. Journal, Vol. 43, pp. 143-214, Jan., 1964 (Part I).

7. Hingorani, G. D. "Error Rates for a Class of Binary Receivers," IEEE Transactions on Comm. Tech., Vol. COM-15, pp. 209-215, April, 1967.

8. Schwartz, M., W. R. Bennett, and S. Stein. Communication Systems and Techniques, McGraw-Hill Book Co., Inc., New York, Ch. 8, 1966.

9. Walker, W. F. "The Error Performance of a Class of Binary Communication Systems in Fading and Noise," IEEE Transactions on Comm. Systems, Vol. CS-12, pp. 28-45, March, 1964.

10. Hancock, J. C. and G. D. Hingorani. "A Transmitted Reference System for Communication in Random or Unknown Channels," IEEE Transactions on Comm. Tech., Vol. COM-13, pp. 293-301, Sept., 1965.

11. Hancock, J. C. and G. D. Hingorani. "A Sequential Transmitted Reference System for Communication in Random or Unknown Channels," Convention Record, First Annual IEEE Communications Convention, Boulder, Colorado, June, 1965.

12. Spilker, J. J. "Some Effects of a Random Channel on Transmitted Reference Signals," IEEE Transactions on Comm. Tech., Vol. COM-13, pp. 377-379, Sept., 1965.

13. Price, R. and P. E. Green. "A Communication Technique for Multipath Channels," Proceedings of the IRE, Vol. 46, pp. 555-570, March, 1958.

14. Hollis, James L. "An Experimental Equipment to Reduce Teleprinter Errors in the Presence of Multipath," IRE Transactions on Comm. Systems, Vol. CS-7, pp. 185-188, Sept., 1959.

15. Aein, J. M. and J. C. Hancock. "Reducing the Effects of Intersymbol Interference with Correlation Receivers," IEEE Transactions on Information Theory, Vol. IT-9, pp. 167-175, July, 1963.

16. Schwarzlander, H. and J. C. Hancock. "Signal Optimization for Digital Communication over Channels with Memory," Convention Record, Symposium on Signal Transmission and Processing, pp. 56-61, Columbia University, New York, 1965.

17. Quincy, E. A. and J. C. Hancock. "Jointly Optimum Waveforms and Receivers for Channels with Memory," Technical Report TR-EE 66-7, Purdue University, Lafayette, Indiana, June, 1966.

18. Rappeport, M. A. "Automatic Equalization of Data Transmission Facility Distortion Using Transversal Equalizers," IEEE Transactions on Comm. Tech., Vol. COM-12, pp. 65-73, Sept., 1964.

19. Lucky, R. W. "Automatic Equalization for Digital Communication Systems," Bell System Tech. Journal, Vol. 44, pp. 547-588, April, 1965.

20. Lucky, R. W. "Techniques for Adaptive Equalization of Digital Communication Systems," Bell System Tech. Journal, Vol. 45, pp. 255-286, Feb., 1966.

21. Schreiver, K. E., H. L. Funk, and E. Hopner. "Automatic Distortion Correction for Efficient Pulse Transmission," IBM Journal of Res. and Dev., Vol. 9, pp. 20-30, Jan., 1965.

22. Gorog, E. "A New Approach to Time-Domain Equalization," IBM Journal of Res. and Dev., Vol. 9, pp. 228-232, July, 1965.

23. Stein, S. "Theory of a Tapped Delay Line Fading Simulator," Convention Record, First Annual IEEE Communications Convention, pp. 601-607, Boulder, Colorado, June, 1965.

24. Bello, P. A. and B. D. Nelin. "Predetection Diversity Combining with Selectively Fading Channels," IRE Transactions on Comm. Systems, Vol. CS-10, pp. 32-42, March, 1962.

25. Bello, P. A. "Some Techniques for the Instantaneous Real-Time Measurement of Multipath and Doppler Spread," IEEE Transactions on Comm. Tech., Vol. COM-13, pp. 285-292, Sept., 1965.

26. Bartlett, M. S. An Introduction to Stochastic Processes, Cambridge University Press, New York, Section 5.11, 1955.

27. Cochran, W. G. Sampling Techniques, Second edition, John Wiley and Sons, New York, Sections 2.7 and 2.13, 1963.

28. Proakis, J. G., P. R. Drouilhet, Jr., and R. Price. "Performance of Coherent Detection Systems Using Decision Directed Channel Measurement," IEEE Transactions on Comm. Systems, Vol. CS-12, pp. 54-63, March, 1964.

29. Abramowitz, M. and I. A. Stegun. Handbook of Mathematical Functions, Dover Publications, Inc., New York, p. 231, 1965.

30. Bailey, C. C. "Tapped Delay Line Simulation of Randomly Time-Variant Channels," Memorandum Report 66-2, Electronic Systems Research Laboratory, School of Electrical Engineering, Purdue University, Lafayette, Indiana, Sept., 1966.

31. Stein, S. "The Q Function and Related Integrals," Research Report No. 467, Applied Research Laboratory, Sylvania Electronic Systems, Waltham, Mass.

32. DiDonato, A. R. and M. P. Jarnagin. "A Method for Computing the Circular Coverage Function," Mathematics of Computaion, Vol. 16, pp. 347-355, July, 1962.

33. Weingarten, Harry and A. R. DiDonato. "A Table of Generalized Circular Error," Mathematics of Computation, Vol. 15, pp. 169-173, April, 1961.

APPENDIX A

ERROR PROBABILITY CALCULATIONS FOR THE G-F CHANNEL AND SQUARE PULSE SIGNALING

APPENDIX A

ERROR PROBABILITY CALCULATIONS FOR THE G-F CHANNEL AND SQUARE PULSE SIGNALING

In this appendix we show some of the details of the calculation of the error probability expression for the G-F channel with square pulse signaling. Examination of Equation (2-8) shows that this requires that we compute the three moments $\overline{u^*v}$, $\overline{|u|^2}$, and $\overline{|v|^2}$ conditioned on the various given modulation sequences S. These moments, when used with Equations (2-8), (2-7), (2-4), and (2-5) respectively, yield the desired error probability. For computing these three desired moments, it is convenient to set up the following notation:

$$
\begin{aligned}
m_{11}^{abcd} &= \overline{|u|^2} \quad \text{given} \quad S = (a,b,c,d) \\
m_{00}^{abcd} &= \overline{|v|^2} \quad \text{given} \quad S = (a,b,c,d) \qquad \text{(A-1)} \\
m_{10}^{abcd} &= \overline{u^*v} \quad \text{given} \quad S = (a,b,c,d)
\end{aligned}
$$

Now it can be shown that these three moments can all be computed from the following relation (5):

$$m_{rs}^{abcd} = \int_{-\infty}^{\infty} p(\tau) B_r^{abcd}(\tau) [B_s^{abcd}(\tau)]^* d\tau + 32EN_0\delta_{rs}$$

$$a,b,c,d,r,s = 0,1 \qquad \text{(A-2)}$$

where $p(\tau)$ is the delay spread correlation function defined by Equation (1-4), δ_{rs} is the Kronecker delta, and where B is given by

$$B_k^{abcd}(\tau) = \int_{-\infty}^{\infty} x^*_{abcd}(t - kT_b)[s_1(t + \tau) - s_0(t + \tau)]dt \qquad \text{(A-3)}$$

Here $x_{abcd}(t)$ is the transmitted signal (see Figure 1) given that S = (a,b,c,d) and s_0 and s_1 are the pulse signals discussed in Section 1.4. For the case which we are considering, s_0 and s_1 are real and anticorrelated, so we may simplify (A-1) to

$$B_k^{abcd}(\tau) = 2\int_{-\infty}^{\infty} x^*_{abcd}(t-kT_b)s(t+\tau)dt \qquad \text{(A-4)}$$

where

$$s_1(t) = s(t) = -s_0(t)$$

We now recall that the square pulse was defined in Equation (2-12) by

$$s(t) = \begin{cases} \sqrt{2E/T_b} & , \quad 0<t<T_b \\ 0 & , \quad \text{otherwise} \end{cases} \qquad \text{(A-5)}$$

Substituting (A-5) into (A-4) the following B functions are obtained:

$$B_0^{1111}(\tau) = 4E \quad , \quad |\tau| < T_b$$

$$B_1^{1111}(\tau) = 4E \quad , \quad |\tau| < T_b$$

$$B_0^{0110}(\tau) = \begin{cases} 4E(1 + 2\tau/T_b) & , -T_b < \tau \leq 0 \\ 4E & , 0 < \tau < T_b \end{cases}$$

$$B_1^{0110}(\tau) = \begin{cases} 4E & , -T_b < \tau \leq 0 \\ 4E(1 - 2\tau/T_b) & , 0 < \tau < T_b \end{cases}$$

$$B_0^{0111}(\tau) = 4E \quad , \quad |\tau| < T_b$$

$$B_1^{0111}(\tau) = B_1^{0110}(\tau) \quad , \quad |\tau| < T_b$$

$$B_0^{0101}(\tau) = 4E(-1 + 2|\tau|/T_b), \quad |\tau| < T_b$$

$$B_1^{0101}(\tau) = 4E(1 - 2|\tau|/T_b), \quad |\tau| < T_b$$

$$B_0^{1100}(\tau) = -B_1^{0110}(\tau) \quad , \quad |\tau| < T_b$$

$$B_1^{1100}(\tau) = B_0^{0110}(\tau) \quad , \quad |\tau| < T_b$$

$$B_0^{0100}(\tau) = B_0^{1100}(\tau) \quad , \quad |\tau| < T_b$$

$$B_1^{0100}(\tau) = B_1^{0101}(\tau) \quad , \quad |\tau| < T_b$$

In Equation (2-10) the delay spread correlation function for the G-F channel is given by

$$p(\tau) = \sigma_0^2 \sqrt{\pi} B_c \exp[-(\pi B_c \tau/2)^2] \qquad \text{(A-7)}$$

We must now evaluate the various required moments using Equation (A-2). This equation requires integration over the

infinite interval on τ. However, the B functions are evaluated in (A-6) only for $|\tau| < T_b$, i.e., only adjacent-baud intersymbol interference is accounted for. We therefore will approximate the moments by using Equation (A-2) but inserting in it the B-function expressions in (A-6) instead of exact B functions which would be valid for all τ. This approximation is justifiable if the $p(\tau)$ term in the integrand has tails which are extremely small for $|\tau| > T_b$. This condition should be assured if the e^{-2} point on the $p(\tau)$ function is not allowed to exceed T_b. This will insure that at least 99.5% of the area under the $p(\tau)$ function will lie in the region $|\tau| < T_b$. We therefore require

$$\frac{4}{\pi B_c} < T_b$$

or

$$d = \frac{1}{T_b B_c} < \frac{\pi}{4} = .786$$

This inequality gives the condition for which the exact B functions can be replaced in (A-2) by B functions which take into account only adjacent-baud intersymbol interference. Thus, we can interpret this restriction as indicating the range of data rates for which the intersymbol interference is essentially entirely caused by pulse overlap from only adjacent bauds. Using the above approximation, the following values are found for the required conditional moments.

$$\underline{1111} \quad m_{00}^{1111} = 32E(\sigma_0^2 E + N_0)$$

$$m_{11}^{1111} = m_{00}^{1111}$$

$$m_{10}^{1111} = 32\sigma_0^2 E^2$$

$$\underline{0110} \quad m_{00}^{0110} = 32\sigma_0^2 E^2(1-4c_1 d+4c_2 d^2) + 32\,EN_0$$

$$m_{11}^{0110} = m_{00}^{0110}$$

$$m_{10}^{0110} = 32\sigma_0^2 E^2(1 - 4c_1 d)$$

$$\underline{0111} \quad m_{00}^{0111} = m_{00}^{1111}$$

$$m_{11}^{0111} = m_{00}^{0110}$$

$$m_{10}^{0111} = 32\sigma_0^2 E^2(1 - 2c_1 d) \qquad \text{(A-8)}$$

$$\underline{0101} \quad m_{00}^{0101} = 32\sigma_0^2 E^2(1-8c_1 d+8c_2 d^2) + 32EN_0$$

$$m_{11}^{0101} = m_{00}^{0101}$$

$$m_{10}^{0101} = -32\sigma_0^2 E^2(1 - 8c_1 d + 8c_2 d^2)$$

$$\underline{1100} \quad m_{00}^{1100} = m_{00}^{0110}$$

$$m_{11}^{1100} = m_{00}^{0110}$$

$$m_{10}^{1100} = -m_{10}^{0110}$$

$$\underline{0100} \quad m_{00}^{0100} = m_{00}^{0110}$$

$$m_{11}^{0100} = m_{00}^{0101}$$

$$m_{10}^{0100} = -32\sigma_0^2 E^2(1 - 6c_1 d + 4c_2 d^2)$$

where $c_1 = 1/\pi\sqrt{\pi}$, and $c_2 = 1/\pi^2$.

We can now use the moment expression of (A-8) in Equation (2-8) to obtain the following values for the R's. Recalling that $r = \sigma_0^2 E/N_0$, we find

$$R_{1111} = 2r$$

$$R_{0110} = \frac{2r(1 - 4c_1 d)}{1 + r(4c_2 d^2)}$$

$$R_{0111} = \frac{2r(1 - 2c_1 d)}{\sqrt{1 + 2rE(d) + r^2 H(d)} - r(1 - 2c_1 d)}$$

with $$E(d) = 1 - 2c_1 d + 2c_2 d^2$$

$$H(d) = 1 - 4c_1 d + 4c_2 d^2$$

$$R'_{0101} = 2r(1 - 8c_1 d + 8c_2 d^2) \qquad \text{(A-9)}$$

$$R'_{1100} = \frac{2r(1 - 4c_1 d)}{1 + r(4c_2 d^2)}$$

$$R'_{0100} = \frac{2r(1 - 6c_1 d + 4c_2 d^2)}{\sqrt{1 + 2rA(d) + r^2 B(d)} - r(1 - 6c_1 d + 4c_2 d^2)}$$

with $$A(d) = 1 - 6c_1 d + 6c_2 d^2$$

$$B(d) = 1 - 12c_1 d + (12c_2 + 32c_1^2)d^2 - 64c_1 c_2 d^3 + 32c_2^2 d^4$$

It is desirable to simplify the somewhat unwieldy expressions for R_{0111} and R'_{0100}. To develop such a simplification we will make use of the power series

$$\sqrt{1 + x} = 1 + \frac{1}{2}x - \frac{1}{2}\cdot\frac{1}{4}x^2 + \frac{1}{2}\cdot\frac{1}{4}\cdot\frac{3}{6}x^3 - \ldots \qquad \text{(A-10)}$$

which we will truncate after the first three terms since the quantity x will be required to be much less than 1. In the

expression for R_{0111}, we are interested in

$$\sqrt{1 + 2rE(d) + r^2H(d)} = \sqrt{1+2r(1-2c_1d+2c_2d^2) + r^2(1-4c_1d+4c_2d^2)}$$

$$= (1 + r)\sqrt{1-4c_1dg(r)+4c_2d^2g(r)} \qquad \text{(A-11)}$$

where

$$g(r) = r/(1+r)$$

Using (A-10) in (A-11) and dropping all terms of order d^3 and higher, we obtain

$$\sqrt{1 - 4c_1dg(r) + 4c_2d^2g(r)} = 1-2c_1dg(r)+2d^2[c_2g(r)- c_1^2g^2(r)] \qquad \text{(A-12)}$$

Thus R_{0111} becomes

$$R_{0111} = \frac{2r(1 - 2c_1d)}{(1+r)\{1-2c_1g(r)d + 2d^2[c_2g(r)-c_1^2g^2(r)]\}-r(1-2c_1d)} \qquad \text{(A-13)}$$

In the expression for R'_{0100}, we are interested in

$$\sqrt{1 + 2rA(d) +r^2B(d)} =$$

$$\sqrt{1+2r(1-6c_1d+6c_2d^2)+r^2[1-12c_1d+(12c_2+32c_1^2)d^2-64c_1c_2d^3+32c_2^2d^4]} \qquad \text{(A-14)}$$

Using techniques identical to those above, we obtain

$$R'_{0100} \approx \frac{2r(1 - 6c_1 d + 4c_2 d^2)}{(1+r)\{1-6c_1 g(r)d+2d^2[3c_2 g(r)-c_1^2 g^2(r)]\}-r(1-6c_1 d+4c_2 d^2)} \qquad \text{(A-15)}$$

The above approximations have been used in the expressions of Equation (2-15).

All the generalized SNR's which have been found here except for R_{1111} differ from those of Bello and Nelin. In Figure 23, the irreducible error probability computed from the expressions of this appendix and from Bello and Nelin's expressions are compared. As can be seen, there is a discernable difference between the two results, although they differ by less than an order of magnitude.

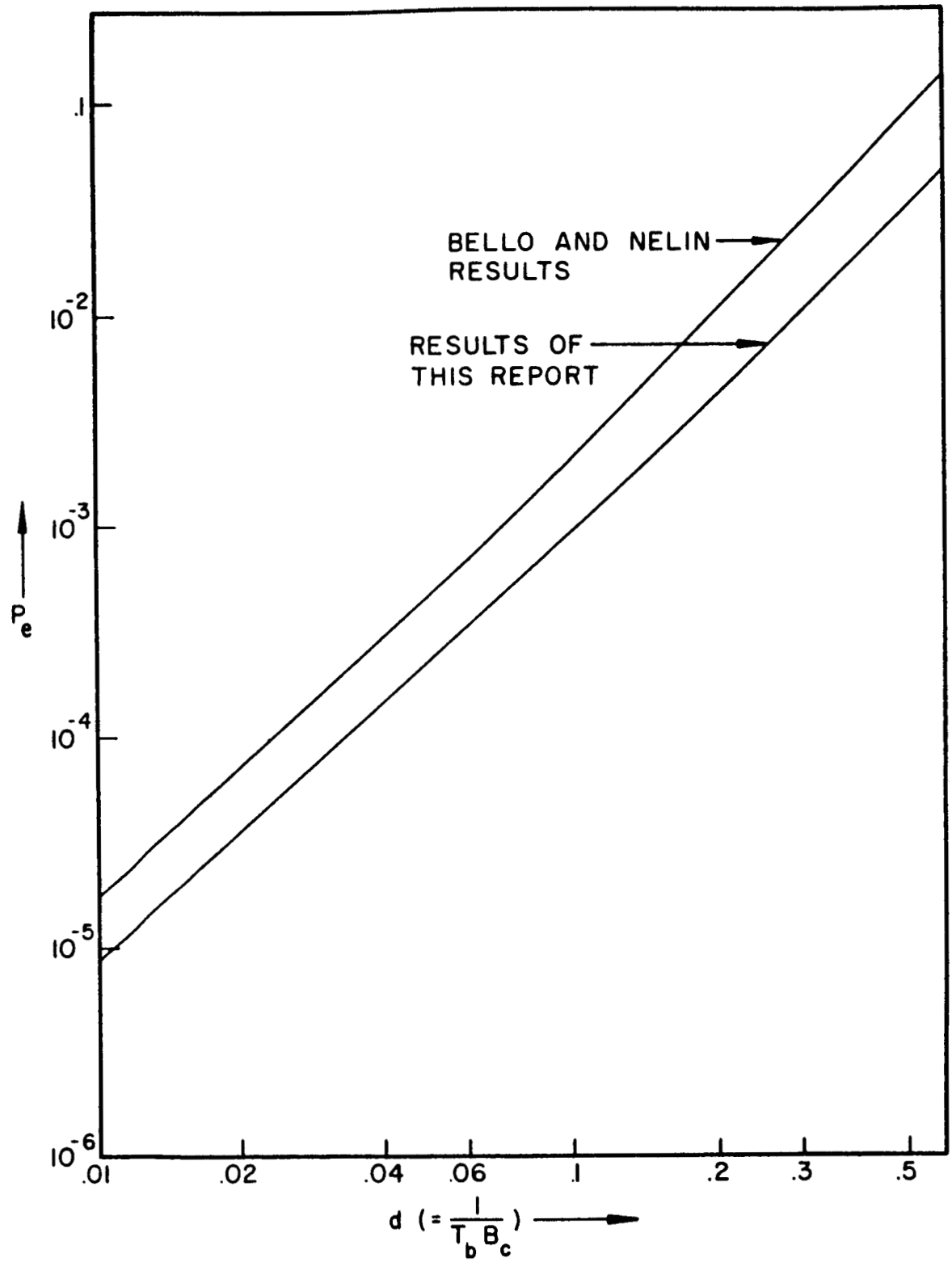

Figure 23. Comparison of Irreducible Error Probability from Bello and Nelin's Results and from Results of this Report.

APPENDIX B

ERROR PROBABILITY CALCULATIONS FOR THE S-F CHANNEL AND SQUARE PULSE SIGNALING

APPENDIX B

ERROR PROBABILITY CALCULATIONS FOR THE S-F CHANNEL AND SQUARE PULSE SIGNALING

In this appendix, details of the error probability calculations for the S-F channel with square pulse signaling are presented. Much of this work parallels the developments of Appendix A, and some reference to equations in that appendix will be necessary. Since the work of both Appendix A and this appendix are concerned with square pulse signaling, an examination of Equations (A-2) and (A-4) shows that the B functions of Appendix A will be identical to the B functions required for this work. Furthermore, we see that in evaluating the conditional moments through the use of (A-2), the only change required from the previous work is to replace $p(\tau)$ for the G-F channel by $p(\tau)$ for the S-F channel. From Equation (2-11), it can be seen that the delay spread correlation function for the S-F channel is given by

$$p(\tau) = \begin{cases} R_0 & , |\tau| \leq T_m \\ 0 & , |\tau| > T_m \end{cases} \qquad \text{(B-1)}$$

Using this expression in (A-2) yields

$$m_{rs}^{abcd} = R_0 \int_{-T_m}^{T_m} B_r^{abcd}(\tau)[B_s^{abcd}(\tau)]^* d\tau + 32EN_0\delta_{rs} \qquad (B-2)$$

At this point we note that since the B functions have been given in (A-6) only for values of τ less than T_b in absolute value, the integral in (B-2) can only be evaluated if $T_m < T_b$. Since we have defined $d = \frac{T_m}{T_b}$ in this case, we see that we now have the restriction

$$d \leq 1$$

We note that unlike the situation encountered in Appendix A, no approximation is required to evaluate (B-2) as long as the above restriction is met. Thus, this restriction can be considered to define the range of d for which our adjacent-baud intersymbol interference analysis will be valid, or equivalently it is the range of d over which we are assured that adjacent-baud overlap is the only source of intersymbol interference in the system.

When the B functions of (A-6) are substituted into (B-2), it is found that the resulting expressions greatly resemble the expressions obtained in (A-8) of Appendix A. The resemblance comes from the fact that corresponding to each power of d in the expressions of (A-8) there is a similar power of d in the corresponding evaluation of (B-2), only the coefficient of the term being different. Thus, (B-2) could be

evaluated by making the following substitutions in the expressions of (A-8).

$$\sigma_0^2 \longrightarrow R_0 T_m$$

$$d/\pi\sqrt{\pi} \longrightarrow d/4$$

$$d^2/\pi^2 \longrightarrow d^2/6$$

The conditional moments are thus found to be

$$\underline{1111} \quad m_{00}^{1111} = 32E(R_0 E T_m + N_0)$$

$$m_{11}^{1111} = m_{00}^{1111}$$

$$m_{10}^{1111} = 32R_0 T_m E^2$$

$$\underline{0110} \quad m_{00}^{0110} = 32R_0 T_m E^2 (1-4c_3 d+4c_4 d^2) + 32EN_0$$

$$m_{11}^{0110} = m_{00}^{0110}$$

$$m_{10}^{0110} = 32R_0 T_m E^2 (1 - 4c_3 d)$$

$$\underline{0111} \quad m_{00}^{0111} = m_{00}^{1111}$$

$$m_{11}^{0111} = m_{00}^{0110}$$

$$m_{10}^{0111} = 32R_0 T_m E^2 (1 - 2c_3 d)$$

$$\underline{0101} \quad m_{00}^{0101} = 32R_0 T_m E^2 (1-8c_3 d+8c_4 d^2)+32EN_0 \qquad \text{(B-3)}$$

$$m_{11}^{0101} = m_{00}^{0101}$$

$$m_{10}^{0101} = -32R_0 T_m E^2 (1 - 8c_3 d + 8c_4 d^2)$$

$$\underline{1100} \qquad m_{00}^{1100} = m_{00}^{0110}$$

$$m_{11}^{1100} = m_{00}^{0110}$$

$$m_{10}^{1100} = -m_{10}^{0110}$$

$$\underline{0100} \qquad m_{00}^{0100} = m_{00}^{0110}$$

$$m_{11}^{0100} = m_{00}^{0101}$$

$$m_{10}^{0100} = -32R_0T_mE\ (1 - 6c_3d + 4c_4d^2)$$

where

$$c_3 = 1/4$$

$$c_4 = 1/6$$

We can now use the above moment expressions in Equation (2-8) to obtain the following values for the R's. Because of the great similarity in the basic form of the expressions for the m's in (A-8) and (B-3), we also find a similarity in the forms for the R's of Equation (A-9) and for the present case. Recalling that r is now given by R_0T_mE/N_0, we find

$$R_{1111} = 2r$$

$$R_{0110} = \frac{2r(1 - 4c_3d)}{1 + r(4c_4d^2)}$$

$$R_{0111} = \frac{2r(1 - 2c_3d)}{\sqrt{1 + 2rE(d) + r^2H(d)} - r(1 - 2c_3d)}$$

with

$$E(d) = 1 - 2c_3 d + 2c_4 d^2$$

$$H(d) = 1 - 4c_3 d + 4c_4 d^2$$

$$R'_{0101} = 2r(1 - 8c_3 d + 8c_4 d^2)$$

$$R'_{1100} = \frac{2r(1 - 4c_3 d)}{1 + r(4c_4 d^2)}$$

$$R'_{0100} = \frac{2r(1 - 6c_3 d + 4c_4 d^2)}{\sqrt{1 + 2rA(d) + r^2 B(d)} - r(1-6c_3 d+4c_4 d^2)}$$

with

$$A(d) = 1 - 6c_3 d + 6c_4 d^2$$

$$B(d) = 1-12c_3 d+(12c_4+32c_3^2)d^2-64c_3 c_4 d^3 + 32c_4^2 d^4$$

(B-4)

As was the case in Appendix A, it is possible to simplify the expressions for R_{0111} and R_{0100}. Since we are dealing with expressions which are identical in form to those of Appendix A, we can write the approximations for R_{0111} and R_{0100} directly as

$$R_{0111} = \frac{2r(1 - 2c_3 d)}{(1 + r)\{1 + 2c_3 g(r)d+2d^2[c_4 g(r)-c_3^2 g^2(r)]\}-r(1-2c_3 d)}$$

$$R'_{0100} = \frac{2r(1 - 6c_3 d + 4c_4 d^2)}{(1+r)\{1-6c_3 g(r)d+2d^2[3c_4 g(r)-c_3^2 g^2(r)]\}-r(1-6c_3 d+4c_4 d^2)}$$

These approximations have been used in the expressions of Equation (2-19).

APPENDIX C

ERROR PROBABILITY CALCULATIONS FOR THE S-F CHANNEL AND RAISED COSINE SIGNALING

In this appendix, details of the error probability calculations for the S-F channel with raised cosine signaling are presented. The general method for carrying out these calculations is the same as that used in Appendix A, but the use of the raised cosine signal causes significant changes in the way the computation must be carried out.

As was the case in Appendix A, we first note that Equation (2-8) calls for us to compute the three moments $\overline{u^*v}$, $\overline{|u|^2}$, and $\overline{|v|^2}$ conditioned on the various possible transmitted sequences. Using the definitions of Equation (A-1), we find that the conditional moments can be evaluated by evaluating Equations (A-2) and (A-3). The B functions of (A-3) can be determined by considering the raised cosine signal as given in Equation (2-14)

$$s(t) = \sqrt{2BE}\,[\mathrm{sinc}(2Bt-\tfrac{1}{2})+\mathrm{sinc}(2Bt-\tfrac{3}{2})] \qquad (C\text{-}1)$$

Now the B functions of (A-4) are given by

$$B_k^{abcd}(\tau) = 2\int_{-\infty}^{\infty} x^*_{abcd}(t-kT_b)\,s(t+\tau)\,dt \qquad (C\text{-}2)$$

where $x_{abcd}(t)$ is the transmitted signal given S = (a,b,c,d). We can write $x_{abcd}(t)$ in terms of s(t) as follows

$$x_{abcd}(t) = \sum_{i=1}^{4} s_i s[t + (3 - i)T_b] \qquad (C-3)$$

$$a,b,c,d = 0,1$$

where

$$\begin{aligned} s_1 &= 2a - 1 \\ s_2 &= 2b - 1 \\ s_3 &= 2c - 1 \\ s_4 &= 2d - 1 \end{aligned} \qquad (C-4)$$

Thus the B functions can be written

$$B_k^{abcd}(\tau) = 2 \sum_{i=1}^{4} s_i \int_{-\infty}^{\infty} s^*[t + (3 - i - k)T_b]s(t + \tau)dt$$

$$= 2 \sum_{i=1}^{4} s_i I(3 - i - k, \tau) \qquad (C-5)$$

where

$$I(j,\tau) \equiv \int_{-\infty}^{\infty} s^*(t + jT_b)s(t + \tau)dt \qquad (C-6)$$

Substituting (C-1) into (C-6) and using the fact that

$$\int_{-\infty}^{\infty} \text{sinc}(x + a)\text{sinc}(x + b)dx = \text{sinc}(a - b)$$

we find

$$I(j,\tau) = 2E\left[\tfrac{1}{2}\,\mathrm{sinc}(2B\tau-2j-1) + \mathrm{sinc}(2B\tau-2j) + \tfrac{1}{2}\,\mathrm{sinc}(2B\tau-2j+1)\right] \tag{C-7}$$

The B functions can now be used to compute the conditional moments with the aid of Equation (A-2)

$$m_{rs}^{abcd} = \int_{-\infty}^{\infty} p(\tau) B_r^{abcd}(\tau)\,[B_s^{abcd}(\tau)]^* d\tau + 32EN_0\delta_{rs}$$

$$a,b,c,d,r,s = 0,1 \tag{C-8}$$

Substituting the $p(\tau)$ function for the S-F channel [see Equation (B-1)], and the B-function expression of (C-5), we obtain

$$m_{rs}^{abcd} = R_0 \int_{-T_m}^{T_m} B_r^{abcd}(\tau)\,[B_s^{abcd}(\tau)]^* d\tau + 32EN_0\delta_{rs}$$

$$= 4R_0 \sum_{i=1}^{4} \sum_{k=1}^{4} s_i s_k \int_{-T_m}^{T_m} I(3-i-r,\tau) I^*(3-k-s,\tau) d\tau + 32EN_0\delta_{rs}$$

$$= 4R_0 \sum_{i=1}^{4} \sum_{k=1}^{4} s_i s_k J(3-i-r,3-k-s,T_m) + 32\,EN_0\delta_{rs} \tag{C-9}$$

where

$$J(m,u,L) \equiv \int_{-L}^{L} I(m,\tau) I^*(u,\tau) d\tau \tag{C-10}$$

The problem of evaluating the required conditional moments now becomes one of evaluating the J functions. To do this, we first reduce J to a sum of finite convolutions of sinc functions. These convolution integrals are then evaluated in terms of known functions. When (C-6) is substituted into (C-10), the J function becomes

$$J(m,u,L) = 4E^2 \sum_{j=-1}^{1} \sum_{n=-1}^{1} (1 - \tfrac{1}{2}|j|)(1-\tfrac{1}{2}|n|) \int_{-L}^{L} \operatorname{sinc}(2B\tau-2m+j) \cdot \operatorname{sinc}(2B\tau - 2u + n)\,d\tau$$

$$= 4E^2 \sum_{j=-1}^{1} \sum_{n=-1}^{1} (1- \tfrac{1}{2}|j|)(1- \tfrac{1}{2}|n|)K(j-2m,n-2u,2BL) \qquad \text{(C-11)}$$

where

$$K(p,q,M) \equiv \int_{-M}^{M} \operatorname{sinc}(x+p)\operatorname{sinc}(x+q)\,dx \qquad \text{(C-12)}$$

The evaluation of the integral K will be discussed at the end of this appendix. We now point out that the conditional moments can be written in terms of K by combining (C-11) with (C-9). We obtain

$$m_{rs}^{abcd} = \frac{8R_0E^2}{B} \sum_{i=1}^{4} \sum_{k=1}^{4} s_i s_k \sum_{j=-1}^{1} \sum_{n=-1}^{1} (1-\tfrac{1}{2}|j|)(1-\tfrac{1}{2}|n|) \cdot K[j-2(3-i-r),n-2(3-k-s),2BT_m] + 32EN_0\delta_{rs} \qquad \text{(C-13)}$$

Now we know that the error probability is dependent only on the parameters r and d. Thus, in order to compute the error probability, relationships must be found which relate the constants in (C-13) to r and d. To do this it is necessary to note from Equation (2-8) that if all three moments for a given sequence abcd are multiplied by the same constant, then the value of R_{abcd} is not changed. Thus the resulting conditional probability is not changed. Making use of this fact, we multiply m_{rs}^{abcd} in (C-13) above by $(EN_0)^{-1}$ to obtain

$$\tilde{m}_{rs}^{abcd} = \frac{8R_0E}{BN_0} \sum_{i=1}^{4} \sum_{k=1}^{4} s_i s_k \sum_{j=-1}^{1} \sum_{n=-1}^{1} (1 - \tfrac{1}{2}|j|)(1 - \tfrac{1}{2}|n|)$$

$$\cdot K[j-2(3-i-r),\ n-2(3-k-s),\ 2BT_m] + 32\delta_{rs} \qquad \text{(C-14)}$$

Now we see that two constants are required to evaluate this expression - $\frac{R_0E}{BN_0}$ and BT_m. Recalling that r and d have been defined as

$$d \equiv \frac{T_m}{T_b} = BT_m$$

$$r \equiv \frac{2R_0T_mE}{N_0}$$

we see that the constants required to evaluate (C-14) are given by

$$\frac{R_0E}{BN_0} = \frac{r}{2d}$$

$$BT_m = d \qquad \text{(C-15)}$$

Thus, given r and d, (C-15) and (C-14) can be used to determine the conditional moments to be used in (2-8) which then determines the error probability.

To evaluate the integral K we must consider two cases, $p = q$ and $p \neq q$. We consider the case where $p \neq q$ first. If $p \neq q$, we can write

$$K(p,q,M) = \int_{-M}^{M} \frac{\sin \pi(x + p)}{\pi(x + p)} \frac{\sin \pi(x + q)}{\pi(x + q)} dx$$

$$= \frac{1}{\pi^2} \left[\frac{1}{q - p} \int_{-M}^{M} \frac{\sin \pi(x + p) \sin \pi(x + q)}{(x + p)} dx + \right.$$

$$\left. \frac{1}{p - q} \int_{-M}^{M} \frac{\sin \pi(x+p) \sin \pi(x+q)}{(x + q)} dx \right] \qquad \text{(C-16)}$$

Now

$$\int_{-M}^{M} \frac{\sin \pi(x+p) \sin \pi(x+q)}{(x + p)} dx$$

$$= \frac{1}{2} \cos \pi(p - q) \int_{2\pi(p - M)}^{2\pi(p + M)} \frac{1 - \cos(y)}{y} dy$$

$$- \frac{1}{2} \sin \pi(p - q) \int_{2\pi(p - M)}^{2\pi(p + M)} \frac{\text{sir}(y)}{y} dy \qquad \text{(C-17)}$$

$$= \frac{1}{2} \cos \pi(p - q) \{\text{Cin}[2\pi(p + M)] - \text{Cin}[2\pi(p - M)]$$

$$- \frac{1}{2} \sin \pi(p - q) \{\text{Si}[2\pi(p + M) - \text{Si}[2\pi(p - M)]\}$$

where Si(x) and Cin(x) are defined by (29)

$$\mathrm{Cin}(x) = \int_0^x \frac{1 - \cos(y)}{y}\, dy$$

$$\mathrm{Si}(x) = \int_0^x \frac{\sin(y)}{y}\, dy \qquad \text{(C-18)}$$

Similarly, we can show that

$$\int_{-M}^{M} \frac{\sin \pi(x + p) \sin \pi(x + q)}{(x + q)}\, dx$$

$$= \frac{1}{2} \cos \pi(q - p)\{\mathrm{Cin}[2\pi(q + M)] - \mathrm{Cin}[2\pi(q - M)]\}$$

$$- \frac{1}{2} \sin \pi(q - p)\{\mathrm{Si}[2\pi(q + M)] - \mathrm{Si}[2\pi(q - M)]\} \qquad \text{(C-19)}$$

Using (C-17) and (C-19) in (C-16), we obtain

$$K(p,q,M) = \frac{1}{2} \frac{\cos(p - q)}{\pi^2(p - q)} \{\mathrm{Cin}[2\pi(q + M)]$$

$$- \mathrm{Cin}[2\pi(q - M)] - \mathrm{Cin}[2\pi(p + M)] + \mathrm{Cin}[2\pi(p - M)]\}$$

$$+ \frac{1}{2} \frac{\sin(p-q)}{\pi^2 (p-q)} \{\mathrm{Si}[2\pi(p+M)] - \mathrm{Si}[2\pi(p - M)]$$

$$+ \mathrm{Si}[2\pi(q + M)] - \mathrm{Si}[2\pi(q - M)]\} \qquad \text{(C-20)}$$

If $p = q$, $K(p,q,M)$ can be evaluated as follows:

$$K(p,p,M) = \int_{-M}^{M} \frac{[\sin \pi(x + p)]^2}{(x + p)^2}\, dx$$

$$= \int_{\pi(p-M)}^{\pi(p+M)} \frac{\sin^2 y}{y^2}\, dy = -\frac{1}{2\pi(p+M)} + \frac{1}{2\pi(p-M)}$$

$$+ \frac{\cos[2\pi(p+M)]}{[2\pi(p+M)]} - \frac{\cos[2\pi(p-M)]}{[2\pi(p-M)]}$$

$$+ \mathrm{Si}[2\pi(p+M)] - \mathrm{Si}[2\pi(p-M)]$$

The conditional moments m_{00}, m_{11}, and m_{10} can now be computed by using Equations (C-20) and (C-21) in Equation (C-14). The graphical results shown in Figure 7 through 10 of Chapter II were all obtained by using a digital computer to evaluate these equations.

APPENDIX D

COMPUTER SIMULATION PROGRAMS

APPENDIX D

COMPUTER SIMULATION PROGRAMS

This appendix is devoted to a presentation of some of the details of the digital computer simulation programs which were used for this research. For all the computer experiments reported herein, the objective was to evaluate the error probabilities for a specified communication system and channel model. With one exception, it was necessary to compute an average error probability for a system employing a random channel. The method used to compute error probabilities of this type was a Monte Carlo technique and can be divided into three major steps:

1. Generate a sample from an appropriately defined ensemble of random channels.
2. Compute the system error probability conditioned upon the generated channel sample.
3. Compute the average error probability for this entire ensemble of channels generated.

A general block diagram of the computer program is shown in Figure 24. As indicated in this figure, the program was designed to compute error probabilities for several SNR's during the course of an experiment.

The generation of the channel impulse responses is accomplished by linear filtering of a set of uncorrelated pseudo-random Gaussian variates. Details of the filtering scheme and specification of the weighting factors are given elsewhere (30). Since the experiments performed with this system employed frequency domain techniques, the channel impulse response is converted into its (discrete) Fourier transform. Thus the transmission of a given signal through the channel filter and the receiver matched filter can be represented by multiplying the channel transfer function $H(f)$ by the squared modulus of the signal spectrum, $|S(f)|^2$. Also, any other desired operation such as adaptively controlled receiver filtering or channel transfer function modification is performed at this point. Next the resulting composite transform is inverse transformed to form time samples of the entire linear system's response to a signal pulse. This response, which we will denote as $u_0(t)$ is sometimes called the pulse transfer characteristic of the communication system. When only adjacent-baud intersymbol interference is being considered, then only $u_0(-T_b)$, $u_0(0)$, and $u_0(T_b)$ are computed.[1] Next, for a given modulation sequence[2] $S = (a,b,c,d)$, the values of $u(T_b)$ and $v(T_b)$ are computed (see Figure 3). These are given by

---

[1]For simplicity, we will assume that the pulse transmission characteristic is centered about $t = 0$.

[2]As in the analysis of Chapter II, we will compute the error probability for the decision made at $t = T_b$.

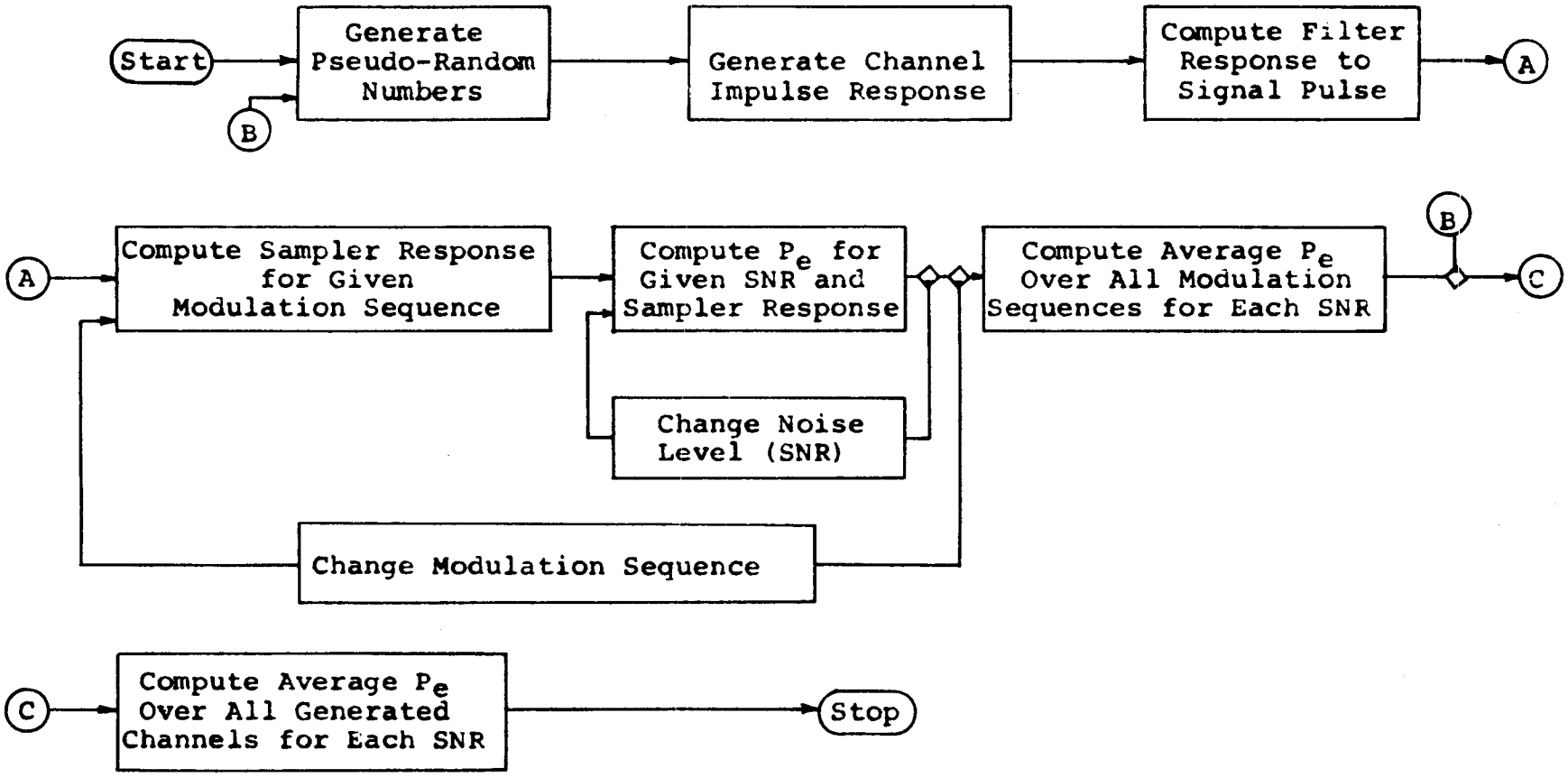

The diamond-shaped boxes are decision boxes. The program branches out of the shaded corner of the box until the required number of cycles is completed, at which time the branch out of the unshaded corner of the box is taken.

Figure 24. Block Diagram of Computer Simulation Program.

$$\hat{u} = u(T_b) = s_2 u_0(T_b) + s_3 u_0(0) + s_4 u_0(-T_b)$$

$$\hat{v} = v(T_b) = s_1 u_0(T_b) + s_2 u_0(0) + s_3 u_0(-T_b) \qquad \text{(D-1)}$$

where

$$s_1 = 2a - 1$$

$$s_2 = 2b - 1$$

$$s_3 = 2c - 1$$

$$s_4 = 2d - 1$$

Once $\hat{u}$ and $\hat{v}$ are specified along with the SNR, the error probability conditioned on the given modulation sequence and the given channel can then be computed as (8)

$$P_e(\hat{u},\hat{v},r) = \frac{1}{2}[1-Q(\sqrt{B},\sqrt{A}) + Q(\sqrt{A},\sqrt{B})] \qquad \text{(D-2)}$$

where

$$A = \frac{(\hat{u} - \hat{v})^2 r}{4K_c E}$$

$$B = \frac{(\hat{u} + \hat{v})^2 r}{4K_c E}$$

$$K_c = \begin{cases} 2\sigma_0^2 & \text{for the G-F channel} \\ 2R_0 T_m & \text{for the S-F channel} \end{cases}$$

and where $Q(x,y)$ is the Marcum Q function. This error probability expression can be more easily evaluated with the use

of a digital computer when it is rewritten in an equivalent form (31):

$$P_e(\hat{u},\hat{v},r) = \frac{1}{2}\left[1 \pm V\left(\left|\sqrt{A} - \sqrt{B}\right|, \frac{\left|\sqrt{A} - \sqrt{B}\right|}{\sqrt{A} + \sqrt{B}}\right)\right] \qquad \text{(D-3)}$$

where the plus sign applies if $B \geq A$ and the minus sign applies otherwise. The V function, which arises in studies of damage probabilities associated with ballistic weapons, is defined by

$$V(K,L) = \frac{1}{L}\int_0^K \exp\left[-\frac{(1 + L^2)}{4L^2}x^2\right] I_0\left[\frac{(1 - L^2)}{4L^2}x^2\right]x\,dx \qquad \text{(D-4)}$$

This function is sometimes called the generalized circular error function or the elliptic normal probability function (32). An efficient digital computer scheme has been developed for evaluating this function (33). This scheme was used as a subprogram of the simulation program to evaluate Equation (D-3).

Equation (D-3) allows the computation of the conditional error probability given the channel impulse response and the specific modulation sequence S. It is therefore necessary to compute the average probability of error for all possible modulation sequences. This is done by evaluating Equation (D-3) for each possible modulation sequence. If one adjacent baud of intersymbol interference is being considered, this means that $2^4 = 16$ different modulation sequences must be

accounted for. If intersymbol interference from two bauds distant from the detection interval is to be considered, then $2^6 = 64$ different sequences must be considered. However, as indicated in Equation (2-3), certain simplifications are possible which reduce the number of evaluations to six and twenty for the one and two-baud cases respectively.

Once the error probability averaged over the additive noise and overall possible modulation sequences is computed for a specified channel impulse response, a new pseudo-random impulse response is generated. The error probability is then computed for the new impulse response and the process is repeated for a prespecified number of times. Then the average error probability is computed for all the channels generated. This is done by simply computing the sample mean of the various conditional error probabilities. Writing $\hat{P}_e$ as the estimate for the complete system error probability and P_n for the individual channel-conditioned error probabilities, we have

$$\hat{P}_e = \frac{1}{N} \sum_{n=1}^{N} P_n$$

where N is the total number of channel samples generated. At the same time the sample variance of the set of conditional probabilities was computed. This is simply

$$\hat{\sigma}^2(P_n) = \frac{1}{N-1} \sum_{n=1}^{N} (P_n - \hat{P}_e)^2$$

This number is then used to compute the estimated standard deviation of the error probability estimate. This is given by

$$\hat{\sigma}(\hat{P}_e) = \left[\frac{\hat{\sigma}^2(P_n)}{N}\right]^{\frac{1}{2}}$$

This estimate is used as a basis for judging the accuracy of the error probability estimate and consequently to judge the required number of channel samples which must be generated in order to obtain adequate experimental results.

We conclude this appendix by briefly describing the modifications of the basic simulation program just described which were made to obtain the various experimental results given in this report. The most extensive modification required was for the experimental results of Figures 11, 12, and 13 in Chapter III. These figures indicate the error probability for a DPSK system whose transmission channel consists solely of a time-invariant linear delay distortion filter. Since this case was concerned with a non-random time invariant filter, the entire Monte-Carlo feature of the simulation program was unnecessary. That is, it was simply necessary to generate one channel with the proper transfer function and compute the error probability averaged over the additive white noise and the possible modulation sequences. Thus, for a given L, the channel transfer function was defined to be

$$H(f) = \exp[j\pi T_b^2 Lf].$$

From this, the corresponding values of $u_0(-T_b)$, $u_0(0)$, and $u_0(T_b)$ were computed. Then, since two adjacent bauds of intersymbol interference were to be computed, Equations (D-1) and (D-3) were evaluated the required twenty times and the resulting average error probability recorded.

In Chapter IV the results of three experiments are recorded. The first of these is a simulation of the non-adaptive communication system which was analyzed in Chapter II. This system is simulated by the program with no modifications. That is, after the pseudo-random channel transfer function is generated, it is immediately multiplied by the composite signal-matched filter spectrum $|S(f)|^2$ and inverse transformed. The Monte Carlo procedure is used with a number of random channels sufficient to make the estimated standard deviation of the estimate reasonably small.

The second experiment described in Chapter IV is the simulation of a flat Rayleigh fading communication system. For this experiment the basic simulation program was used, but the pseudo-random channel transfer functions were modified before being multiplied by $|S(f)|^2$. The modification consisted of replacing the frequency-dependent transfer function by its value at the center frequency, thus making it a constant across the baud. Writing $H(f)$ for the generated transfer function and $H_m(f)$ for the transfer function after modification, we can express this as

$$H_m(f) = H(0)$$

The third experiment described in Chapter IV consists of determining the error probability for the non-adaptive system discussed in Chapter II when it is subject separately to the phase and amplitude distortion effects of a Gaussian random channel. For this experiment the basic simulation program was again used, but the pseudo-random channel transfer functions were modified in the following manner before being multiplied by $|S(f)|^2$:

$$H_m(f) = |H(f)|$$

for the pure amplitude selective fading case, and

$$H_m(f) = H(0)[H(f)/|H(f)|]$$

for the pure phase distortion fading case.

In Chapter V, experimental results for two adaptive receiver systems operating with the Gaussian frequency selective fading channel were investigated. These systems consist of a channel measurement system along with an adaptively controlled linear filter placed between the channel output and the matched filter input. Since the transmission system from signal generator to receiver matched filter is entirely linear, the method of implementing this experiment is basically the same as for the second experiment of Chapter IV described above. Specifically, as soon as the pseudo-random

channel transfer function is generated, the required measurement is made. Then three transfer functions were multiplied together - the channel transfer function H(f), the signal-matched filter spectrum $|S(f)|^2$, and the equalization filter transfer function $H_c(f)$. The remainder of the simulation program was unchanged. For the ideal system of Section 5.3, $H_c(f)$ was set equal to the quadratic function of f which would exactly compensate for the measured phase characteristic. For the physically realizable system, $H_c(f)$ was set equal to the all-pass phase function given in Equation (5-5), where (5-7) and (5-8) were used to determine ω_r and α.

RECENT RESEARCH PUBLICATIONS
SCHOOL OF ELECTRICAL ENGINEERING
PURDUE UNIVERSITY

TR-EE66-1 TOWARD BRAIN MODELS WHICH EXPLAIN MENTAL CAPABILITIES – (Report No. 1)
R. J. Swallow, Support: E. E. Department Research

TR-EE66-2 ON THE ASYMPTOTIC STABILITY OF FEEDBACK CONTROL SYSTEMS CONTAINING A SINGLE TIME-VARYING ELEMENT
Z. V. Rekasius and J. R. Rowland, NASA Institutional Grant (SUB-UNDER NRG 14-005-021) PRF #4220-52-285, January, 1966

TR-EE66-3 ANALOGUE DEMODULATION ON A FINITE TIME INTERVAL
J. C. Hancock and P. W. Brunner, NSF Grant #GP-2898, PRF #3955-50-285, April, 1966

TR-EE66-4 STEADY STATE ANALYSIS OF LINEAR NETWORKS CONTAINING A SINGLE SINUSOIDALLY VARYING ELEMENT.
B. J. Leon and J. V. Adams, Grant #GK26, PRF #4108-50-285, May, 1966

TR-EE66-5 CYBERNETIC PREDICTING DEVICES
A. G. Ivakhnenko and V. G. Lapa. Translated by Z. J. Nikolic, April, 1966

TR-EE66-6 ON THE STOCHASTIC APPROXIMATION AND RELATED LEARNING TECHNIQUES
K. S. Fu, Y. T. Chien, Z. J. Nikolic and W. G. Wee, National Science Foundation GK-696, PRF #4502, April, 1966

TR-EE66-7 JOINTLY OPTIMUM WAVEFORMS AND RECEIVERS FOR CHANNELS WITH MEMORY
J. C. Hancock and E. A. Quincy, NSF GP-2898, PRF 3955 and NASA NSG-553, PRF 3823, June 1966

TR-EE66-8 AN ADAPTIVE PATTERN RECOGNIZING MODEL OF THE HUMAN OPERATOR ENGAGED IN A TIME VARYING CONTROL TASK
K. S. Fu and E. E. Gould, National Science Foundation Grant GK-696; PRF #4502, May, 1966

TR-EE66-9 ANALYSIS OF A WIDEBAND RANDOM SIGNAL RADAR SYSTEM
G. R. Cooper and Ronald L. Gassner, National Science Foundation Grant GK-189 PRF #4243, August, 1966.

TR-EE66-10 OPTIMAL CONTROL IN BOUND PHASE-COORDINATE PROCESSES
J. Y. S. Luh and J. S. Shafran, NASA/JPL No. 950670, PRF #3807, July, 1966

TR-EE66-11 ON THE OPTIMIZATION OF MIXTURE RESOLVING SIGNAL PROCESSING STRUCTURES
J. C. Hancock and W. D. Gregg, NSF GP-2898;-PRF #3955; NASA NGR-15-005-021;-PRF #4219, October, 1966.

TR-EE66-12 OPTIMAL CONTROL OF ANTENNA POINTING SYSTEM
J. Y. S. Luh and G. E. O'Connor, Jr., NASA/JPL No. 950670; PRF #3807, August, 1966

TR-EE66-13 DESIGN OF LARGE SIGNAL SETS WITH GOOD APERIODIC CORRELATION PROPERTIES
G. R. Cooper and R. D. Yates, Lockheed Electronics Company, Contract #29951, PRF #4195, September, 1966

TR-EE66-14 A PRELIMINARY STUDY OF THE FAILURE MECHANISMS OF CdSe THIN FILM TRANSISTORS
R. J. Schwartz and R. C. Dockerty, U.S. Naval Avionics Facility, N0016366C0096 A02, PRF #4850-53-285, September, 1966

TR-EE66-15 REAL-TIME ESTIMATION OF TIME-VARYING CORRELATION FUNCTIONS
G. R. Cooper and W. M. Hammond, NSF Contract No. GK-189; PRF #4243-50-285, October, 1966

TR-EE66-16 ON THE FINITE STOPPING RULES AND NONPARAMETRIC TECHNIQUES IN A FEATURE-ORDERED SEQUENTIAL RECOGNITION SYSTEM
K. S. Fu and Y. T. Chien, National Science Foundation GK-696, PRF #4502, October, 1966

TR-EE66-17 FAILURE MECHANISMS IN THIN-FILM RESISTORS
H. W. Thompson, Jr. and R. F. Bennett, Naval Avionics Facility, Contract No. N0016366 C0096; Task Order No. A02, October, 1966

TR-EE66-18 DISTRIBUTION FREE, MINIMUM CONDITIONAL RISK LEARNING SYSTEMS
E. A. Patrick, Air Force Avionics Laboratory (AVWC), Contract AF 33 (615) 3768, November 1966

TR-EE66-19 THRESHOLD STUDY OF PHASE LOCK LOOP SYSTEMS
John C. Lindenlaub and John Uhran, NASA Grant NsG-553, November, 1966

TR-EE66-20 A STUDY OF LEARNING SYSTEMS OPERATING IN UNKNOWN STATIONARY ENVIRONMENTS
K. S. Fu and Z. J. Nikolic, NSF Grant GK-696, PRF 4502, November 1966

RECENT RESEARCH PUBLICATIONS
SCHOOL OF ELECTRICAL ENGINEERING
PURDUE UNIVERSITY

(Continued from inside back cover)

TR-EE66-21 FIVE RESULTS ON UNSUPERVISED LEARNING SYSTEMS
E. A. Patrick, G. Carayannopoulos, J. P. Costello, Air Force Avionics Laboratory (AVWC), Wright Patterson Air Force Base, Contract AF 33(615)3768

TR-EE66-22 THE RADIATION PRODUCED BY AN ARBITRARILY ORIENTED DIPOLE IN AN INFINITE, HOMOGENEOUS, WARM, ANISOTROPIC PLASMA
Floyd V. Schultz and Robert W. Graff, Joint Services Electronics Program, Contract ONR N00016-66-C0076-A04

TR-EE66-23 HARMONIC GENERATION USING THE VARACTOR CAPABILITIES OF THE PLASMA SHEATH
R. A. Holmes and R. T. Hilbish, Joint Services Electronics Program, Contract ONR N00016-66-C0076-A04

TR-EE66-24 AN INVESTIGATION OF THE INTERFACE STATES OF THE GERMANIUM-SILICON ALLOYED HETEROJUNCTION
H. W. Thompson and A. L. Reenstra, Joint Services Electronics Program, Contract ONR N00016-66-C0076-A04

TR-EE67-1 PARAMETER ESTIMATION WITH UNKNOWN SYMBOL SYNCHRONIZATION
J. C. Hancock and T. L. Stewart, NSF Grant GP-2898, PRF 3955-50-285, January 1967

TR-EE67-2 NONLINEAR OSCILLATION OF A GYROSCOPE
Chikaro Sato, PRF 4891, National Science Foundation Grant No. GK-01235

TR-EE67-3 ON THE DESIGN OF SPECIFIC OPTIMAL CONTROLLERS
V. B. Haas and S. Murtuza, NASA, NGR 15-005-021

TR-EE67-4 ON THE ANALYSIS AND SYNTHESIS OF CONTROL SYSTEMS USING A WORST CASE DISTURBANCE APPROACH
V. B. Haas and A. S. Morse, NASA, NGR 15-005-021

TR-EE67-5 ANALYSIS AND SYNTHESIS OF MULTI-THRESHOLD THRESHOLD LOGIC
K. S. Fu and W. C. W. Mow, Contract ONR-N00016-66-C0076,A04 Joint Services Electronic Program

TR-EE67-6 ESTIMATION OF SONAR TARGET PARAMETERS
G. R. Cooper and J. U. Kincaid, National Science Foundation Grant GK-189, PRF 4243

TR-EE67-7 ON GENERALIZATIONS OF ADAPTIVE ALGORITHMS AND APPLICATION OF THE FUZZY SETS CONCEPTS TO PATTERN CLASSIFICATION
K. S. Fu and W. G. Wee, National Science Foundation Grant GK-696, PRF 4502

TR-EE67-8 COMPUTER AIDED ANALYSIS AND SYNTHESIS OF MULTIVALUED MEMORYLESS NETWORKS
L. O. Chua and W. H. Stellhorn, National Science Foundation Grant GK-01235, Joint Services Electronics Program Contract ONR-N00016-66-C0076-A04, PRF 4711

TR-EE67-9 OPTIMUM FINITE SEQUENTIAL PATTERN RECOGNITION
K. S. Fu and G. P. Cardillo, National Science Foundation Grant GK-696, PRF 4502

TR-EE67-10 MINIMUM SENSITIVITY OPTIMAL CONTROL FOR NONLINEAR SYSTEMS
V. Haas and A. Steinberg, NASA NGR 15-005-021, PRF 4558

TR-EE67-11 RANDOM SIGNAL RADAR (Final Report)
G. R. Cooper and C. D. McGillem, NASA, NsG-543

TR-EE67-12 INTRODUCTION TO THE PERFORMANCE OF DISTRIBUTION FREE, MINIMUM CONDITIONAL RISK LEARNING SYSTEMS
E. A. Patrick and F. P. Fisher II, Naval Ship Systems Command Contract N00024-67-C-1162 PRF No. 4925-53-2859

TR-EE67-13 P-I-N THERMO-PHOTO-VOLTAIC DIODE
R. J. Schwartz and C. W. Kim, Joint Services Electronic Program Contract ONR-N00014-67 A00226-004

TR-EE67-14 ESTIMATION OF PROBABILITY DENSITY AND DISTRIBUTION FUNCTIONS
R. L. Kashyap and C. C. Blaydon, National Science Foundation Grant GK-1970, PRF 5181, and Joint Services Electronics Program Contract N00014-67-A0226-0004, PRF 4711.

TR-EE67-15 OPTIMIZATION OF STOCHASTIC CONTROL PROCESSES WITH RESPECT TO PROBABILITY OF ENTERING A TARGET MANIFOLD
J. Y. S. Luh and G. E. O'Connor, Jr., Jet Propulsion Laboratory Contract 950670, PRF 3807

TR-EE67-16 CODES FOR UNSUPERVISED LEARNING OF SOURCE AND BINARY CHANNEL PROBABILITIES
E. A. Patrick and G. Carayannopoulos, Air Force AF 33(615)3768, PRF 4575